Title	Tactile sensorization of highly-deformable materials for enriching physical interactions
Author(s)	川節, 拓実
Citation	大阪大学, 2018, 博士論文
Version Type	VoR
URL	https://doi.org/10.18910/70749
rights	
Note	

Doctoral Dissertation

Tactile sensorization of highly-deformable materials for enriching physical interactions

Takumi Kawasetsu

July 2018

Graduate School of Engineering
Osaka University

Thesis Supervisor: Minoru Asada
Title: Department of Adaptive Machine Systems,
Graduate School of Engineering, Osaka University

Thesis Committee: Minoru Asada, Chair
Koh Hosoda
Fumikazu Miyasaka

Preface

This work has been carried out by Takumi Kawasetsu from 2015 to 2018 under the supervision of Professor Minoru Asada at the Department of Adaptive Machine Systems, Graduate School of Engineering, Osaka University, Japan.

Abstract

The aims of this doctoral dissertation are

- to propose a tactile sensorization method of highly-deformable materials for enriching physical interaction
- to propose a feasible configuration for fabricating tactile sensors based on the proposed tactile sensorization approaches
- to investigate and evaluate performances of the fabricated tactile sensors.

Tactile sensation is an important modality for robots interacting with unknown environments, including human beings. Tactile senses various types of physical force interactions that occur in contact boundaries. For instance, tactile sensors are employed to measure multi-axis force, slippage, or vibration that appear between the sensor and the environment. In order to obtain rich tactile information, the physical interactions between a robot and the environment should be enriched as a prerequisite. A feasible approach for enriching physical interaction is to develop a tactile sensor covered with a soft material. This is because the soft surface of a tactile sensor 1) fits the shape of a contact target to obtain contact information from a broad contact area; 2) accepts enriched human touch patterns such as pinching, twisting, tapping, pushing, and stroking; and 3) enhances occasions of social touching by providing humans with a comfortable tactile impression. Therefore, numerous studies have proposed various flexible and soft tactile sensors for measuring enriched physical interaction. However, conventional sensors have several structural and functional disadvantages in terms of sensitivity and durability owing to the mismatch between material softness and sensing mechanism.

To address this issue, this dissertation introduces two approaches in which soft and thick materials function as flexible tactile sensors by employing electromagnetic phenomena. Both approaches employ a magnetorheological elastomer (MRE) as the surface of the proposed tactile sensor. An MRE is a functional magnetic elastic material in which particles with a high magnetic permeability (e.g., iron particles), are mixed with an elastic material (e.g., silicon rubber). Both approaches utilize electromagnetic phenomena to sensorize the MRE by measuring the displacement of magnetic particles caused by the applied contact force to the MRE. To evaluate these approaches, this dissertation addresses the following:

1. In the first approach, the MRE sheet is tactile-sensorized by employing a magnet and magnetic transducer pair. The MRE sheet and a silicon rubber sheet are simply laminated onto the magnet and transducer. The normal force applied to the MRE sheet causes the displacement of magnetic particles in the MRE sheet, thereby changing the magnetic field distribution generated by the magnet around the magnetic transducer. As a result, the MRE sheet itself functions as a flexible tactile sensor because the applied contact force can be measured with the magnetic transducer as a change in the magnetic field. To investigate how the magnetic field changes with applied contact force, the following experiments are conducted: 1) magnetic field simulation with a simple model of the proposed sensor for reference; and 2) investigation of sensor responses by experiments with the fabricated sensor.

2. In the second approach, the MRE functions as a flexible tactile sensor by employing an inductor. Here, the MRE sheet and a silicon rubber sheet are simply laminated onto the inductor, e.g., a coil printed with a trace on a circuit board. Since the MRE contains magnetic particles with high magnetic permeability, the distance between the MRE and inductor determines its inductance. Consequently, the MRE itself will function as a flexible tactile sensor because the applied force can be measured by monitoring the inductance. The sensor responses, i.e., the change in inductance caused by the applied contact force, are investigated by experiments with a fabricated sensor.

3. As an extension of the second approach, the MRE is tri-axis tactile-sensorized

by employing four inductors. A disk-shaped MRE (a ferromagnetic marker) embedded in cylindrical silicon rubber is placed on the four inductors. In this structure, the three-dimensional displacement of the ferromagnetic marker can be estimated by the summation or difference of four inductances. The sensor responses, i.e., the change in the four inductances caused by the applied tri-axis force, are investigated by experiments with a fabricated sensor.

The proposed sensors can resolve issues with conventional flexible tactile sensors as well as enrich physical interaction.

Acknowledgments

First of all, I express my gratitude to Professor Minoru Asada, who is a principal adviser of this work. He guided me to the exciting and challenging field of robotics as well as cognitive developmental robotics, which was advocated by him and some researchers. He also has given me many chances to study on high-level and make valuable connections with many researchers. His critical comments and great supports have enabled me to accomplish this work.

I am also very grateful to Assistance Professor Hisashi Ishihara. His comments from both engineering and cognitive developmental robotics viewpoints have always given me an opportunity to review this study from the viewpoint. I learned important things not only to advance my own research but also to spend happy life as a researcher. His powerful leading and big supports have enabled me to accomplish this work. This work would not be possible without his support.

Professor Koh Hosoda and Associate Professor Fumikazu Miyasaka have spared their valuable time to discuss the meanings of the research on flexible tactile sensors. Their meaningful suggestions and discussions gave me a chance to reaffirm my stance on the study. I would like to thank them.

I also thank all the present and the past members in Emergent Robotics Laboratory at Osaka University. I would like to thank Mr. Takato Horii, who proposed a flexible tactile sensor using a magnetorheological elastomer and magnetic phenomena, for his valuable discussions and suggestions on this study. He has given me essential advices on how to discover interesting topics of study.

Dr. Yuji Kawai and Mr. Jihoon Park have given me valuable suggestions and great opportunities to study cognitive developmental robotics as well as engineering since I entered this laboratory. Mr. Kohei Fukuda and Mr. Takashi Morishige have tackled some issues on my study. The members in Ishihara group, Mr. Yoshihiro Nakata, Mr. Nobuyuki Ota, Mr. Ryosuke Yokoo, Mr. Yuki Yamashita, Mr. Binyi Wu, Mr. Souma Ohkita, Mr. Naoki Umeda, and Mr. Jeffrey Queisser gave me valuable discussions and suggestions on this study. I also thank Mr. Ryo Iwaki, Mr. Jorge Luis Copete, and Mr. Jyh-Jong Hsieh, who have worked together as the same Ph.D students in this laboratory. Other members who are not mentioned here also have supported me to accomplish my study.

I would like to thank the members in Robocon Project at Nara National College of Technology. Mr. Hiroaki Ota and Mr. Yuta Yanagisawa have gave me essential advices on electromagnetic phenomenon, including the sensing mechanisms of the proposed sensor. Mr. Yuito Sugata supported me to summarize the results as well as to conduct some experiments. Mr. Shota Hamaguchi designed and fabricated a robotic arm for coming experiments.

Finally, I also thank my family. They have supported me in every way. None of this work and my life would be possible without their great supports.

July 5th, 2018
Takumi Kawasetsu

Contents

Preface **iii**

Abstract **v**

Acknowledgments **ix**

1 Introduction **1**

1.1 Tactile sensors for enriching physical interactions 2

1.2 Tactile sensorization of highly-deformable material 5

1.3 Research objective 6

1.4 Outline of the dissertation 8

2 Related works **11**

2.1 Summary of state-of-the-art tactile sensors 11

2.1.1 Type A, Transducers are placed inside a flexible covering . . . 12

2.1.2 Type B, The flexible covering functions as a transducer 13

2.1.3 Type C, Transducers are mounted onto the surface of the robot frame 14

2.1.4 Type D, Transducers are placed inside the robot with their markers inside the covering 15

2.1.5 Summary 17

2.2 Key ideas of the proposed sensor 17

3 Tactile sensorization with a magnet and a magnetic transducer **21**

3.1 Background 22

3.2 Proposed sensor 24
3.2.1 Structure and Sensing Mechanism 24
3.2.2 Fabricated Sensor 25
3.3 Simulations and experiments 26
3.3.1 Magnetic field simulation 27
3.3.2 Experiments with the fabricated sensor 28
3.3.3 Thickness dependency in the sensor responses 31
3.3.4 Contact Speed dependency in the sensor response 34
3.3.5 Spatial Response 39
3.4 Discussion 44
3.4.1 Simulations and real experiments 44
3.4.2 Sensor Response and Contact Speed 47
3.4.3 Spatial Response 48
3.4.4 Usefulness of the Mexican-Hat-Like Spatial Response for Tactile Information Processing 53
3.5 Summary 54

4 Tactile sensorization with an inductor **55**
4.1 Background 56
4.2 Proposed sensor 57
4.2.1 Structure and Sensing Mechanism 57
4.2.2 Fabricated Sensor 58
4.3 Experiments and results 60
4.3.1 Sensor response curve 60
4.3.2 Spatial Response Properties 61
4.3.3 Sensor response caused by approaching metallic materials . . . 64
4.3.4 Interference between inductors 67
4.4 Discussions 71
4.4.1 Sensor response caused by approaching metallic materials . . . 73
4.4.2 Interference between two inductors 74
4.5 Summary 76

5 Tri-axis tactile sensorization with four inductors 77
5.1 Background 77
5.2 Proposed Tri-axis Tactile Sensor 80
5.2.1 Developed sensor 80
5.2.2 Sensing mechanism 81
5.3 Experiments 84
5.3.1 Sensor calibrations 84
5.3.2 Tri-axis force sensing 89
5.4 Discussions 90
5.4.1 Sensor calibration and tri-axis force sensing 90
5.4.2 Advantages of the proposed sensor 91
5.5 Summary 92

6 Discussion 95
6.1 Difference between the proposed approaches 95
6.2 Advantages of the proposed approaches 96
6.2.1 Advantages in practical applications 97
6.2.2 Adjustability of sensor performances 98
6.3 Issues of the proposed approach 100
6.4 An insight for a tactile hardware filter 101

7 Conclusion 103
7.1 Summary of the proposed approaches 103
7.1.1 Tactile sensorization of a magnetorheological elastomer based on a magnetic field measurement 104
7.1.2 Tactile sensorization of a magnetorheological elastomer based on an inductance measurement 104
7.2 Future works 105

Bibliography 107

List of Tables

3.1 Parameters of each element. BE and MRE stand for base elastomer and magnetorheological elastomer, respectively. 28
3.2 Thickness differences of each elastomer sheet between three types of sensors. Type A is the same elastomer with the one used in the first experiment. 32
4.1 Characteristics of the prepared three spiral inductors 58
4.2 Summary of the measured responses. 64
4.3 Parameters of the MRE sheet. 67
5.1 Root mean squared errors between the estimated and measured tri-axis force across 10 trials 90

List of Figures

1.1 Function of soft surface of tactile sensors: (a) a hard object touches a hard surface, i.e., the surface of a tactile transducer; (b) a soft object touches a hard surface; (c) a hard object touches a soft surface; and (d) a soft object touches a soft surface. The soft surface reduces the reaction force that occurs in the touched object and enriched the contact information obtained because of the broad contact area. . . 4

1.2 Proposed approaches for tactile sensorization of a soft and flexible magnetorheological elastomer (MRE): (a) a flexible tactile sensor employing a magnet and magnetic transducer; (b) a flexible tactile sensor employing an inductor. In both approaches, the applied contact force can be measured as a deformation of the surface MRE based on electromagnetic techniques. 8

2.1 Schematics of the structures of conventional flexible tactile sensors holding a thick flexible contact layer: (a) type A—transducers with associated wiring are placed inside a flexible covering; (b) type B—a flexible covering functions as a transducer; (c) type C—transducers are mounted onto the surface of the robot frame; and (d) type D—transducers are placed inside the robot while their markers are embedded into flexible covering. 12

2.2 Schematics of the structures of the proposed sensors: (a) tactile sensorization approach employing a magnet and magnetic transducer pair; (b) tactile sensorization approach employing an inductor. 18

3.1 Basic structure of the proposed flexible tactile sensor, which can detect an applied normal force and vertical deformation. 23

3.2 Schematic of the structure and sensing mechanism of the proposed sensor. A flexible dual-layer elastomer, which is composed of magnetorheological and nonmagnetic elastomers, is placed on the robot frame. A magnet and magnetic transducer are mounted inside the robot. The magnetic transducer detects the deformation of the surface of the dual-layer elastomer as the change in magnetic flux distribution generated by the magnet. 25

3.3 Overview of the fabricated tactile sensor. (a) Appearance of the sensor. A black magnetorheological elastomer was laminated onto a white translucent base elastomer, and the top surface was covered by a thin protective plastic film. (b) Appearance of the sensor when viewed from the bottom. A magnet is mounted at the center of a printed circuit board, and a GMR sensor is placed 10 mm away from the magnet. . . 26

3.4 Simulation model of the proposed sensor used in the magnetic field simulation. The model consists of a magnetorheological elastomer sheet, a base elastomer sheet, a board, a magnetic transducer, a permanent magnet, and the air. The geometric and material parameters for each element are summarized in Table 3.3.1. 27

3.5 Simulation result of magnetic flux density penetrating the magnetic sensor against applied depth with the second order fitted curve. . . . 29

3.6 Experimental setup for investigating the sensor response. The sensor was mounted on a z-axis stage holding a digital force gauge with a plastic cylindrical indenter with a diameter of 20 mm. The output voltage of the sensor was amplified by an amplification circuit and was then measured with an oscilloscope. 29

3.7 The sensor output voltage versus the applied normal force. The solid lines indicate the moving averages of the sensor outputs with an interval of 10 ms. Each arrow represents the direction of applied vertical deformation. 31

3.8 The sensor output voltage versus the applied vertical deformation. The solid lines indicate the moving averages of the sensor outputs with an interval of 10 ms. The sensor output quadratically increased with the applied vertical deformation. White diamond and square plots represent simulated value calculated by different relative permeability μ_r of MRE: 2 and 1.5, respectively. 32

3.9 Comparison of sensor output changes against the applied normal force among the three types of the sensors. 33

3.10 Comparison of sensor output changes against the applied vertical deformation among the three types of the sensors. White squares, triangles, and circles indicate simulated value of type A, type B, and type C sensor, respectively. 33

3.11 Overview of the fabricated tactile sensor. (a) Appearance of the sensor. A black magnetorheological elastomer was laminated onto a white translucent base elastomer, and the top surface was covered by a thin protective plastic film. (b) Appearance of the sensor when viewed from the bottom. A magnet is mounted at the center of a printed circuit board, and a GMR sensor is placed 10 mm away from the magnet. . . 35

3.12 Experimental setup for investigating the sensor response. The sensor was mounted on a three-axis stage holding a digital force gauge with a plastic cylindrical indenter with a diameter of 10 mm. The output voltage of the sensor was amplified by an amplification circuit and was then sent to a personal computer via an analog-to-digital converter. 36

3.13 Sensor response curves with a contact speed V of 0.1 mm/s: (a) the sensor output versus the applied normal force and (b) the sensor output versus the indenter depth. In both plots, the solid lines and shaded regions indicate the average value and twice the standard deviation (2σ), respectively. The arrows indicate the direction of the applied load. 38

3.14 Sensor output versus time for three different contact speeds: (**a**,**b**,**c**) Sensor outputs with three different contact speeds $V = 0.1$, 1, and 10 mm/s, respectively. 40

3.15 Measurement region and positions of the spatial response. The black dots indicate the center position of the applied load, i.e., the center of the indenter. The indenter was moved from $(x, y) = (-40, 40)$ to $(40, 40)$ in 1 mm steps based on the index numbers 1, 2, ..., 6,561 of the dots. 41
3.16 Measured spatial response for a depth of 4 mm. The shape of spatial response exhibits an approximately elliptical Mexican-hat-like bipolar shape whose major axis corresponds to the line connecting the centers of the magnet and GMR sensor. 42
3.17 Line profiles of the measured spatial responses with at seven different depths: (**a**,**b**) Sensor outputs along the x and y axes through the point (x_o, y_o) = (3, 0), respectively. 43
3.18 Measured spatial response with a sponge sheet instead of the base elastomer sheet at a depth of 4 mm. The shape of spatial response exhibits an approximately elliptical Gaussian-like shape whose major axis corresponds to the line connecting the centers of the magnet and GMR sensor. 44
3.19 Line profiles of the measured spatial responses with the sponge sheet instead of the base elastomer sheet: (**a**,**b**) Sensor outputs along the x and y axes through the point (x_{os}, y_{os}) = (2, 0), respectively. 45
3.20 Comparison between the measured and fitted responses for a depth of 4 mm: (**a**) two-dimensional fitted response and (**b**,**c**) line profiles along the x and y axes through the center (x_o, y_o) = (0, 0), respectively. . 52
4.1 Appearance of the proposed sensor and its cross-sectional schematic. An spiral inductor is printed on a printed circuit board while magnetorheological and nonmagnetic base elastomer sheets cover the board. 58
4.2 An appearance of the fabricated flexible tactile sensor. The sensor consists of a mangetorheological elastomer sheet, a non-magnetic elastomer sheet, and a printed circuit board holding a spiral inductor. . 59
4.3 Inductor parameters of a two-layer planar spiral inductor printed on both surface of a rigid circuit board. 59

4.4 Experimental setup for measuring the sensor response curves. A normal force was applied to the sensor surface by a three-axis robot stage with a cylindrical indenter. A personal computer captured the inductance and the outputs of a force–torque sensor via an inductance-to-digital converter and analog-to-digital converter. 60

4.5 Measured sensor response curves versus (a) the applied normal force and (b) the applied vertical deformation across 10 trials. The inset shows a magnification of the initial part of the curve. The solid line and dots indicate the mean value of the inductance, and the arrows depict the direction of the applied normal force. The shaded region indicates twice the standard deviation (2σ) of the inductance. 62

4.6 Measurement region and positions of the spatial response. The black dots indicate the center position of the applied load, i.e., the center of the indenter. The indenter was moved from $(x, y) = (-40, 40)$ to $(40, 40)$ in 1 mm steps based on the index numbers 1, 2, ..., 6,561 of the dots. 63

4.7 Spatial response of the sensor with a type A inductor. The color indicates that the inductance changed from its initial value. 64

4.8 Experimental condition for investigating the sensor response versus approaching metal cube. 65

4.9 Measured inductance change versus the distance from the inductor. The solid line indicates the mean value of the inductance across 5 trials. 66

4.10 Maximum inductance change obtained with the nine different elastomers and the aluminum cube. The characters indicate the type of the elastomer. 68

4.11 An appearance of the fabricated sensor for investigating the interference between two inductors: (a) appearance of the sensor; (b) bottom view of the sensor. The sensor consists of a mangetorheological elastomer sheet, a non-magnetic elastomer sheet, and flexible printed circuit boards holding spiral inductors. 69

4.12 Inductance change versus the applied normal force across 10 trials. The solid line and shaded gray region indicate the mean value of the inductance and twice the standard deviation (2σ) of inductance, respectively. The inductance monotonically increases with the applied normal force. 70

4.13 Inductor interval distance d versus inductance changed caused by the interference of two inductors. The dots and their error bars indicate the mean value and twice the standard division (2σ) of measure inductance change across 10 trials. For reference, the dotted line indicate the inductance change when a vertical deformation of 6 mm is applied. . 71

4.14 Inductance change versus applied vertical deformation. The solid and dotted lines indicate the mean value of measure inductance change when a neighbor inductor with an interval of 20 mm was driven or not driven across 5 trials, respectively. 72

5.1 Appearance of the proposed tri-axis tactile sensor. The sensor consists of four spiral inductors printed on a flexible printed circuit board (FPCB) and a disk-shaped magnetorheological elastomer (MRE; ferromagnetic marker) embedded in a cylindrical elastomer made of a silicon rubber. The inductances of the inductors are determined by the positional relationship between the ferromagnetic marker and each inductor because the marker contains iron particles with a high magnetic permeability. Therefore, the sensor can estimate applied tri-axis forces by monitoring the inductance changes caused by three-dimensional (3D) displacements of the marker. 79

5.2 Schematic and design parameters of the developed tri-axis tactile sensor: (a) Design parameters for an inductor printed on the FPCB; (b) arrangement of inductors and ferromagnetic marker in x-y plane; (c) arrangement of inductors and ferromagnetic marker in x-z plane. . . . 82

5.3 Fabrication processes: (a) a ferromagnetic marker; (b) a cylindrical elastomer containing the ferromagnetic marker. 83

5.4 Experimental setup for investigating the sensor responses. The proposed sensor is mounted on a three-axis robot stage holding a force–torque sensor (F/T sensor). Contact force is applied to the sensor using a plastic flat object attached to the tip of the F/T sensor. An inductance-to-digital converter measures the inductances and sends them to a personal computer (PC), while an analog-to-digital converter captures the output of the F/T sensor and sends it to the PC. 85

5.5 Converted inductances L_x, L_y, and L_z versus the applied normal force F_z across 10 trials. The solid and dotted lines indicate the mean value of the converted inductance and applied shear force, respectively. The shaded region indicates twice the standard deviation (2σ) of each inductance. The inductance value L_z increases with the applied normal force, while L_x and L_y do not significantly increase. 86

5.6 Converted inductances versus the applied shear force F_x across 10 trials. The solid and dotted lines indicate the mean values of the converted inductance and applied shear and normal force, respectively. The shaded region indicates twice the standard deviation (2σ) of the inductance. The result demonstrates that the converted inductance value L_x increase in accordance with the applied shear force F_x, while L_z does not significantly increase. 87

5.7 Converted inductances versus the applied shear force F_y across 10 trials. The solid and dotted lines indicate the mean values of the converted inductance and applied shear and normal force, respectively. The shaded region indicates twice the standard deviation (2σ) of the inductance. The result demonstrates that the converted inductance value L_y increase in accordance with the applied shear force F_y, while L_z does not significantly increase. 88

5.8 Comparison between measured and estimated tri-axis force applied to the proposed sensor: (a) applied normal force F_z versus time; (b), (c) applied shear force F_x and F_y versus time, respectively. The solid gray line indicates the measured tri-axis force with the F/T sensor (i.e., reference force), while the solid black line indicates the estimated tri-axis force based on the measured inductance values. The dotted red line indicates the estimation error (i.e., difference of the measured and estimated force) for reference. 94

Chapter 1

Introduction

Tactile is an essential modality for robots interacting with unknown environments and human beings. Tactile sensation mainly measures force information during physical interactions that occur in contact boundaries; for instance, tactile sensors are employed to measure the multi-axis force, slippage, or vibration that emerge between the sensor and contact object. Such force information will be important and indispensable for robots that perform a wide variety of tasks requiring physical interactions with the environment.

One of the biggest challenges in robotics is dexterous grasping. Grasping tasks have been increasingly complex when handling various objects such as soft, fragile, and nonuniform-shaped objects. Tactile sensing plays important roles in grasping tasks to handle such objects, requires precise contact force control. In industrial robot applications, there is a great demand for robots, e.g., robotic arms, which require tactile sensing in order to perform grasping tasks including precise force control.

Another major challenge is to develop social and communication robots working in human environments. These robots are expected to perform tasks, e.g., housework, together with or instead of humans; thus these tasks also require precise force control as humans utilize tactile sensations in their daily activities. In addition, such robots should always be aware of unexpected contact with humans and objects because their working spaces could dynamically change. Several studies have proposed that these robots should be equipped with whole body tactile sensing to monitor contact and to reduce risks associated with unexpected contact between robots and environments.

Communication robots are expected to understand the emotions and intentions of humans as well as behave intelligently like humans. In the above example, tactile sensors are used to actively measure force information, i.e., the sensor approaches for touching an object. In contrast, in the case of communication robots, the sensor is touched by humans to physically interact with each other. Therefore, the sensor should have the capacity to measure various kinds of touch, e.g., grasping, patting, stroking, pinching, etc., for enriching physical interactions between robots and humans. Rich physical interaction between humans and such robots will provide essential information for performing these tasks. In addition, tactile sensors will function as a tactile display, conveying tactile feelings to humans. Therefore, tactile sensors should be developed to consider how humans feel tactile impressions of the sensor as well as what kind of information the sensor can obtain.

According to the above examples, tactile sensing is required in numerous applications in robotics. However, tactile sensor development is still in its early stage; therefore tactile sensing is still missing in the field of robotics. To this end, a significant number of studies have proposed various tactile sensors for measuring rich physical interaction [1–8].

1.1 Tactile sensors for enriching physical interactions

Tactile sensors measure tactile information when touching an environment or touched by an environment. In order to obtain rich tactile information, physical interactions between a robot and the environment should be enriched as a prerequisite. One feasible approach for enriching physical interaction is to develop a tactile sensor covered with a soft material.

The surface material of tactile sensors is an important element because the sensor surface functions as a kind of a spatiotemporal filter against applied force information to the sensor, i.e., the sensor surface itself determines the sensor response. In other words, tactile transducers, which are placed in, under, or outside the sensor surface, cannot measure the applied force information directly. Here, we focus on a tactile sensor with a soft surface covering for enriching tactile interaction, as shown in Fig. 1.1. In the condition where a hard object touches a hard surface, contact information will be obtained from a limited contact area because the contact region will be almost a point. Such point contact reduces the obtained contact information (Fig. 1.1 (a)), and a large reaction force will be applied to the touched object. When a soft object touches a hard surface, the object itself will deform, as shown in Fig. 1.1 (b). As a result, the contact information can be obtained from a broad contact area. However, these reaction forces and the deformation that occurs in contact objects can damage fragile objects. In contrast, employing a soft material as the sensor surface enables the application of a smaller reaction force to the contact object (Fig. 1.1 (c)). When the soft object touches the soft surface, both the object and surface will deform in accordance with their softness ratio, i.e., employing a softer surface allows a fragile object to be touched with smaller reaction force. Consequently, the sensor can even touch a fragile object with a broad contact area to provide increased contact information. In addition, the sensor covered with a soft surface can measure the three-dimensional (3D) deformation of its surface to measure more contact patterns such as a pinching, a twisting, simple tapping, pushing, and stroking.

Soft surfaces provide other advantages in several applications. For instance, grasping can be more stable using the soft surface because the surface can deform to accurately fit the shape of a grasping target. This deformable surface enables us to grasp soft and fragile objects. On the other hans, a hard surface causes stress concentration on the grasping target, making it difficult to grasp soft and fragile objects. In terms of sensor durability, a soft surface can protect a contact target as well as the transducers mounted under the surface because the surface functions as a shock absorber against a large contact force or impact that occurs in intense physical interactions. For instance, personal robots working with humans should have a soft covering to reduce the risk of causing unintentional harm to humans when the robot and human make physical contact with each other. In addition, a soft sensor surface gives a good tactile impression to interacting humans, which can encourage humans to touch the robots. For this purpose, several studies have been reported where the whole body of the robots is covered with soft materials such as rubber, elastomer, and elastic foam [9–12].

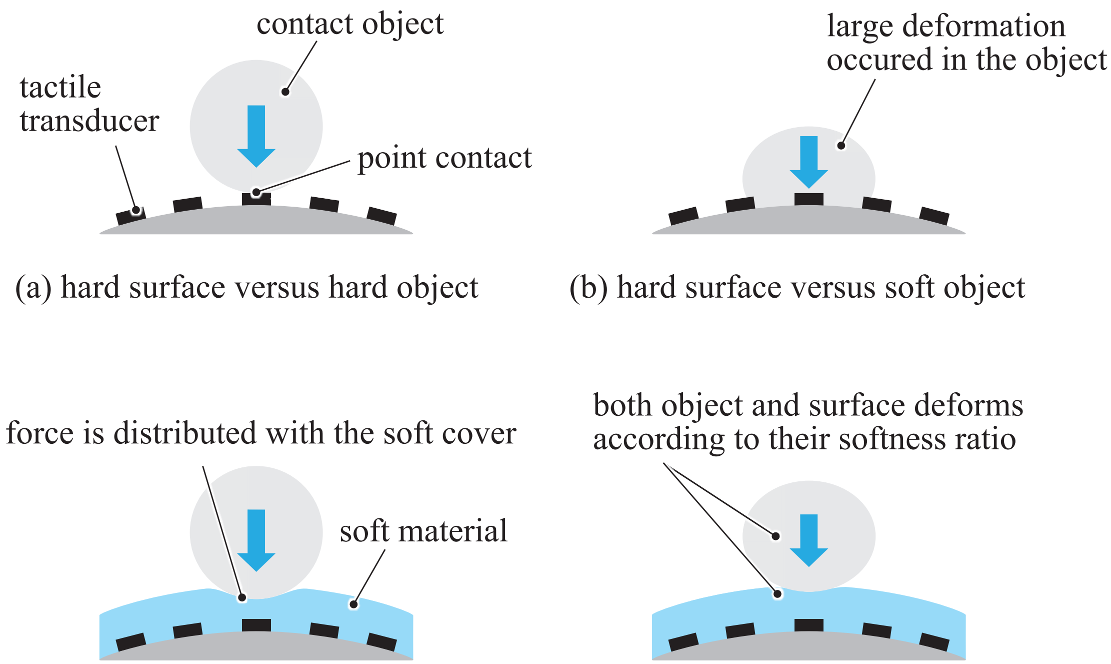

(a) hard surface versus hard object (b) hard surface versus soft object

(c) soft surface versus hard object (d) soft surface versus soft object

Figure 1.1: Function of soft surface of tactile sensors: (a) a hard object touches a hard surface, i.e., the surface of a tactile transducer; (b) a soft object touches a hard surface; (c) a hard object touches a soft surface; and (d) a soft object touches a soft surface. The soft surface reduces the reaction force that occurs in the touched object and enriched the contact information obtained because of the broad contact area.

In conclusion, the surface of a tactile sensor should be covered with a soft surface in order to enrich the physical interaction and provide the above mentioned advantages. However, a soft surface raises several issues in relation to its softness and material characteristics. The next section provides methods for developing a tactile sensor with a soft sensor surface, and considers the issues that result from employing a soft material as the surface.

1.2 Tactile sensorization of highly-deformable material

To develop a tactile sensor covered with a soft surface, the tactile sensorization of a highly-deformable material is one of the feasible approaches. This approach employs a wide variety of transducers to convert tactile information applied to the surface into electrical signals. One example is the employment of force transducers, e.g., a strain or pressure transducer to convert strains or pressures into electrical signals, respectively. These transducers are typically placed inside the soft surface to directly measure the deformation of the material. However, tactile transducers inside the soft surface often suffer from physical damage caused by the applied contact force; sometimes, a large impact can be applied to the transducer and its wiring. Such physical damage makes difficult to develop tactile sensors for practical applications. In addition, solid transducers and their wiring placed inside the soft surface decrease the softness of the sensor surface.

Another approach to sensorize a highly-deformable material is to place the tactile transducer under the sensor surface where contact force is applied. The advantage is the simple structure in which a highly-deformable sheet material (e.g., elastomer sheet or sponge sheet) is simply laminated onto tactile transducers (e.g., pressure transducer). In addition, the sensor surface without any sensing elements allows easy replacement of the damaged surface without reconnection of the elements.

A common issue with the above two approaches is that the soft sensor surface deteriorates the sensor performance. One study that investigated the filtering effect of the surface material of a tactile sensor reported that a soft surface functions as a low-pass filter against the applied contact force [13]. This investigation showed that the soft cover decreased the sensitivity and a spatial and temporal resolution in the measurement of contact force. In addition, several researchers have pointed out that a tactile sensor with an elastic covering has a hysteresis property [14] in its sensor response curve versus applied contact force because of the viscosity of the elastic materials. These effects of the soft surface on the sensor response are also important issues that need to be resolved.

A feasible approach to address the above issues is to place the tactile transducer outside the sensor surface where contact force is applied. This configuration can increase the durability of tactile transducers and their wiring because no contact force reaches the transducers and their fragile electronic elements, e.g., wiring. Employing magnetic technology [15] is one of the promising approaches to place the tactile transducer outside of the sensor surface. Generally, a magnet is placed inside a soft surface material while a magnetic transducer is placed outside the material. The force applied to the sensor surface can be estimated by monitoring the change in magnetic field distributions because the applied force displaces the magnet embedded in the soft sensor surface. However, solid elements inside the elastic materials decrease the durability and softness of the material.

Optical tactile sensors [16] is an approach similar to the one with magnetic tactile sensors described above. In optical tactile sensors, optical markers are placed inside a soft transparent material while a camera is placed outside the material. The force applied to the sensor surface can be estimated by monitoring the displacement of the markers embedded in the soft sensor surface. One of the issues in optical tactile sensors is that it is difficult to fabricate compact and thinner sensors because of their optical system. Another issue is that the temporal performance of the sensor depends on the sampling rate of the camera used, which is generally insufficient to acquire temporally fast contact, e.g., a vibration.

In summary, employing magnetic and optical technologies can provide tactile sensors with high durability of transducers and high maintainability for easy replacement of the sensor surface covered with a soft surface. However, they have several issues, especially with regard to keeping the sensor surface soft and miniaturizing the sensor. This dissertation provides two tactile sensorization approaches for highly-deformable materials to address these issues.

1.3 Research objective

The purpose of this dissertation is to propose a method for the tactile sensorization of highly-deformable materials for enriching physical interaction. This dissertation introduces two approaches in which soft materials function as flexible tactile sensors by employing electromagnetic phenomena. Figure 1.2 summarizes the proposed approaches. Both approaches employ an MRE as the surface of the proposed tactile sensor. An MRE is a functional magnetic elastic material in which particles with high magnetic permeability (e.g., iron particles) are mixed with an elastic material (e.g., silicon rubber). Both approaches utilize electromagnetic phenomena that allow us to sensorize the MRE by measuring the displacement of magnetic particles caused by the contact force applied to the MRE.

In the first approach, the MRE is tactile-sensorized by employing a magnet and magnetic transducer pair. The normal force applied to the MRE causes the displacement of magnetic particles in the MRE, thereby changing the magnetic field distribution generated by the magnet around the magnetic transducer. The MRE itself functions as a flexible tactile sensor because the applied force is measured with the magnetic transducer as a change in magnetic field. To predict and investigate the sensor response, magnetic field simulation is a promising method for tactile sensors employing magnetic field measurements. However, the highly-deformable MRE containing magnetic particles leads to difficulties in simulations of changes in magnetic field because of the complex deformation of the MRE and displacement of magnetic particles. Therefore, this dissertation conducts the following experiments: 1) magnetic field simulation with a simple model of the proposed sensor for reference; and 2) investigation of sensor responses by experiments with the fabricated sensor.

In the second approach, the MRE functions as a flexible tactile sensor by employing an inductor. Here, the MRE sheet and a silicon rubber sheet are simply laminated onto the inductor, e.g., a coil printed with a trace on a circuit board. Since the MRE contains magnetic particles with high magnetic permeability, the distance between the MRE and inductor determines its inductance. Consequently, the MRE itself will function as a flexible tactile sensor because the applied force is measured by monitoring the inductance. As with the first approach, it is difficult to accurately predict the deformation of the MRE and the change in the inductance caused by the displacement of magnetic particles. Therefore, the sensor responses, i.e., the change in inductance caused by the applied contact force, are investigated by experiments with a fabricated sensor. Since this approach employed electromagnetic phenomena for sensing the applied contact force, electromagnetic interference occurred between

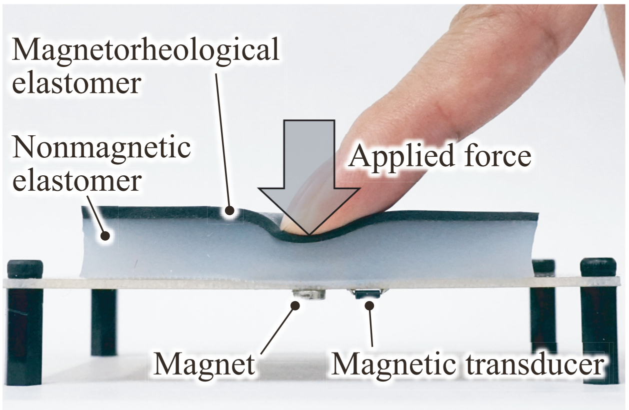

(a)

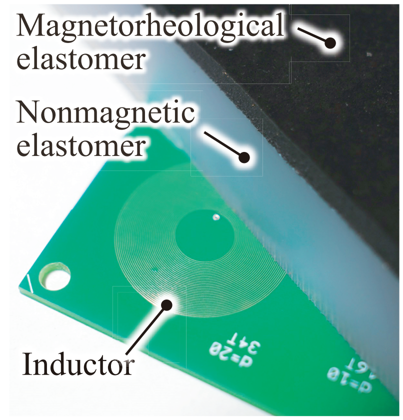

(b)

Figure 1.2: Proposed approaches for tactile sensorization of a soft and flexible magnetorheological elastomer (MRE): (a) a flexible tactile sensor employing a magnet and magnetic transducer; (b) a flexible tactile sensor employing an inductor. In both approaches, the applied contact force can be measured as a deformation of the surface MRE based on electromagnetic techniques.

the sensor and external magnetic material or between the sensors themselves. This interference is also investigated and discussed. In addition, the tri-axis tactile sensorization method is proposed using four inductors and a disk-shaped MRE.

1.4 Outline of the dissertation

This dissertation consists of seven chapters including this one. The contents of each chapter can be summarized as follows:

Chapter 1. Introduction

The purpose of this dissertation is to propose a flexible tactile sensor that can acquire rich tactile information by tactile sensorization of a highly flexible material. First, this chapter discusses the importance of tactile sensing in the field of robotics, and describes the kind of tactile sensor that should be developed for enriching physical interaction according to the structure and surface material. Next, the requirements for tactile sensors for effective tactile sensing are discussed, and two approaches are proposed to meet these requirements.

Chapter 2. Related works

An overview of the state-of-the-art in flexible and soft tactile sensors is provided. Although numerous approaches have been proposed to develop a wide-variety of tactile sensors, this dissertation categorizes them into four types based on their structure, and identifies the open issues to be resolved. Finally, the key ideas of the proposed approach in this dissertation are summarized with comparisons between conventional and the proposed approach.

Chapter 3. Tactile sensorization with a magnet and magnetic transducer

The first approach, which employs a magnet and magnetic transducer pair, is presented. An MRE, which is a highly-deformable silicon rubber containing iron particles, can be tactile-sensorized by employing the magnet and magnetic transducer. This approach enables the development of a tactile sensor covered with a soft sensor surface that contains no fragile transducers and solids. Simulations and experiments with the fabricated sensors show that the proposed approach can measure the applied normal force by monitoring changes in the magnetic field. The spatial response of the proposed sensor is also investigated and discussed in terms of its advantages in tactile information processing.

Chapter 4. Tactile sensorization with an inductor

The second approach, which employs an inductor, is proposed for the tactile sensorization of a highly-deformable MRE. Employing an inductor (instead of the magnet and a magnetic transducer used in the first approach) enables the fabrication of a tactile sensor with a compact and thin transducer. Experiments with the fabricated sensor demonstrate that the proposed approach can measure the applied normal force by monitoring changes in inductance. The influence of inductor size on sensor responses such as a sensitivity, noise-to-signal ratio, and spatial response are also investigated. The proposed sensor measures the applied contact force with changes in inductance. However, an approach for metallic materials can also change the inductance. The experimental results show that the inductance monotonically decreased in accordance with the approach for metallic materials. The occurrence of electromagnetic interference between inductors is also investigated.

Chapter 5. Tri-axis tactile sensorization with four inductors

This chapter introduces an approach for tri-axis tactile sensorization of an MRE based on the sensing mechanism of the second approach described in Chapter 4. By employing four spiral inductors, the 3D displacement of the MRE can be obtained, i.e., the sensor can measure the tri-axis force applied to the sensor surface. Experiments with the fabricated sensor demonstrate that the sensor can estimate the applied tri-axis force by calculating the sum or difference of the changes in inductance from the four inductors.

Chapter 6. Discussions

This chapter summarizes and discusses the results obtained in this dissertation. First, we discuss the difference between the two proposed approaches for tactile sensorization of an MRE. Then, the advantages of the proposed approaches are also discussed in terms of their structure, material, and sensor performance. The open issues of the proposed approaches are also summarized and discussed. Finally, insights for a tactile hardware filter using the proposed approaches are provided.

Chapter 7. Conclusions

Finally, conclusions and future works are provided. The proposed tactile sensorization approaches enable us to fabricate a highly-deformable soft and flexible tactile sensor with high durability, maintainability, and sensitivity. However, they have several issues caused by their sensing mechanism based on electromagnetic phenomena. These issues are discussed as works for the near future.

Chapter 2

Related works

Tactile sensors are still in the early stages of development although there are great expectations for utilization of tactile sensations in the field of robotics. Therefore, research in this field has focused on developing various tactile sensors. This chapter summarizes existing tactile sensors covered with soft materials. These sensors are categorized into four types according to their structures. Finally, the key ideas of the two proposed tactile sensorization approaches are summarized with comparisons between conventional and the proposed approaches.

2.1 Summary of state-of-the-art tactile sensors

Since various types of tactile sensors have been proposed (see the reviews [17–19]), this section summarizes the issues with conventional flexible tactile sensors with a thick flexible contact layer. We first define the three parts of a flexible tactile sensor: flexible covering, frame, and inside of the frame (illustrated in Fig. 2.1(a)). The flexible covering is the outermost part where the contact force is applied. The frame holds the flexible covering and protects the inside of the frame. Tactile transducers are placed either inside or on these three parts as follows.

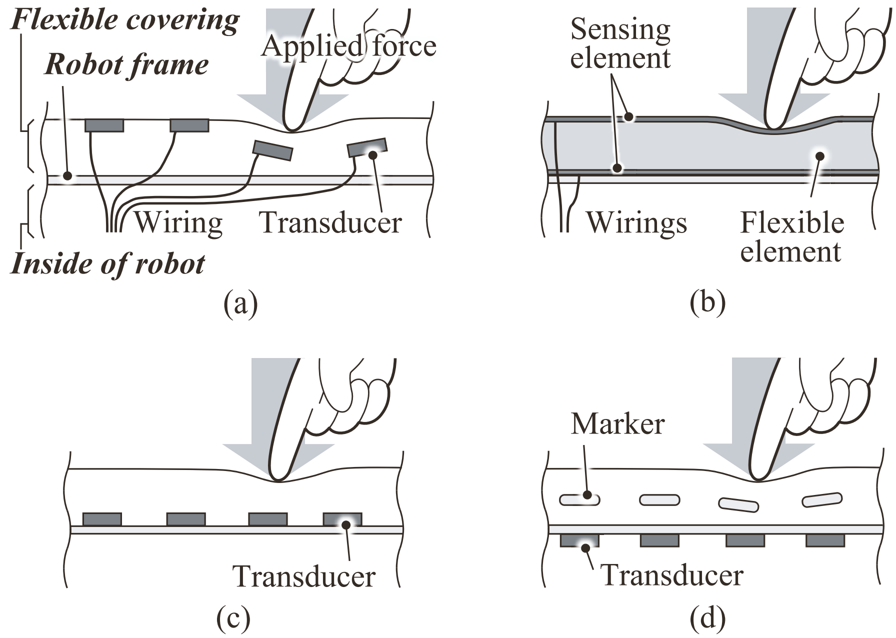

Figure 2.1: Schematics of the structures of conventional flexible tactile sensors holding a thick flexible contact layer: (a) type A—transducers with associated wiring are placed inside a flexible covering; (b) type B—a flexible covering functions as a transducer; (c) type C—transducers are mounted onto the surface of the robot frame; and (d) type D—transducers are placed inside the robot while their markers are embedded into flexible covering.

2.1.1 Type A, Transducers are placed inside a flexible covering

For this type of sensor (Fig. 2.1(a); e.g., [11, 20–34]), the transducers are placed with the associated electrical wiring inside the flexible covering. The transducers inside the covering directly capture the deformation or vibration of the covering.

Hosoda et al. [20, 21] proposed a flexible tactile sensor in which strain gauges and polyvinylidene fluoride (PVDF) films are placed inside the flexible covering at different positions, poses, and depths. These transducers mounted differently in several locations inside the covering can measure different deformation and vibration information. The structure of the sensors imitated the human fingertip, i.e., the sensor consists of a bone, an inner and outer rubber layer (which have different softness), and randomly distributed transducers inside the rubber; they claimed that this structure realized high sensing performance. They demonstrated that this different deformation and vibration information conveys important information on the classification task of touched materials.

However, Goka et al. [15] pointed out that the wiring in the soft and flexible covering might be damaged by large deformation of the covering. Therefore, they developed a magnetic tactile sensor (we classified this sensor here as Type D, as described below). Recent progress in stretchable electronics techniques [35–37] for wiring may resolve this issue.

2.1.2 Type B, The flexible covering functions as a transducer

In this approach, the sensors employed a flexible covering that functioned as a transducer, e.g., using capacitive [14, 31, 38–45] or resistive technology [46–53]. The transducer consists of a flexible functional element inserted between a pair of sensing elements such as a stretchable electrode. These sensors can measure the applied load with high sensitivity since the transducers capture the surface deformation directly.

Capacitive tactile sensor

Maiolino et al. [14] developed a large-scale flexible tactile sensor which employs a capacitive technology for the skin of the humanoid robot iCub. This sensor consists of three parts: an electrode, a conductive sheet, and flexible and soft dielectric material. A capacitor can be made by putting the dielectric material between the electrode and conductive sheet, which functions as the other electrode. The sensor can measure the applied normal force by monitoring the change in capacitance because the applied normal force causes a change in the distance between the electrode and conductive sheet. They successfully applied tactile sensations to the body of the humanoid robot iCub by attaching a large number of electrodes to the body, and then placing an elastic dielectric sheet and a conductive fabric sheet.

Resistive tactile sensor

Shimojo et al. [50] proposed a flexible tactile sensor employing resistive technology. This sensor also consists of three parts: two conductive sheets and a flexible and soft pressure-conductive material. A resistive network can be made by putting the pressure-conductive material between the conductive sheets. They succeeded in estimating the center of contact force on a large sensing area with only four pieces of wiring by measuring the change in current distributions caused by the applied contact force. To fabricate a large-scale tactile sensor, the number of wires is one of the issues. This approach is a feasible solution for reducing the number of wires.

One drawback of these approaches is that the electrical wire connected to the surface sheet requires a wiring connection. A large number of wires, which connect the flexible covering and inside of the robot, might diminish the maintainability.

2.1.3 Type C, Transducers are mounted onto the surface of the robot frame

For these sensors (Fig. 2.1(c); e.g., [10, 54–59]) the transducers are mounted onto the outer surface of the robot frame. Because their flexible covering has no wiring or transducers, there are no problems with wiring disconnection and replacement of the cover is easy.

Minato et al. [54] developed the child humanoid robot CB^2, whose entire body is covered with soft skin, including tactile sensing. They installed a toral of 197 PVDF films under the robot's surface sheet made of soft silicon rubber. Mukai et al. [56] also developed the human-interactive robot "RI-MAN", in which tactile sensors were installed in three parts of the body: the chest and both arms. They employed a pressure transducer mounted on a comb-shaped flexible printed circuit board (PCB) to develop a large-scale tactile sensor system attached to robot surfaces, including complex shapes. Their proposed sensor was attached to the curved surface of the robot's body and covered with an elastic sponge sheet.

Shimojo [13] pointed out that the flexible covering functions as a spatial low-pass filter for a tactile transducer when the sensor elements are installed under the covering. Therefore, the sensitivity and spatial resolution will be diminished by a soft covering such as a compressible sponge sheet.

2.1.4 Type D, Transducers are placed inside the robot with their markers inside the covering

For this type of sensor (Fig. 2.1(d)), the transducers can be removed from the part where the contact force is applied; instead, the transducers are placed inside the robot. The applied loads are estimated by capturing the displacement of the markers embedded inside the covering.

Magnetic tactile sensor

An example of this type of sensor is a magnetic tactile sensor (e.g., [15, 60–71]) employing magnetic technology. In these sensors, magnetic transducers are placed inside the robot, and magnets are placed inside the flexible covering as their magnetic markers. To measure the applied forces, these sensors detect the changes in the magnetic field caused by the displacement of the magnet.

Goka et al. [15] proposed a magnetic tactile sensor using a disk-shaped magnet, four magnetic transducers, and four inductors. As a magnetic transducer, they used a giant magnetoresistance (GMR) sensor which can measure the magnitude of the magnetic field penetrating the sensor body in one-direction. The GMR sensors and inductors were installed at the bottom surface of a PCB in four different orientations while a cylindrical elastic silicon rubber containing the magnet was placed on the circuit board. In this configuretion, the applied tri-axis force caused the 3D displacement of the magnet and a 3D change in the magnetic field distribution around the GMR sensors. As a result, the sensor can estimate the applied tri-axis force using the combined outputs of the four GMR sensors. In addition, the inductors can generate an induced electromotive force depending on the change in the magnetic field. Because faster change in the magnetic field generates larger induced electromotive force, the inductors can respond to fast displacement of the magnet, e.g., caused by slip between the surface elastic rubber and contact target. Therefore, the sensor can measure slip information as well as the applied tri-axis force.

Tomo et al. [64, 72] proposed a similar magnetic tactile sensor using a small magnet and a 3D GMR sensor which could measure the 3D change in magnetic field distribution. Their sensor required a magnet and only one 3D GMR sensor. They also succeeded in fabricating a miniaturized 16-sensor array to install at the tip of the robotic finger. The development of a miniaturized magnetic tactile sensor array is a biggest challenge because such a sensor array requires several magnet, and their magnetic fields generated will cause interference between the magnets. They proposed an air gap structure in the silicon rubber containing several magnets to avoid or reduce the effect of interference between the magnets.

One remaining issue with this approach is that replacing the covering containing the magnets requires precise positioning with the corresponding magnetic transducers because their positional relationship determines the response. In addition, the sensor requires the installation of a hard marker (in this case, a permanent magnet) in the soft covering, which will decrease the softness of the covering.

Vision-based tactile sensor

A similar configuration can be implemented by using an image sensor with markers [73–84]. This type of sensor can also separate the transducers from the flexible covering.

One example of this approach is the Finger Vision proposed by Yamaguchi et al. [80]. A USB camera was employed to measure the displacement of the markers installed in transparent soft silicon rubber. This approach enabled the measurement of force flow distribution on a large sensing area using only one camera. They installed this sensor to the tip of a robot hand, which succeeded ino grasping a knife for cutting an apple dexterously.

Simonomura et al. [83, 84] proposed an interesting approach to develop a flexible tactile sensor with extremely high temporal resolution. They employed a bio-inspired event-driven camera for measuring the displacement of the markers embedded in transparent silicon rubber. The event-driven camera could potentially measure the displacement of the markers in microseconds. This fast measurement offers a novel approach to address tactile information.

Because these sensors require an optical system, their structure will be difficult to miniaturize and make thinner.

Inductive tactile sensor

Wang et al. [85] proposed a flexible tri-axis tactile sensor in which a square-shaped aluminum film attached to soft silicon rubber was placed on four inductors printed on flexible circuit boards. In this configuration, an eddy current was generated inside the film when the film approached the inductor. As a result, the inductance decreased because the eddy current generated a magnetic flux that weakened the original magnetic flux produced by the inductor. Therefore, the applied tri-axis force can be estimated from the four inductance changes caused by the displacement of the film. In other words, the film functions as a magnetic displacement marker which can be captured as inductance changes. The advantage of this kind of sensor is its simple structure. On the other hand, the drawback is that its surface is not stretchable and soft because the sensing mechanism requires the use of highly conductive material.

2.1.5 Summary

In summary, flexible tactile sensors have several problems such as fracture of the sensing elements by large amount of deformation, decreased sensitivity caused by soft covering, and poor maintainability. Our proposed flexible tactile sensor can provide a solution to these problems.

2.2 Key ideas of the proposed sensor

The proposed approaches enable the sensorization of an MRE as a flexible tactile sensor. The key idea is that the sensor can measure the applied force as the displacement of magnetic particles in the MRE based on the electromagnetic phenomenon. As shown in Fig 2.2, the distribution of magnetic permeability around the contact areas changes with the displacement of magnetic particles in the MRE sheet. This dissertation provides a method to convert this distribution change in magnetic permeability into contact force information applied to the surface of the MRE sheet.

The first approach described in Chapter 3 converts the distribution change in magnetic permeability into the change in magnetic field by using a permanent magnet. This is because the magnitude of the magnetic field can be measured easily

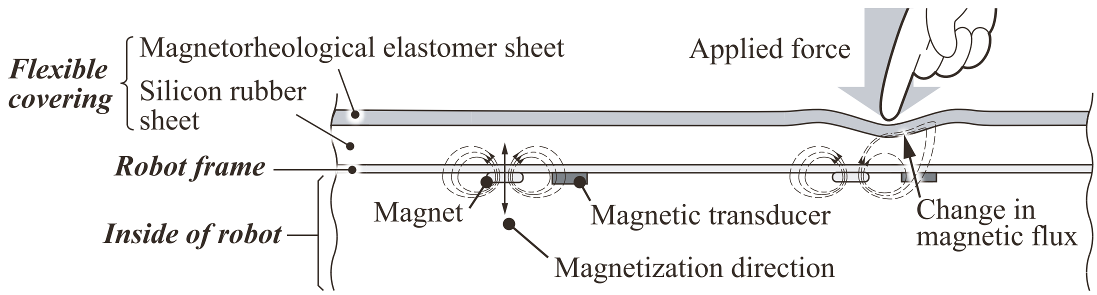

(a) tactile sensorization approach by employing a magnet and a magnetic transducer

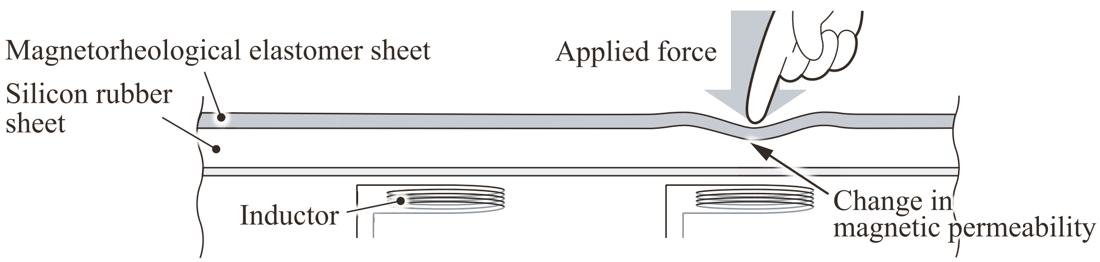

(b) tactile sensorization approach by employing an inductor

Figure 2.2: Schematics of the structures of the proposed sensors: (a) tactile sensorization approach employing a magnet and magnetic transducer pair; (b) tactile sensorization approach employing an inductor.

with a conventional magnetic transducer as this dissertation employed a giant magnetoresistance sensor. Next, the magnetic transducer converts the magnitude of the magnetic field penetrating its body into voltage. Consequently, we can obtain the applied contact force as a voltage value.

In contrast, the second approach described in Chapters 4 and 5 is simpler than the first one. The approach converts the distribution change in magnetic permeability into the change in inductance by using an inductor. In this sense, the inductor functions as a magnetic permeability transducer. Thus, the applied contact force can be obtained as an inductance value.

Both approaches measure the applied contact force as the change in magnetic field or magnetic permeability that occurs around the contact region. These sensing mechanisms enable the measurement of the applied force without the installation of fragile and solid sensing elements, such as a transducer and electrical wiring, inside the soft sensor surface. Further, this sensor structure increases the sensitivity because the sensor can measure the outermost surface deformation by placing the MRE on the sensor surface. Therefore, the proposed tactile sensorization approaches can address the issues with conventional flexible tactile sensors described above.

Chapter 3

Tactile sensorization with a magnet and a magnetic transducer

This chapter describes an approach of a tactile sensorization of a magnetorheological elastomer by employing a pair of a magnet and a magnetic transducer. In this approach, normal force applied to the surface of the magnetorheological elastomer can be measured as a change in magnetic field. This chapter first introduces the method of the tactile sensorization, and an overview of the proposed sensor. Next, magnetic field simulations are provided to analyze the change in magnetic field versus applied normal force. Then, experiments with a fabricated sensor demonstrate that the simulation and real experiment results are well matched, and that the proposed sensor can measure applied normal force by monitoring the change in magnetic field. In addition, we investigated the sensitivity of the sensor, which was found to be high (approximately 161 mV/N with a signal-to-noise ratio of 42.2 dB); however, the sensor has a speed-dependent hysteresis in its sensor response curve. We also investigated the spatial response and observed the following results: (1) the sensor response was a distorted Mexican-hat-like bipolar shape, namely a negative response area was observed around the positive response area; (2) the negative response area disappeared when we used a compressible sponge sheet instead of the incompressible nonmagnetic elastomer. We concluded that the characteristic negative response in the Mexican-hat-like response is derived from the incompressibility of the nonmagnetic elastomer. Finally, discussions and summaries are provided.

3.1 Background

The sense of touch provides essential information for robots working in an unknown environment, handling unknown objects and interacting with humans. A number of researchers has been proposing various types of flexible tactile sensors with safe, flexible and protective coverings intended to provide tactile sensations for robots, e.g., [14, 18, 54]. However, various technical issues remain, such as a large amount of deformation that causes the sensing elements to fracture, deterioration in the sensitivity caused by the thick and soft coverings and a poor maintainability.

To address the above issues in conventional flexible sensors, we proposed a tactile sensorization method of a magnetorheological elastomer, shown in a minimal configuration in Figure 3.1. The proposed sensor has four advantages: (1) the flexible covering contains no solid parts, sensing elements or wiring; (2) the sensor has high sensitivity and extremely low rigidity with respect to the surface deformation of its flexible covering; (3) the electronic and fragile elements in the sensor are completely separated from the parts to which the contact forces are applied; and (4) the flexible covering can be replaced when it becomes damaged and requires no precise positioning.

The tactile sensor obtained with the sensorization method can measure applied normal force by monitoring the change in magnetic field generated by a magnet with a magnetic transducer. However, the complex deformation of the elastomer makes it difficult to predict the sensor response. From the sensor structure, it is expected that the sensor performance can be modified by the following parameters: (1) the thickness of the BE (a thicker BE results in a larger measurement range, while the sensitivity becomes lower); (2) the thickness of the MRE (a thicker MRE results in a higher sensitivity). In addition, the sensor response curve could be changed by the contact speed because a higher contact speed causes the change in deformation behavior of the elastomer. Therefore, the sensor response should be investigated with higher contact speeds, which may be present in a real task. The spatial response of the sensor should be also investigated to determine an appropriate spatial layout for the proposed sensors for large-area implementation. This is because the complex deformation of the elastomer and the complex behavior of the change in magnetic

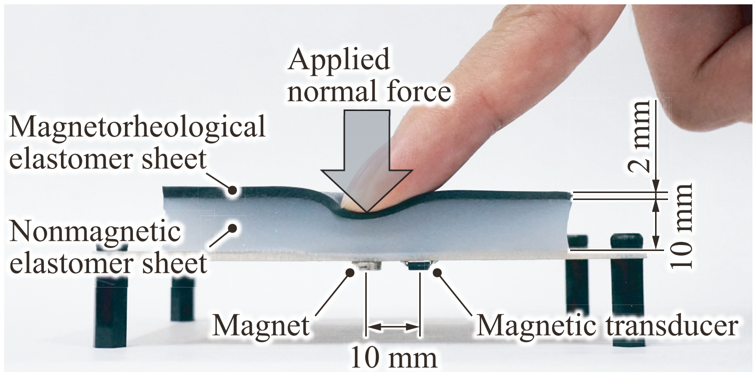

Figure 3.1: Basic structure of the proposed flexible tactile sensor, which can detect an applied normal force and vertical deformation.

field make it difficult to predict the spatial response of the sensor.

In order to investigate these sensor characteristics, we simulated the sensor response with a simple sensor model and compared the results between the simulation and real experiment with a fabricated sensor. We also measured the sensor responses with different contact speeds and the spatial responses with another fabricated sensor. The results can be summarized as follows:

1. the sensor can measure applied normal force and vertical deformation by monitoring the change in magnetic field.

2. the sensitivity and measurement range of the sensor can be modified by the thickness of the elastomer sheets.

3. the sensitivity of the sensor was found to be high (approximately 161 mV/N with a signal-to-noise ratio of 42.2 dB) among flexible tactile sensors with a thick and soft covering.

4. a higher contact speed causes the response to remain after applying a load, and this remaining response was larger at a higher speed.

5. the sensor has a distorted Mexican-hat-like bipolar spatial response, and this bipolar spatial response can be practically fit with an elliptical difference-of-Gaussians function whose major axis corresponds to the line connecting the centers of the magnet and magnetic transducer.

6. the sensor basically has an elliptical Gaussian-like unipolar spatial response versus the applied load; however, the incompressibility of the employed dual-layer elastomer adds a negative response to this unipolar response, and the entire spatial response exhibits a Mexican-hat-like bipolar spatial response.

The remainder of this chapter is organized as follows. The proposed tactile sensorization method and a tactile sensor are introduced in Section 3.2. Section 3.3 provides the methods and results of the simulations and experiments. These results and the fitting function of the proposed sensor are then discussed in Section 3.4. Finally, the summary is presented in Section 3.5.

3.2 Proposed sensor

This section provides an explanation of tactile sensorization method of a magnetorheological elastomer using a magnet and magnetic transducer pair.

3.2.1 Structure and Sensing Mechanism

Figure 3.2 illustrates the structure and sensing mechanism of the proposed sensor obtained with the sensorization method. The sensor is composed of a flexible dual-layer elastomer, a robot frame holding a permanent magnet and a magnetic transducer, which responds to the amount of magnetic flux penetrating its body. As described in Figure 3.2, left, the magnetization of the magnet is in a direction perpendicular to the dual-layer elastomer. The lower layer of the elastomer is a nonmagnetic base elastomer (BE) sheet, whereas the upper one is a magnetorheological elastomer (MRE) sheet, which contains particles with a high magnetic permeability, such as iron particles.

In the absence of a contact force, a certain amount of magnetic flux generated by the magnet penetrates the elastomer and magnetic transducer, as shown in Figure 3.2, left. The force applied to the elastomer surface deforms the top MRE sheet and causes a decrease in the distance between the MRE and the transducer. This distance determines the amount of magnetic flux penetrating the transducer because the magnetic permeability around the transducer is increased by approaching the

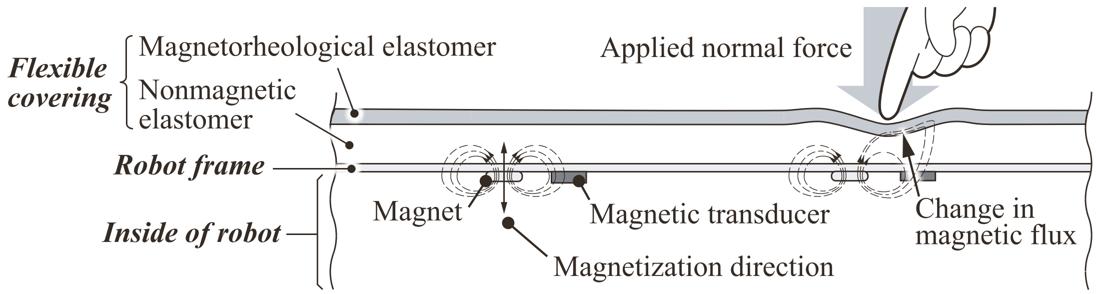

Figure 3.2: Schematic of the structure and sensing mechanism of the proposed sensor. A flexible dual-layer elastomer, which is composed of magnetorheological and non-magnetic elastomers, is placed on the robot frame. A magnet and magnetic transducer are mounted inside the robot. The magnetic transducer detects the deformation of the surface of the dual-layer elastomer as the change in magnetic flux distribution generated by the magnet.

MRE (Figure 3.2, right). As a consequence, the applied force can be estimated by the amount of magnetic flux penetrating the transducer.

3.2.2 Fabricated Sensor

The appearance and an overview of the proposed sensor are shown in Figure 3.3a,b. The dual-layer elastomer is 50 mm long, 50 mm wide and 12 mm thick in which a 2 mm-thick MRE sheet is laminated onto a 10 mm-thick BE sheet. Both elastomer sheets are made of a low-rigidity platinum-cured elastomer (Smooth-on Inc., Macungie, PA, USA, Dragon Skin FX Pro), which is compounded with a plasticizer (Smooth-on Inc., Macungie, PA, USA, Dragon Skin Thinner) with a mass ratio of 200%. We here employed carbonyl iron particles (BASF Corp., Ludwigshafen, Germany, hard grade HQ type) with a particle diameter of 2 µm at a volume ratio of 30%. To make the MRE sheet, we mixed iron particles in the platinum-cured elastomer before curing and poured it into a rectangular female mold until curing.

A disk-shaped neodymium magnet, whose magnetization direction is its axial direction, is mounted at the center of the underside of a printed circuit board (PCB). The diameter and thickness of the magnet are 5 and 1.5 mm, respectively, and its surface magnetic flux density is 0.2 T. As a magnetic transducer, we employ a giant magnetoresistance (GMR) sensor (NVE Corp., Eden Prairie, MN, USA, AA003-02E),

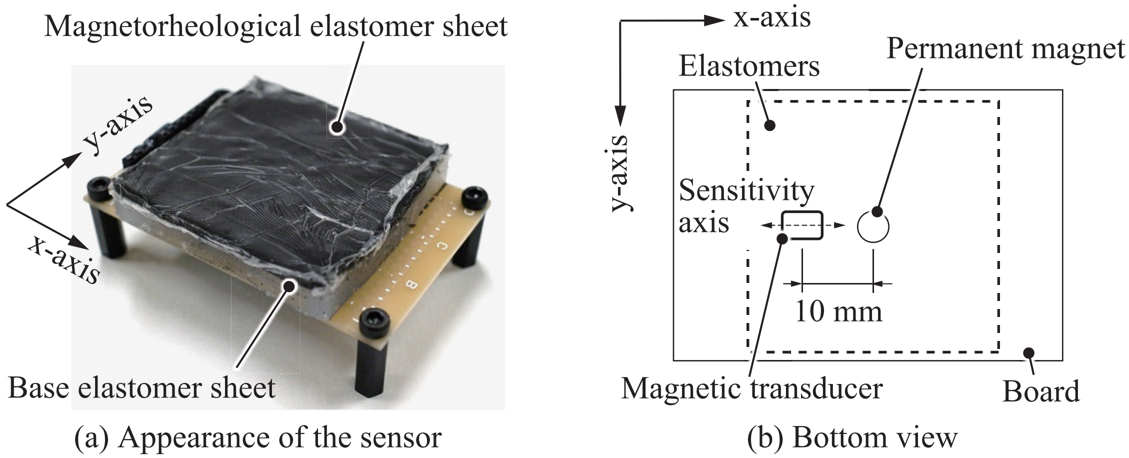

Figure 3.3: Overview of the fabricated tactile sensor. (a) Appearance of the sensor. A black magnetorheological elastomer was laminated onto a white translucent base elastomer, and the top surface was covered by a thin protective plastic film. (b) Appearance of the sensor when viewed from the bottom. A magnet is mounted at the center of a printed circuit board, and a GMR sensor is placed 10 mm away from the magnet.

which offers a high sensitivity to the slight change in magnetic field. The output of the GMR sensor is determined by the amount of the magnetic flux penetrating its body with a sensitivity of 0.1 V/mT (at a supply voltage of 5 V). The GMR sensor is mounted 10 mm from the magnet on the underside of the PCB, as the direction of its sensitivity axis is toward the magnet, i.e., the dashed arrow on the right side of Figure 3.3 (b).

3.3 Simulations and experiments

In this section, we investigated the sensor response versus applied contact force. First, the magnetic flux density around the proposed sensor was calculated with a magnetic field simulator. Next, the actual sensor responses were investigated with the fabricated proposed sensor.

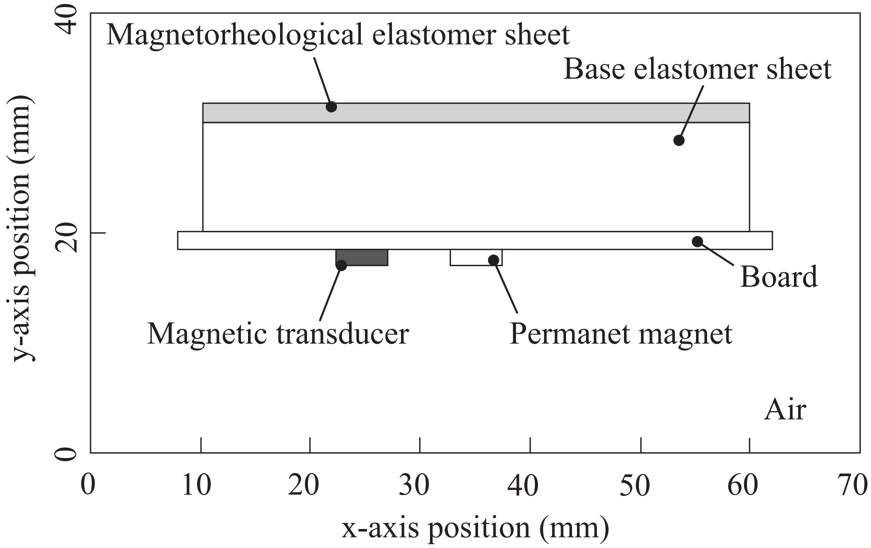

Figure 3.4: Simulation model of the proposed sensor used in the magnetic field simulation. The model consists of a magnetorheological elastomer sheet, a base elastomer sheet, a board, a magnetic transducer, a permanent magnet, and the air. The geometric and material parameters for each element are summarized in Table 3.3.1.

3.3.1 Magnetic field simulation

We investigated the sensor responses with a magnetic field simulator (SATE, Advanced Science Laboratory, Inc., Japan). Figure 3.4 shows a simple structure model for magnetic field simulation. The model consists of a base elastomer (BE) sheet, a magnetorheological elastomer (MRE) sheet, a printed circuit board (PCB), a permanent magnet (PM), a magnetic transducer, and the air. We set the geometric and material parameters of these elements as described in Table 3.3.1. To simplify the simulation, we considered that the magnetic permeability of the MRE sheet is uniform in the entire its body. The magnetic permeability of the MRE sheet was set to 2 according to a study [86].

The magnetic field with this model was calculated in the several conditions in which applying vertical deformations were applied to the surface of the MRE with an indenter with a diameter of 20 mm. In the simulation, the applied vertical deformations were changed from 0 mm to 8 mm with an interval of 0.5 mm. Figure 3.5 demonstrates the simulation results of calculated magnetic flux density. In the figure, the horizontal and vertical axes represent the applied vertical deformation and the

Table 3.1: Parameters of each element. BE and MRE stand for base elastomer and magnetorheological elastomer, respectively.

	Size (mm) WxH	Relative magnetic permeability μ_r	Surface magnetic flux density (T)
Air	other region	1	
BE	50x10	1	
MRE	50x2	2	
Circuit board	54x1.6	1	
Magnetic transducer	5x1.5	1	
Permanent magnet	5x1.5		0.2

calculated magnetic flux density at $x = 25$, $y = 17.5$ (the center position of the magnetic transducer) along the sensitivity axis of the magnetic transducer. The magnetic flux density was subtracted from the value with a vertical deformation of 0 mm, i.e., no load condition, because the proposed sensor measures changes in magnetic flux density from the density under no load. The result shows that the magnetic flux density monotonically and quadratically increased with the applied vertical deformation. We employed a quadratic function $ax^2 + bx + c$ for fitting the calculated magnetic flux density. A least-squares method was applied to obtain these constant values a, b, and c; these values were estimated as follows by using the results presented in Fig. 3.5: $a = 2.0 \times 10^{-6}$, $b = 3.0 \times 10^{-6}$, and $c = 8.2 \times 10^{-7}$.

3.3.2 Experiments with the fabricated sensor

Next, we conducted real experiments with the fabricated sensor. Figure 3.6 shows the experimental setup for investigating the sensor response curve. The proposed sensor was mounted to a z-axis stage (FGS-50E-H, Nidec Corp., Japan) holding a digital force gauge (FGP-5, Nidec Corp., Japan) with a measurement force resolution of 0.01 N and a temporal resolution of 1 ms. The tip of the force gauge was equipped with a plastic cylindrical indenter with a diameter of 20 mm.

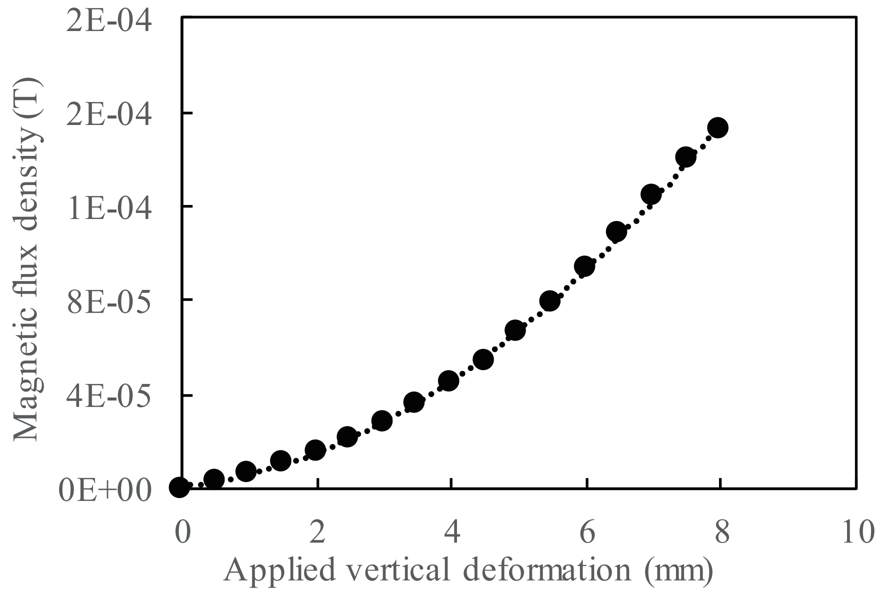

Figure 3.5: Simulation result of magnetic flux density penetrating the magnetic sensor against applied depth with the second order fitted curve.

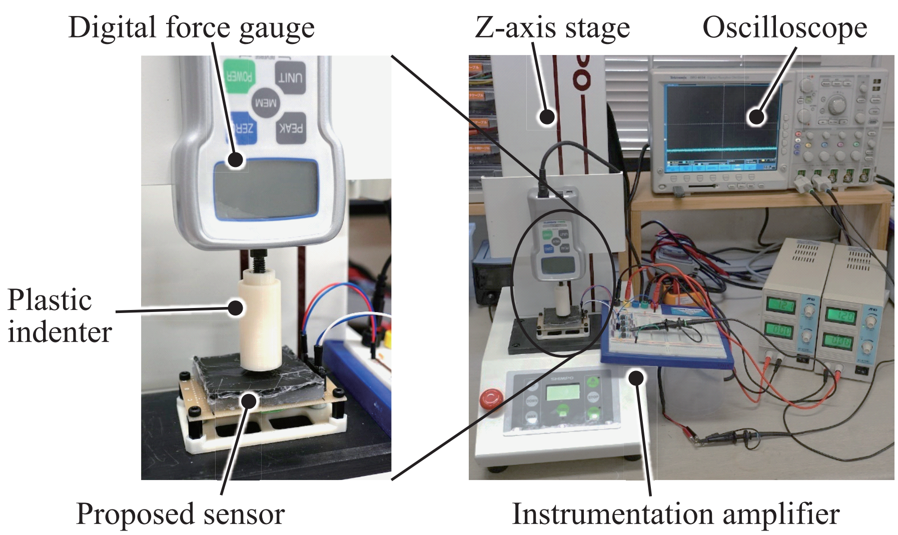

Figure 3.6: Experimental setup for investigating the sensor response. The sensor was mounted on a z-axis stage holding a digital force gauge with a plastic cylindrical indenter with a diameter of 20 mm. The output voltage of the sensor was amplified by an amplification circuit and was then measured with an oscilloscope.

The output of the magnetic sensor was measured with an oscilloscope (DPO 4034, Tektronix, USA) via a differential amplifier with a amplification ratio of 100. The output of the force gauge was also measured with the oscilloscope simultaneously. The sampling period was set to 1 ms.

First, we investigated the sensor responses versus applied normal force and vertical deformations as we already investigated by the simulation described above. The sensor responses were investigated with the following procedure:

1. lower the indenter at a speed of 70 mm/min until the surface of the sensor descends to a depth of 8 mm, which corresponds to the same vertical deformation employed in the simulation experiments described above.

2. wait for 3 s.

3. raise the indenter to its initial position at the same speed.

Figure 3.7 shows the relationship between the sensor response and the applied normal force. The solid lines indicate the moving averages of the sensor outputs with an interval of 10 ms. Each arrow represents the direction of applied normal force. The result demonstrates that the sensor output monotonically increased/decreased with applied normal force, and that the sensor output shows a hysteresis curve.

Figure 3.8 shows the relationship between the sensor response and the applied vertical deformation. The solid lines indicate the moving averages of the sensor outputs with an interval of 10 ms. Each arrow represents the direction of applied vertical deformation. The result demonstrates that the sensor output monotonically increased/decreased with applied vertical deformation, and that the amount of hysteresis was smaller than the result shown in Fig. 3.7.

Next, we compared the results between the simulation and actual experiments. The white diamond plots in Fig. 3.8 represent the simulation result (relative magnetic permeability of the MRE sheet was set to 2) appeared in Fig. 3.5. The simulation results were converted from the magnetic flux density to the voltage with a conversion coefficient of the magnetic sensor (2.6 mV/T). In contrast, the white square plots also represent the simulation result while the relative magnetic permeability of the MRE

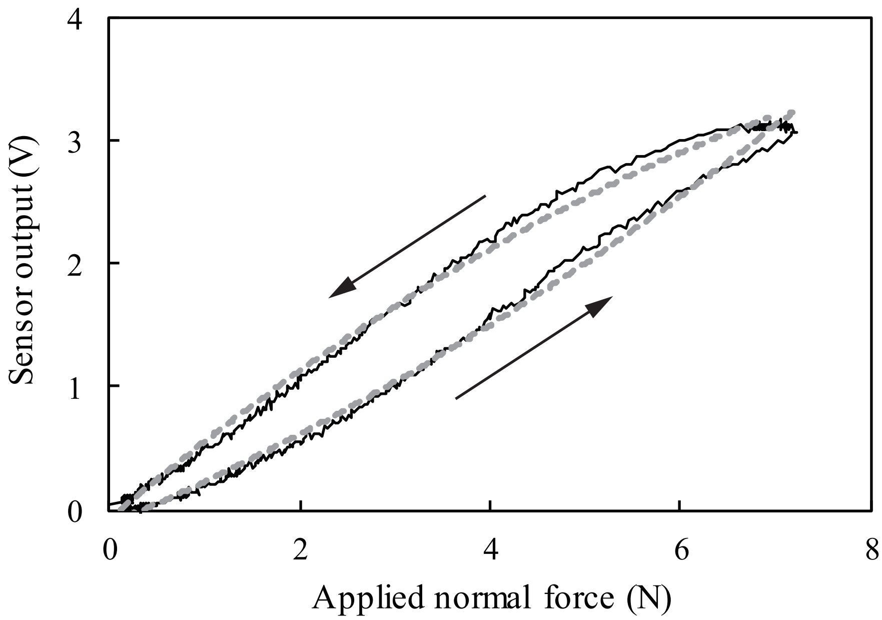

Figure 3.7: The sensor output voltage versus the applied normal force. The solid lines indicate the moving averages of the sensor outputs with an interval of 10 ms. Each arrow represents the direction of applied vertical deformation.

was set to 1.5. The actual sensor response were well matched with the simulation result employing the relative magnetic permeability of 1.5.

3.3.3 Thickness dependency in the sensor responses

The proposed sensor measures applied contact force by detecting an approach of the MRE sheet. Therefore, the sensitivity and measurement range of the sensor will depend on the thickness of both the MRE sheet and BE sheet. We investigated that how the thickness of these two sheets affects its sensor response. Table 3.3.3 summarizes the thicknesses of the three prepared elastomers. Note that the type A elastomer is the same one used in the previous experiment. We employed the same experimental procedure described above while the maximum vertical deformations were set to 8, 2, and 4 mm for the type A, B, and C, respectively.

With the three sensors, Figs. 3.9 and 3.10 show the sensor response curves versus the applied normal force and vertical deformation, respectively. The white square, triangle, and circle plots in Fig. 3.10 are the simulated values with type A, B, and C

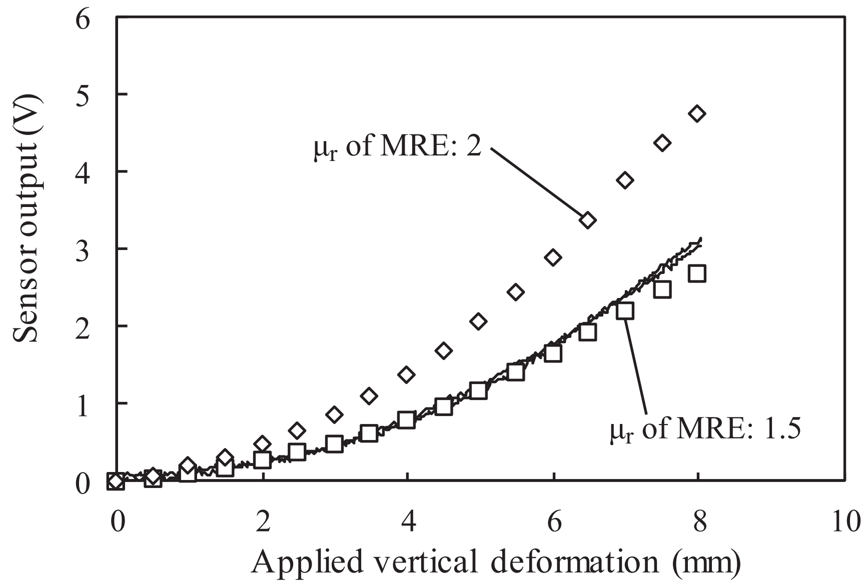

Figure 3.8: The sensor output voltage versus the applied vertical deformation. The solid lines indicate the moving averages of the sensor outputs with an interval of 10 ms. The sensor output quadratically increased with the applied vertical deformation. White diamond and square plots represent simulated value calculated by different relative permeability μ_r of MRE: 2 and 1.5, respectively.

Table 3.2: Thickness differences of each elastomer sheet between three types of sensors. Type A is the same elastomer with the one used in the first experiment.

	Thickness of base elastomer sheet	Thickness of magnetorheological elastomer sheet
Type A	10 mm	2 mm
Type B	5 mm	2 mm
Type C	5 mm	4 mm

elastomers, respectively. Here, the magnetic permeability of the MRE sheet was set to 1.5 which shows a good match between the simulated and measure sensor outputs as shows in Fig. 3.8. Other simulation parameters were the same ones used in the section 3.3.1.

First, we compared the results of the type B and type C sensors. Figure 3.9 demonstrates that the sensor response with the type C was larger than the one with

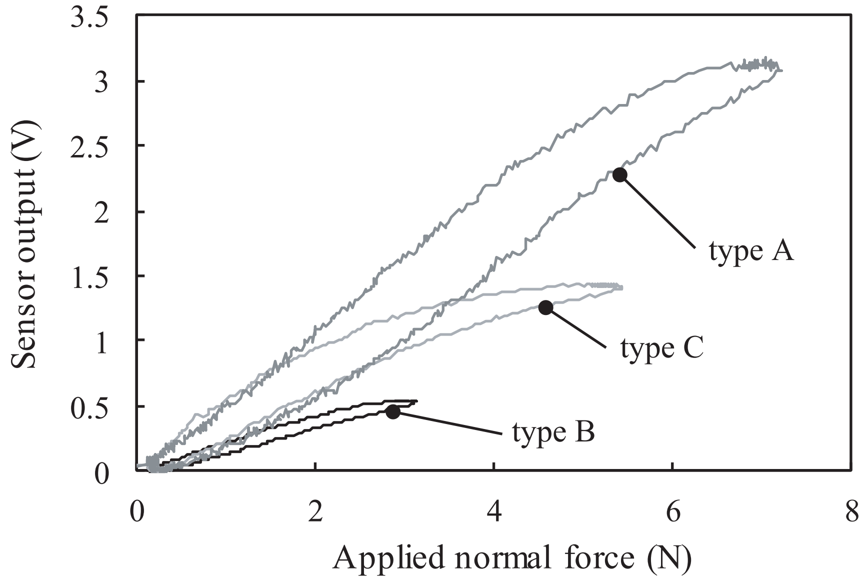

Figure 3.9: Comparison of sensor output changes against the applied normal force among the three types of the sensors.

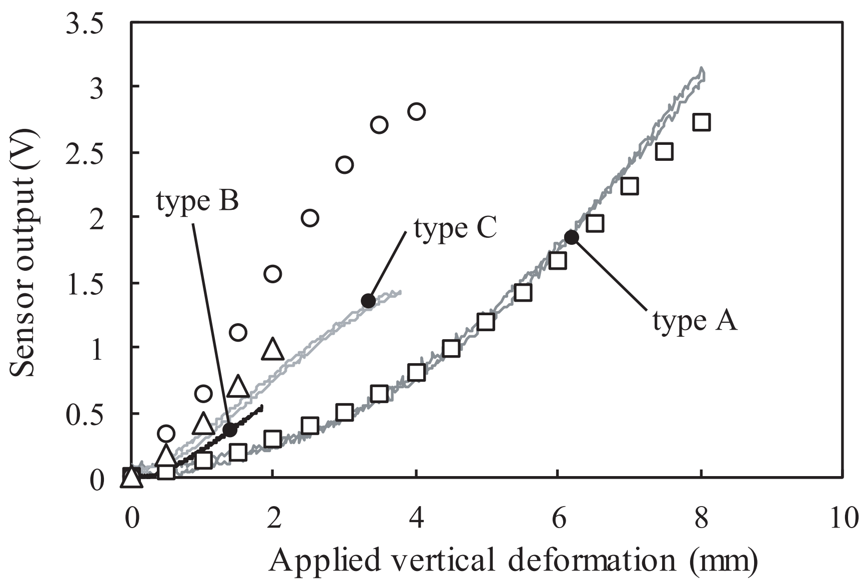

Figure 3.10: Comparison of sensor output changes against the applied vertical deformation among the three types of the sensors. White squares, triangles, and circles indicate simulated value of type A, type B, and type C sensor, respectively.

the type B even under the same applied normal force (approximately 1.9 times when 3 N was applied). Figure 3.10 also demonstrates that the sensor response with the type C was larger than the one with the type B. The slope of the response in the initial stage of applying vertical deformation (the section with the vertical deformation of 0.5 to 1.5 mm) increased by approximately 1.2 times. Therefore, the thicker MRE sheet provides the higher sensitivity in the sensor response. The simulation results of the type B and C also indicate the sensitivity change among these two sensors. However, the simulation result of type C did not match with the measured result. As shown in Figs 3.9 and 3.10, the sensor with the type A elastomer could measure the applied normal force and vertical deformation with the wider measurement range compared to the sensor with the type B elastomer. In contrast, the sensor outputs of the type A sensor was small in the initial stage of applying force. The slope of the response in the initial stage decreased by approximately 0.37 times compared to the type B sensor. Consequently, we confirmed that the sensor performance such as sensitivity and measurement range, can be modified with the thickness of the BE and the MRE sheets.

3.3.4 Contact Speed dependency in the sensor response

Next, we investigated contact speed dependency in the sensor responses. To investigate this, we employed another fabricated another sensor and experimental setup which provides an accurate controlling position and velocity of the indenter.

The appearance of the another fabricated sensor is shown in Fig. 3.11. The dual-layer elastomer is 150 mm long, 150 mm wide and 12 mm thick in which a 2 mm-thick MRE sheet is laminated onto a 10 mm-thick BE sheet. We employed the same elastomer and iron particles descried in the previous section. Here, we set the volume ratio of iron particles in the MRE sheet was 20%.

The magnet and the GMR sensor were also the same ones used in the previous fabricated sensor. The magnet is mounted at the center of the underside of a printed circuit board (PCB) while the GMR sensor is mounted 10 mm from the magnet on the underside of the PCB, as the direction of its sensitivity axis is toward the magnet, i.e., the dashed line on the right side of Figure 3.11 (b). In this study, we mounted

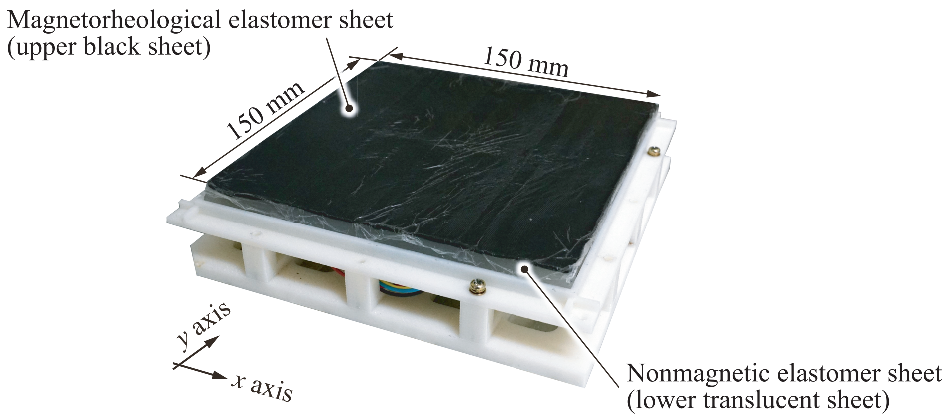

(a)

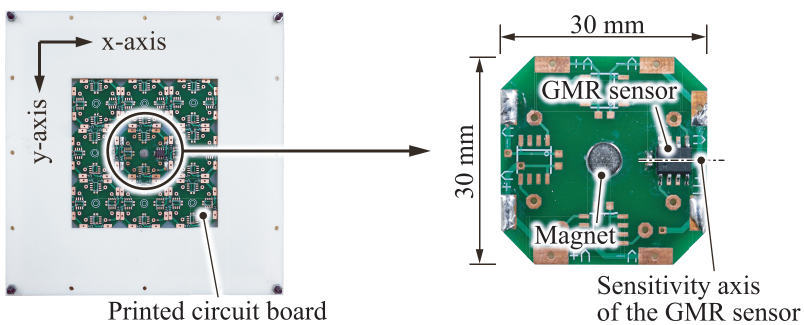

(b)

Figure 3.11: Overview of the fabricated tactile sensor. (a) Appearance of the sensor. A black magnetorheological elastomer was laminated onto a white translucent base elastomer, and the top surface was covered by a thin protective plastic film. (b) Appearance of the sensor when viewed from the bottom. A magnet is mounted at the center of a printed circuit board, and a GMR sensor is placed 10 mm away from the magnet.

only one magnet and one GMR sensor (Figure 3.11 (b), right), even though the PCB could hold many magnets and GMR sensors (planned for future work with a large sensing area).

Figure 3.12 shows the experimental setup which provides an accurate controlling position and velocity of the indenter. The proposed sensor was mounted to a three-axis robot stage (IAI Corp., Shizuoka, Japan, TTA-C3-WA-30-25-10) holding a digital force gauge (Nidec Corp., Kyoto, Japan, FGP-5) with a measurement force resolution of 0.01 N and a temporal resolution of 1 ms. The tip of the force gauge was equipped

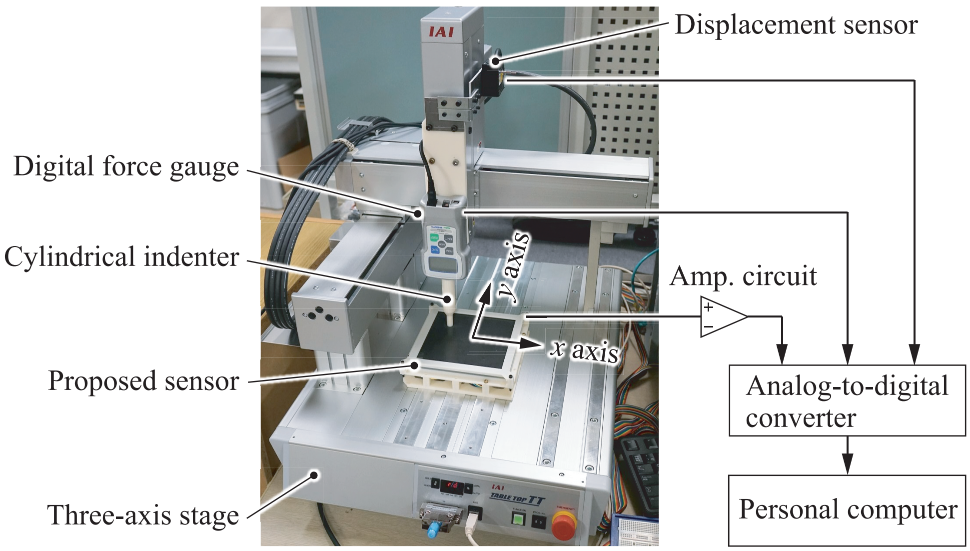

Figure 3.12: Experimental setup for investigating the sensor response. The sensor was mounted on a three-axis stage holding a digital force gauge with a plastic cylindrical indenter with a diameter of 10 mm. The output voltage of the sensor was amplified by an amplification circuit and was then sent to a personal computer via an analog-to-digital converter.

with a plastic cylindrical indenter with a diameter of 10 mm. To measure the vertical displacements precisely, the stage was also equipped with a laser displacement sensor (Omron Corp., Kyoto, Japan, ZX0-LD100A61) with a resolution of 0.08 mm. The output voltage of the GMR sensor was amplified by an amplification circuit with a gain of 200. A personal computer captured the outputs of the amplified sensor, force gauge and displacement sensor via an analog-to-digital converter (CONTEC Corp., Osaka, Japan, ADI12-8GY with CPU-CA20GY) with a sampling rate of 200 Hz.

To investigate how the contact speed affects the sensor response, we measured the response with three different contact speeds $V = 0.1$, 1 and 10 mm/s (10 mm/s is the maximum measurable speed in this setup). The contact point, which corresponds to the center of the indenter, was determined as the position right above the GMR sensor. The sensor responses were investigated with the following procedure:

1. lower the indenter at a speed of V until the surface of the sensor descends to a depth of 6 mm, which corresponds to half of the thickness of the dual-layer elastomer.

2. wait for 10 .

3. raise the indenter to its initial position at a speed of V.

4. wait for 10 s.

5. repeat the above steps 20times.

For a reference, Fig 3.13 shows the sensor responses versus the applied normal force and indenter depth (i.e., vertical deformation) with a contact speed V of 0.1 mm/s, respectively. In both plots, the solid lines and shaded regions indicate the mean value and twice the standard deviation (2σ) of the sensor outputs across 20 trials, respectively. The arrows indicate the directions of the applied load. Each sensor output monotonically increased with the applied normal force and indenter depth. The results in Figure 3.13 (b) indicate that the sensor response increased quadratically with the indenter depth. Although both curves exhibited hysteresis properties, the effect of the hysteresis was larger for the curve of the sensor response versus the normal force. We calculated the sensitivity S (mV/N) during the descending period (dashed line in Figure 3.13 (a)). The estimated sensitivity was S = 161 mV/N or 12.7 mV/kPa (here, we used a cylindrical indenter with a diameter of 10 mm). In addition, the calculated signal-to-noise ratio was 42.2 dB in this setting.

In order to evaluate the contact speed dependency in the sensor response, we measured the sensor outputs with time for three different contact speeds, as shown in Figure 3.14. The solid lines and shaded regions denote the mean value and twice the standard deviation (2σ) of the sensor outputs across 20 trials, respectively. In each plot, the application and removal periods indicate the periods wherein the load was being applied and removed, respectively. The results demonstrate that the sensor outputs varied similar to a quadratic curve for every speed. On the other hand, for speeds of 1 and 10 mm/s, the outputs slightly increased to their steady outputs after the application period. The differences between the outputs just after the application period and the steady outputs were 15.9 and 29.8 mV for speeds of 1 and 10 mm/s, respectively. Furthermore, the outputs remained at small values even though the loads were completely removed, and these remaining outputs gradually returned to the zero level within a few seconds. The remaining outputs were 18.1 and 29.5 mV

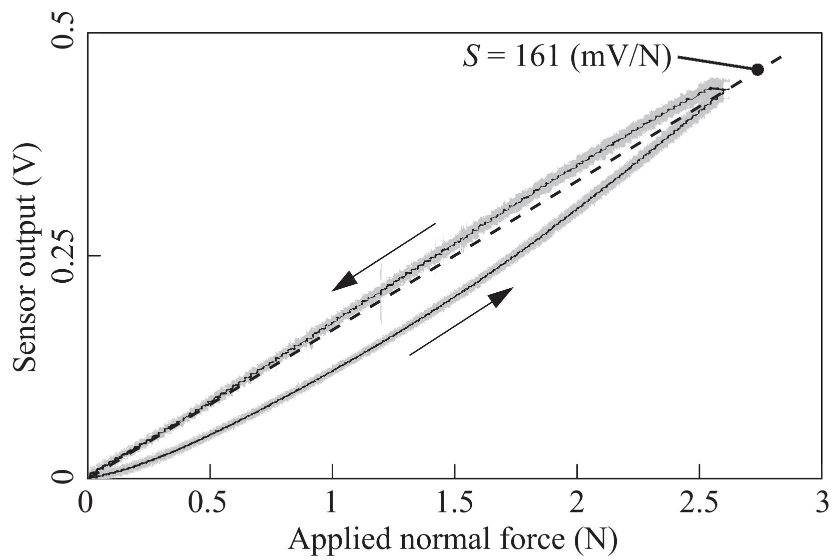

(a)

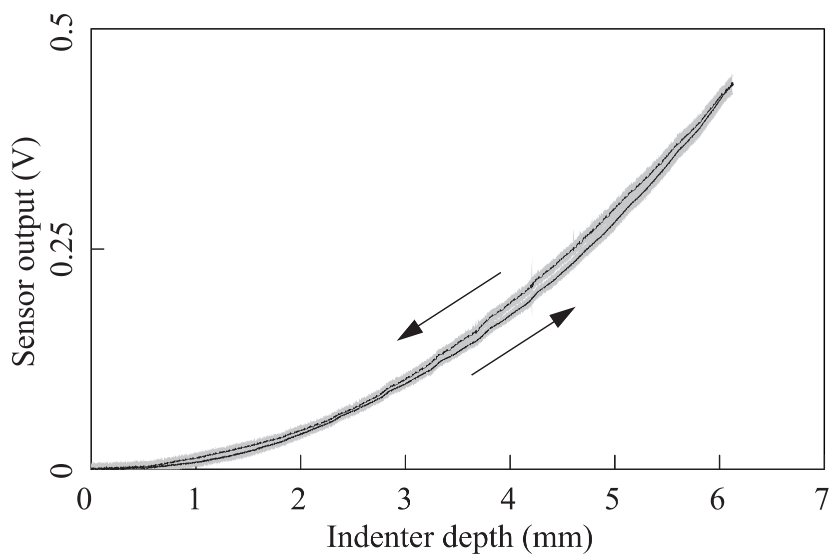

(b)

Figure 3.13: Sensor response curves with a contact speed V of 0.1 mm/s: (a) the sensor output versus the applied normal force and (b) the sensor output versus the indenter depth. In both plots, the solid lines and shaded regions indicate the average value and twice the standard deviation (2σ), respectively. The arrows indicate the direction of the applied load.

for speeds of 1 and 10 mm/s, respectively; thus, a higher speed resulted in a larger remaining output.

3.3.5 Spatial Response

To determine an appropriate spatial layout for the proposed sensor for large-area tactile implementation, the spatial response of the proposed sensor was investigated using the same setup. Figure 3.15 illustrates the measurement region and positions of the spatial response. The black dots in the figure indicate the center positions where the load was applied, i.e., the center of the indenter. In accordance with the index numbers (1, 2, ..., 6561) of the dots, the indenter moved from $x = -40$ mm to $x = 40$ mm and from $y = -40$ mm to $y = 40$ mm in 1-mm steps along each axis. The positions of the magnet and GMR sensor corresponded to (x, y) = (0, 0) and (10, 0), respectively.

At each measurement position, the indenter was lowered from the sensor surface $Z_o = 0$ mm to an arbitrary depth Z_{max}, which was set to each of seven different depths $Z_{max} = 0$, 1, 2, 3, 4, 5 and 6 mm (note that 0 mm means the load was not applied). By subtracting the initial output voltage V_o at Z_o from the output voltage V at Z_{max}, we measured the difference in the sensor outputs (i.e., $V - V_o$) at all measurement points.

Figure 3.16 shows the spatial response measured at a depth of 4 mm ($Z_{max} = 4$ mm) as one example of the measured data. The horizontal and vertical axes indicate the center position of the indenter along the x and y axes, respectively. The color depicts the mean value of the sensor outputs across the three trials; warm colors (yellow, orange and red) and blue indicate positive and negative sensor outputs, respectively. In addition, the white region indicates a region with zero output; in other words, the nonsensitive region of the sensor. The shape of the spatial response exhibited an elliptical Mexican-hat-like bipolar shape whose major axis corresponds to the line connecting the centers of the magnet and GMR sensor. The center of the response was approximately $(x_o, y_o) = (3, 0)$, i.e., the position between the magnet and the GMR sensor along the line connecting the centers of the magnet and GMR sensor.

The results for the other depths are summarized in Figure 3.17 as line profiles

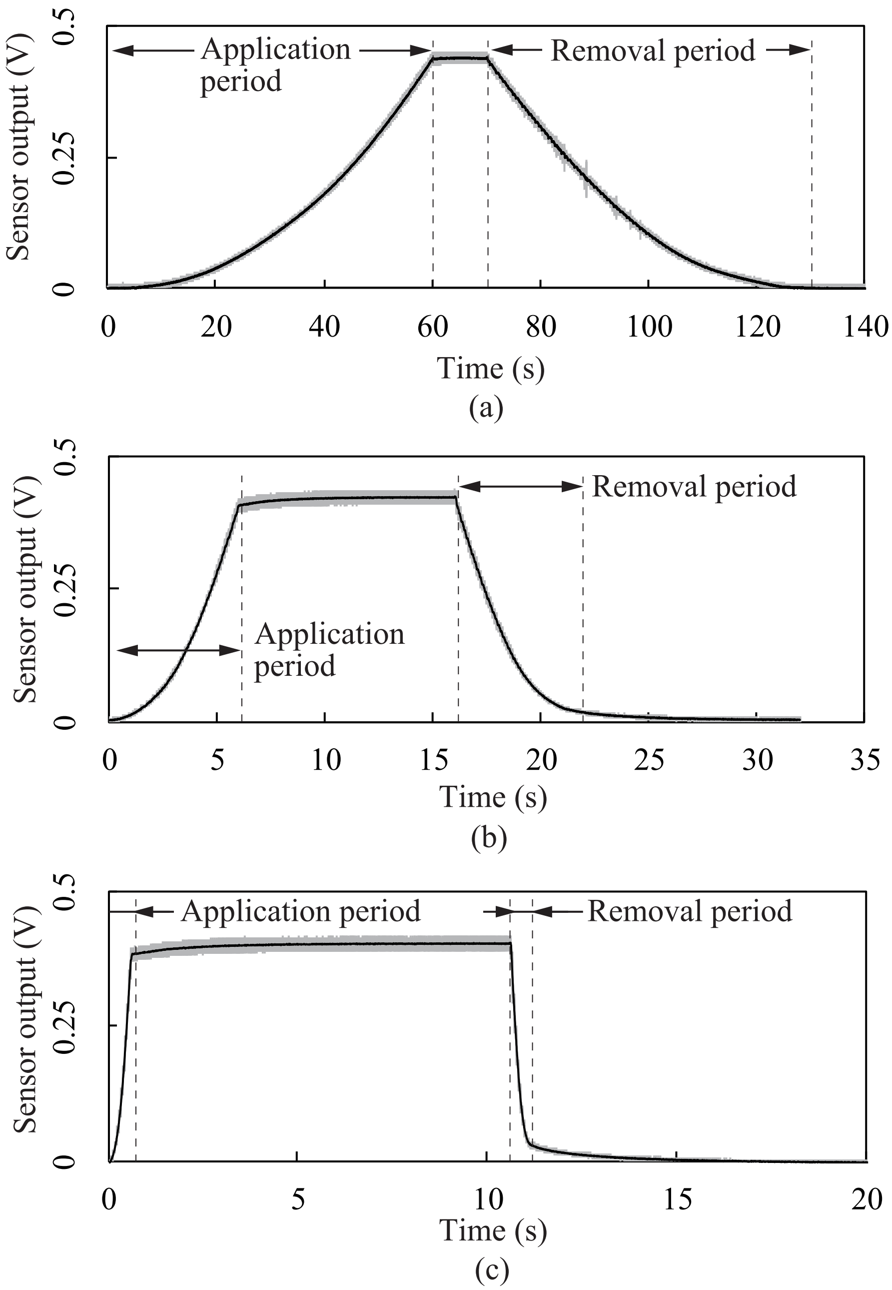

Figure 3.14: Sensor output versus time for three different contact speeds: (**a**,**b**,**c**) Sensor outputs with three different contact speeds $V = 0.1$, 1, and 10 mm/s, respectively.

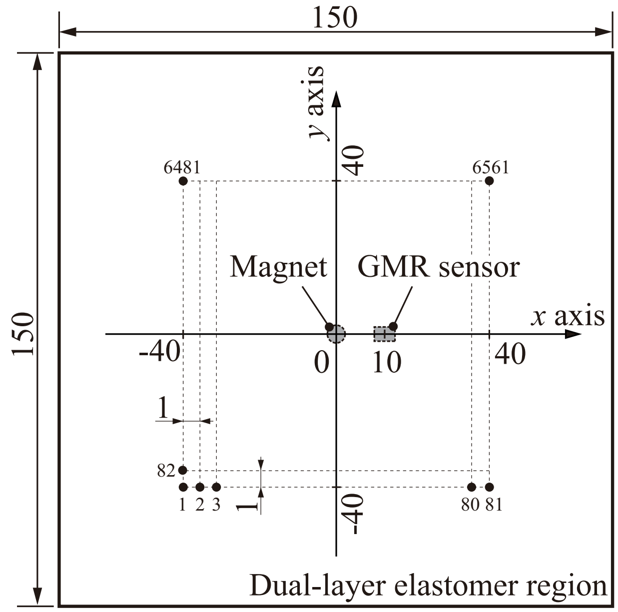

Figure 3.15: Measurement region and positions of the spatial response. The black dots indicate the center position of the applied load, i.e., the center of the indenter. The indenter was moved from $(x, y) = (-40, 40)$ to $(40, 40)$ in 1 mm steps based on the index numbers 1, 2, ..., 6,561 of the dots.

along the x and y axes through the center (x_o, y_o) = (3, 0). These responses exhibit Mexican-hat-like bipolar responses for all depths. In addition, the line profiles indicate that the zero-crossing points were almost the same point, i.e., (x, y) = (–10, 0), (18, 0), (3, –12), and (3, 12) in Figure 3.17, regardless of the depth.

The results demonstrate that the proposed sensor exhibits a Mexican-hat-like bipolar response and not a Gaussian-like response (i.e., a bell-shaped response) generally observed in conventional tactile sensors, e.g., [13, 14]. We hypothesized that such a negative response in the bipolar response does not originate from magnetic transduction, but instead from the incompressible characteristics of the BE. Because the BE is made of an incompressible material, bulging of the BE can occur around the edge of the pushed region (see Figure 3.2, right). This bulging increases the distance between the MRE and the sensing elements and therefore causes the negative response.

To verify this, we replaced the BE sheet with a compressible soft sponge sheet and measured its spatial response with the same setup and procedure. Figure 3.18 shows

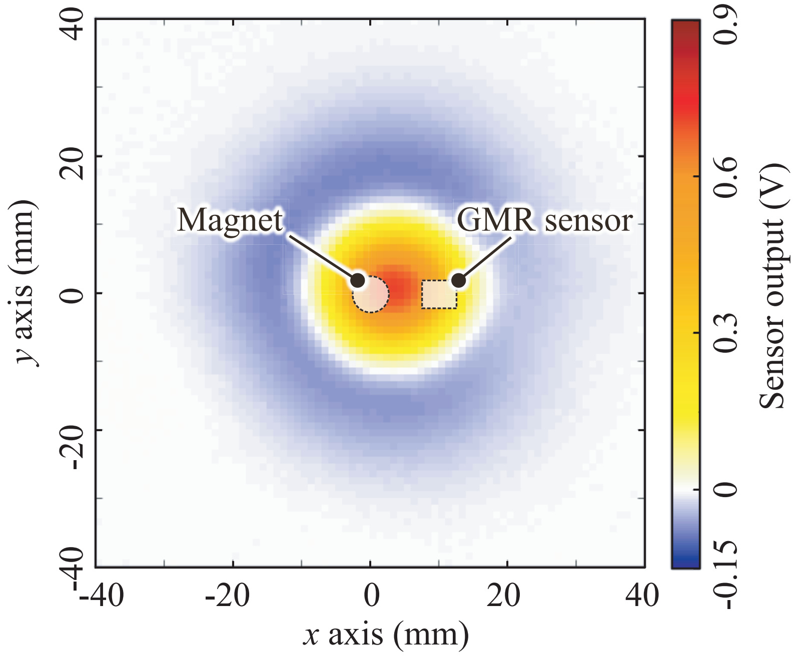

Figure 3.16: Measured spatial response for a depth of 4 mm. The shape of spatial response exhibits an approximately elliptical Mexican-hat-like bipolar shape whose major axis corresponds to the line connecting the centers of the magnet and GMR sensor.

the measured spatial response by using the sponge sheet for a depth of 4 mm (Z_{max} = 4 mm) as one example of the measured data. The result shows that the negative response region clearly disappears and that the spatial response exhibits an elliptical Gaussian-like shape whose major axis corresponds to the line connecting the centers of the magnet and GMR sensor. The center of the response was (x_{os}, y_{os}) = (2, 0), i.e., the position between the magnet and the GMR sensor along the line connecting the centers of the magnet and GMR sensor.

We again summarize the results as line profiles along the x and y axes through the center (x_{os}, y_{os}) = (2, 0). Figure 3.19 shows the line profiles for the seven different depths with the sponge sheet instead of the BE sheet. As in Figure 3.18, negative responses were not observed for all depths. Regardless of the depth, the widths of the responses along the x and y axes were approximately 44 and 40 mm, respectively. These results demonstrate that the negative response is derived from the incompressibility of the BE sheet and not from magnetic transduction.

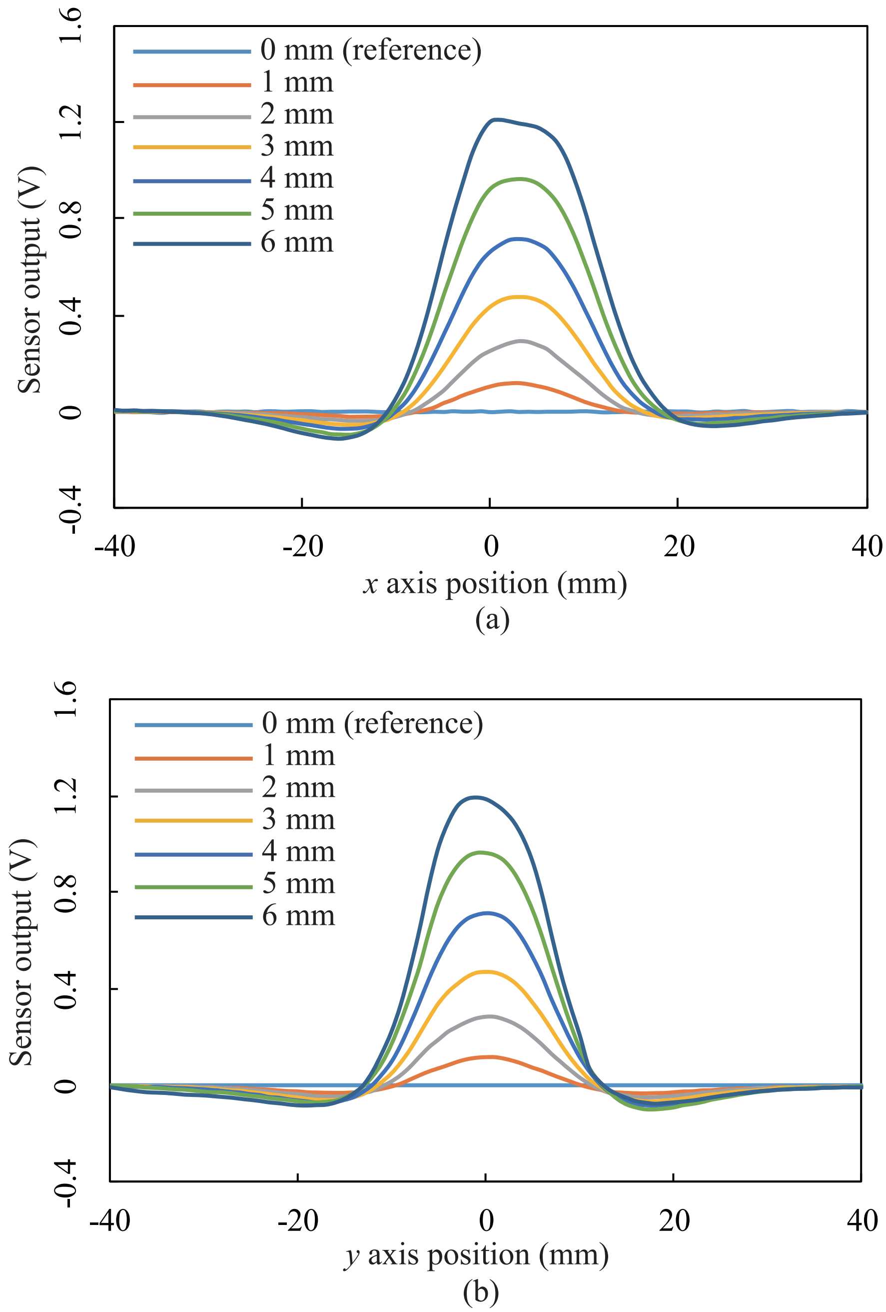

Figure 3.17: Line profiles of the measured spatial responses with at seven different depths: (**a**,**b**) Sensor outputs along the x and y axes through the point (x_o, y_o) = (3, 0), respectively.

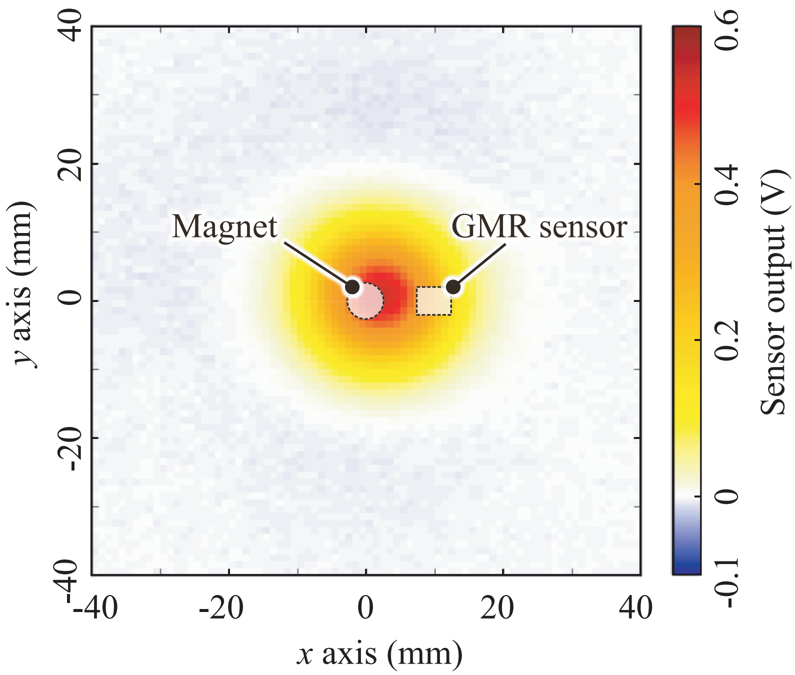

Figure 3.18: Measured spatial response with a sponge sheet instead of the base elastomer sheet at a depth of 4 mm. The shape of spatial response exhibits an approximately elliptical Gaussian-like shape whose major axis corresponds to the line connecting the centers of the magnet and GMR sensor.

3.4 Discussion

This section first summarizes the sensor response curves describing the relationship between the sensor outputs and the contact loads and how the contact speed affects the sensor output. Then, we discuss a model of the spatial response shape and whether the bipolar spatial response is useful for tactile information processing.

3.4.1 Simulations and real experiments

The results of magnetic field simulations and experiments with the fabricated sensor provide the curves showing the fundamental sensor response versus the applied normal force and vertical deformation. The result demonstrated that the applied force and deformation could be estimated from the contact position and shape of the indenter because the curves were either monotonically increasing or decreasing. The curve

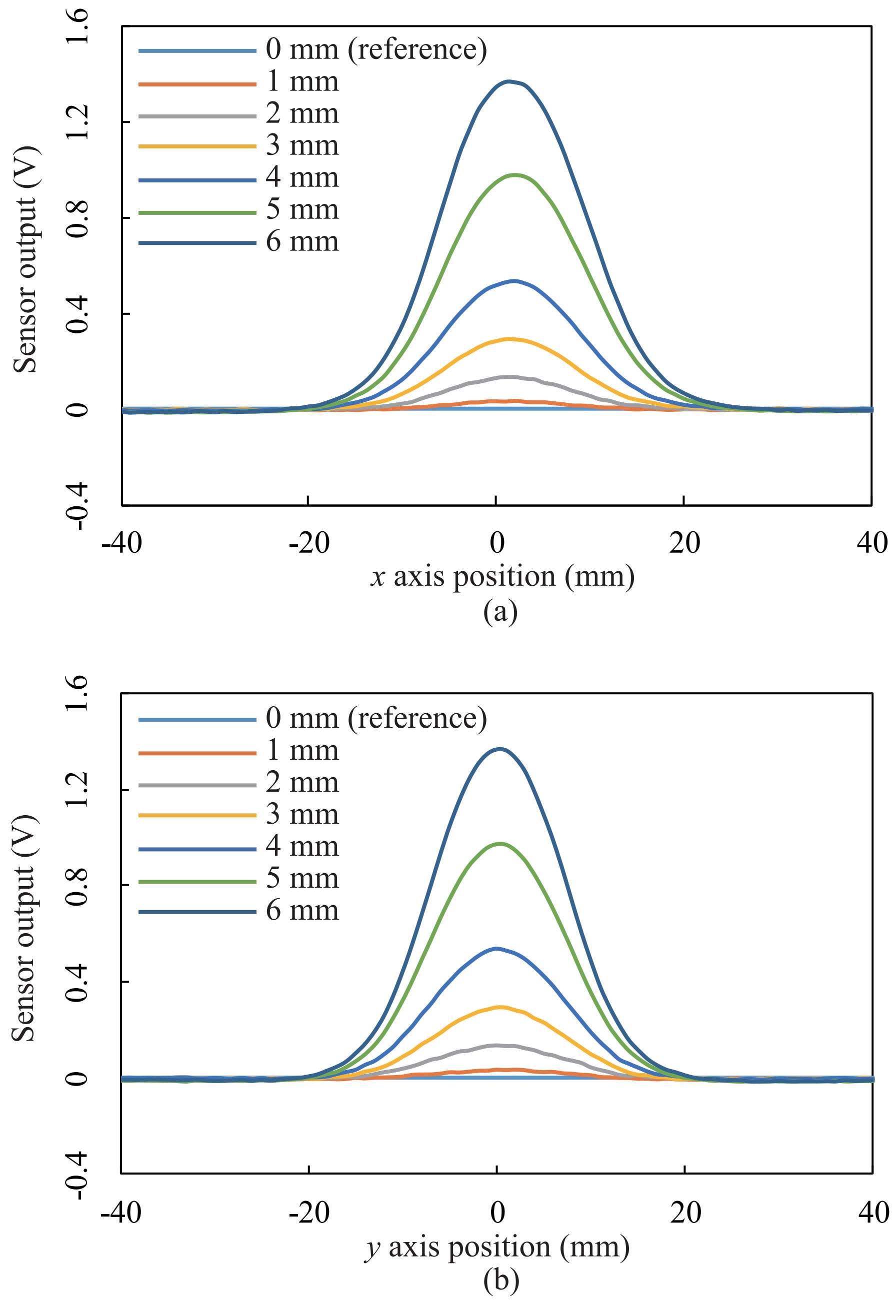

Figure 3.19: Line profiles of the measured spatial responses with the sponge sheet instead of the base elastomer sheet: (**a**,**b**) Sensor outputs along the x and y axes through the point $(x_{os}, y_{os}) = (2,\ 0)$, respectively.

showing the response versus the indenter depth has a smaller hysteresis compared with the curve showing the response versus the applied force. This is because the sensor response is simply determined by the distance between the MRE and the sensing elements on the PCB. While the applied force is removed, the viscosity of the elastomer generates a residual stress. The repulsive force in response to the indenter becomes weak owing to this residual stress; therefore, the hysteresis becomes larger in the curve showing the sensor response versus the applied force.

Figure 3.10 shows that the simulation result with the magnetic permeability of 1.5 was well matched to the measured sensor response. One reason for this is that the magnetic permeability of the MRE sheet used in this study is slightly different from the one of the MRE used in a study [86] because of the difference of magnetic particles distribution. Therefore, a measurement of the magnetic permeability of the MRE sheet will be a future issue. Another reason is that we hypothesized that 1) the magnetic permeability of the MRE sheet was spatially uniform in the magnetic field simulation; 2) the simulation was conducted in two-dimensional plane although the elastomer sheet would show complex deformation against applied contact force.

Next, in the experiments using different elastomers, the sensor response characteristics were changed depending on the thickness of each layer of the elastomer. Although the simulation results and the actual measurement results did not match strictly, this is due to the issues in the current simulation described above. In particular, the simulation result of type C sensor was different from the measured sensor response. We considered that this difference was mainly caused by simulating the MRE sheet having uniform magnetic permeability as discussed above. Since we did not perform processing to uniformly distribute the iron particles in the MRE sheet, the iron particles would concentratedly distributed on the lower surface of the MRE sheet. Therefore, when the MRE sheet is thickened, the iron particles would concentrate on the lower surface, and the magnetic permeability at the lower surface would become high. In order to confirm this concentration effect, we simulated the MRE sheet as a two-layer sheet structure with different magnetic permeability at the top and lower. As a result, we confirmed that the simulated result had a good match with the measured sensor response. Further investigation is necessary for more accurate discussion.

The results obtained in this section can be summarized as follows: (1) A thick MRE sheet has a high sensitivity to applied contact force. In this case, when the thickness of the MRE sheet doubles, the sensitivity against the applied vertical deformation is approximately 1.2 times. (2) A thin BE sheet also provides a high sensitivity; however, the measurement range of the applied contact force is limited. (3) In contrast, the thicker BE sheet decreases the sensitivity to small deformation, and in this case the sensitivity decreased about 0.37 times when the sheet thickness doubled. Consequently, the results suggest that basic sensor performance such as sensitivity and measurement range, can be modified by changing the thickness of both the elastomer sheets.

3.4.2 Sensor Response and Contact Speed

As shown in section 3.3.4, we also evaluated the sensitivity of the sensor, and found that the estimated sensitivity to the applied force was 161 mV/N with a range of forces of 2.5 N and a signal-to-noise ratio of 42.2 dB in this setup. This value demonstrates that the sensor has a high sensitivity (cf. other sensors listed in [17]), even though the proposed sensor was covered by a highly deformable material.

The results of the experiments utilizing different contact speeds indicate that the sensor outputs similarly varied with the applied load. On the other hand, for contact speeds of 1 and 10 mm/s, the sensor output did not return to the zero level immediately after the load was completely removed. The results for both speeds demonstrate that the sensor output requires a certain time (namely, a relaxation time) to return to its zero level. This remaining output means that the top MRE sheet was still lower than its initial position owing to the viscosity of the elastomer. One area of future work is to compensate for these remaining sensor outputs, e.g., by investigating the deformation dynamics and material properties of the elastomer. Another feasible solution will be to employ a low-viscosity elastic material for the elastomer.

3.4.3 Spatial Response

The experimental results indicate that the proposed sensor has a Mexican-hat-like spatial response, i.e., the sensor has positive and negative response regions. We hypothesized that this negative response was generated by the incompressible characteristics of the dual-layer elastomer. Owing to its incompressibility, the volume of the elastomer is constant before and after applying the load. In addition, the elastomer could not expand to the outside because its four sides were fixed (see Figure 3.12). Consequently, the BE right below a contact point moves to surrounding region; then, this moved BE pushes the MRE surface up, which decreases the sensor output. The experiments with the soft sponge sheet instead of the BE sheet demonstrate that the negative response region disappeared and that the response shape become an elliptical Gaussian-like shape.

Comparing the two spatial responses (Figures 3.17 and 3.19), we also found that the spatial response has a large response region; the diameter of the Mexican-hat-like response along its major axis was approximately 80 mm, and the diameter of the Gaussian-like response along its major axis was approximately 44 mm. A large response region could be generated by employing a thick elastomer that causes surface deformation in a broad region; in particular, this deformation region will become broader by using an incompressible BE, as discussed above.

In conclusion, we can summarize the spatial response of the proposed sensor as follows:

1. The distorted Gaussian-like unipolar spatial response shown in Figure 3.18 reflects the spatial response generated by the proposed sensing mechanism, i.e., the change in magnetic field caused by approaching the MRE.

2. The shape of the spatial response is approximately elliptical, whose major axis corresponds to the line connecting the centers of the magnet and GMR sensor.

3. The center of the spatial response (x_{os}, y_{os}) is at a point that is closer to the magnet along the line connecting the centers of the magnet and GMR sensor.

4. The use of an incompressible elastomer adds a negative response to the unipolar

spatial response; then, the entire spatial response becomes a distorted Mexican-hat-like bipolar spatial response, as shown in Figure 3.16.

The following two subsections describe what functions can fit the measured spatial responses.

Modeling of the Sensor Response Generated by Approaching the MRE

Shimojo [13] found that an elastic covering for a tactile sensor functions as a spatial low-pass filter and that its spatial response exhibits a Gaussian-like shape. Because of the elliptical shapes of the responses in Figures 3.18 and 3.19, we employed an elliptical Gaussian function to fit the sensor response generated by approaching the MRE:

$$Res(x, y, z) = \frac{k(z)}{2\pi\sigma^2} \exp\left(-\frac{(x - x_c)^2 + \gamma^2(y - y_c)^2}{2\sigma^2}\right) \tag{3.1}$$

where $k(z)$ is a function of the applied depth z, (x_c, y_c) is the center of the function, σ^2 is the variance and γ is the spatial aspect ratio specifying the ellipticity of the Gaussian function. The results presented in Section 3.3.2 demonstrate that the sensor output increases quadratically with the applied depth; therefore, we employed a quadratic function az^2+bz+c for the function $k(z)$. All parameters were estimated on the basis of a least-squares method, and their estimated values were as follows: x_c = 1.774, y_c = 0.2067, σ = 7.170, γ = 1.074, a = 15.49, b = –16.14 and c = 4.948. The fitting error R^2 (i.e., the squared error of all measurement points for the seven depths) was 2.2047.

Modeling of the Bipolar Response

The bulging of the incompressible BE sheet added a ring-shaped negative response to the ordinary response described in Equation (3.1); thus, the entire response becomes a bipolar response (Figure 3.16). In order to express such a bipolar response, we can practically employ the following two functions: difference of Gaussians (DoG) and Laplacian of Gaussian (LoG) functions. The Mexican-hat-like spatial response is generally fit with these functions.

The DoG function is defined by the difference between two Gaussian functions G_1 and G_2 that have different variances and peak values:

$$DoG(x, y, z) = k(z)\left(G_1(x, y) - G_2(x, y)\right) \tag{3.2}$$

$$G_i(x, y) = \frac{1}{2\pi\sigma_i^2} \exp\left(-\frac{(x - x_c)^2 + \gamma^2(y - y_c)^2}{2\sigma_i^2}\right) \tag{3.3}$$

where $k(z)$ is a function of the applied vertical deformation, σ_i^2 is the variance, (x_c, y_c) is the center position of the DoG function and γ is the spatial aspect ratio that specifies the ellipticity of the DoG function.

On the other hand, the LoG function is defined as a second-order partial differential of a Gaussian function $G(x, y)$:

$$\begin{aligned} LoG(x, y, z) &= k(z)\left(\frac{\partial^2 G(x, y)}{\partial^2 x} + \frac{\partial^2 G(x, y)}{\partial^2 y}\right) \\ &= -\frac{k(z)}{\pi\sigma^4}\left(1 - \frac{(x - x_c)^2 + \gamma^2(y - x_c)^2}{2\sigma^2}\right) \exp\left(-\frac{(x - x_c)^2 + \gamma^2(y - y_c)^2}{2\sigma^2}\right) \end{aligned} \tag{3.4}$$

$$G(x, y) = \frac{1}{2\pi\sigma^2} \exp\left(-\frac{(x - x_c)^2 + \gamma^2(y - y_c)^2}{2\sigma^2}\right) \tag{3.5}$$

where $k(z)$ is a function of the applied vertical deformation, σ^2 is the variance, (x_c, y_c) determines the center position of the LoG function and γ is the spatial aspect ratio that specifies the ellipticity of the LoG function.

We conducted a χ^2 fitting in order to compare the fitting accuracies of these two functions. The calculated values of the DoG function were as follows: x_c = 2.69, y_c = 0.369, σ_1 = 6.32, σ_2 = 14.6, γ = 1.06, a = 4.07, b = 41.5 and c = 0.0911; the χ^2 value was 3.76×10^6. In contrast, the calculated values of the LoG function were as follows: x_0 = 2.61, y_o = 0.468, σ = 8.82, γ = 1.02, a = –282, b = -2.00×10^1 and c = –12.5; the χ^2 value was 6.18×10^6. χ^2 was smaller for the DoG function; thus, we concluded that the DoG function is a practically sufficient fitting of the spatial response of the proposed sensor. Figure 3.20 shows a comparison between the measured and fitted responses for a depth of 4 mm as one example of the fitted response. Figure 3.20a depicts the two-dimensional fitted response (cf. Figure 3.16). Both plots (Figure 3.20b,c) show the line profiles along the x and y axes through the center (x_o, y_o) = (0, 3). The solid and dotted lines indicate the measured and fitted responses, respectively. These plots also demonstrate that the DoG function can express the spatial response of the proposed sensor.

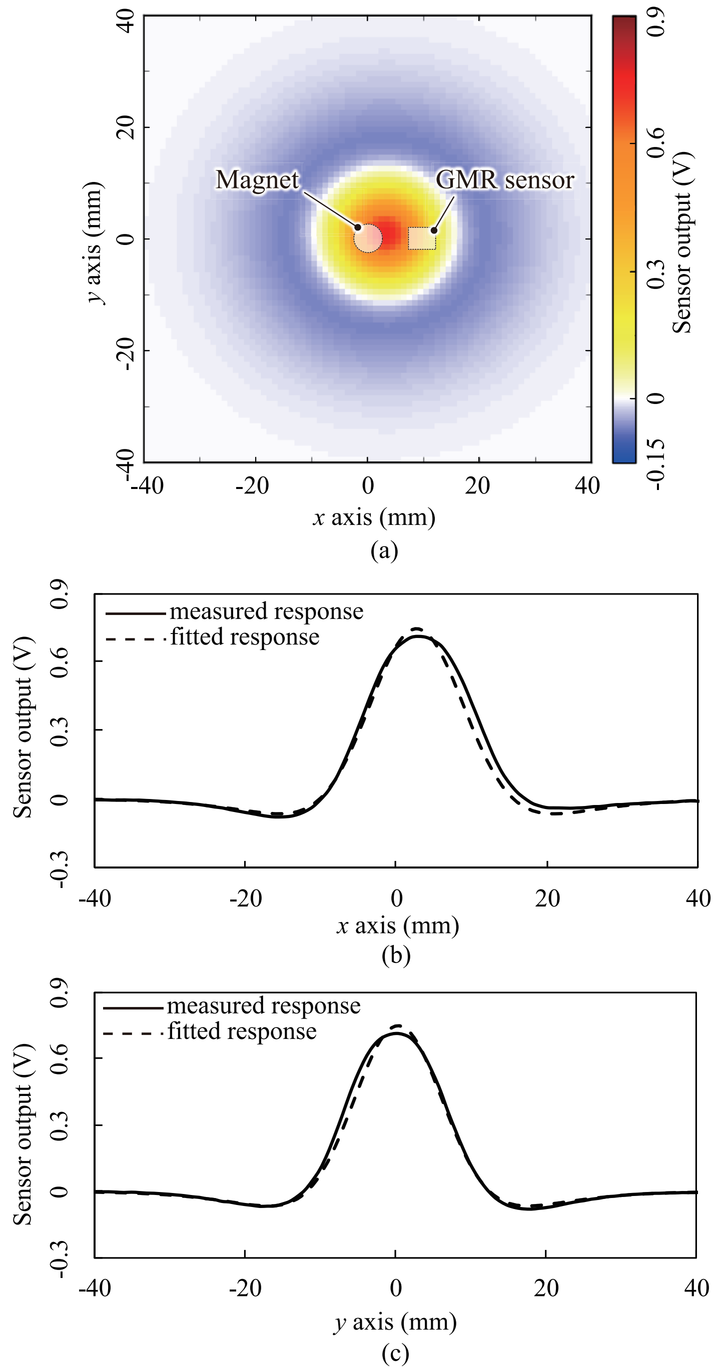

Figure 3.20: Comparison between the measured and fitted responses for a depth of 4 mm: (**a**) two-dimensional fitted response and (**b**,**c**) line profiles along the x and y axes through the center $(x_o, y_o) = (0,\ 0)$, respectively.

3.4.4 Usefulness of the Mexican-Hat-Like Spatial Response for Tactile Information Processing

The experimental results show that the proposed sensor has a Mexican-hat-like bipolar spatial response. Note that the BE sheet in the proposed sensor can be easily replaced with any material possessing a low magnetic permeability, as done with the soft sponge sheet employed in this study. If the negative response is unnecessary for a specific application, the BE sheet can be replaced with a compressible soft material. Accordingly, we can choose whether the negative response is utilized in accordance with real tasks or applications. In this section, we discuss whether the negative response is useful for tactile information processing or not.

Such a spatial response can be fit with a DoG function, which is commonly known as an edge-enhancement filter in computer vision. This means that the sensor could function as a spatial filter and extract DoG-like features at the hardware level. Therefore, the proposed sensor may be able to provide edge-enhanced tactile images (or edge-enhancement features) by implementing many pairs of magnets and GMR sensors arranged in an array. In addition, it is widely known that humans utilize edge information when processing tactile information [87]. We believe that such tactile edge enhancement features will be useful for tactile information processing in the field of robotics.

One example employing a DoG function for tactile processing is a scale-invariant feature transform (SIFT) algorithm, which is used to extract features in computer-vision applications. The SIFT requires various scaling DoG features and is employed in object-shape recognition tasks using a tactile sensory signal [88]. Typically, spatial filtering is accompanied with high computational costs; however, the proposed sensor has the potential to perform filtering processes with DoG features in hardware if the proposed sensor is able to vary its spatial response.

The parameters of the BE, such as the thickness and stiffness, are thought to determine the shape of the spatial response. An area of future research is to investigate how these parameters determine the shape and to develop a design procedure for creating an arbitrary spatial response for the sensor.

3.5 Summary

We proposed a tactile sensorization method of a magnetorheological elastomer based on a magnetic field measurement.We investigated the sensor responses with the magnetic field simulation and real experiments with two fabricated sensors. The simulations and experiments demonstrated that the sensor can measure applied normal force and vertical deformation by monitoring the change in magnetic field, and that these results were well matched. The second experiment indicates that the sensor has a high sensitivity (approximately 161 mV/N with a signal-to-noise ratio of 42.2 dB) and that the sensor can respond to the applied load, even with a high contact speed; however, a high contact speed induces a relaxation time in the sensor output. The third experiment found that the sensor has an elliptical Mexican-hat-like bipolar spatial response whose major axis corresponds to the line connecting the centers of the magnet and magnetic transducer and that employing a incompressible dual-layer elastomer results in a negative response in the bipolar response. We then demonstrated that this bipolar spatial response can be practically fit with an elliptical DoG function. This spatial-filter-like response indicates that the proposed sensor may be able to function as a spatial filter at the hardware level.

In this paper, we evaluated the output with a single-magnet and GMR-sensor pair. Hence, the next step is to focus on the implementation of multiple magnets and GMR sensors. We believe that the combination of outputs from these pairs of devices will enable the estimation of the contact position, the applied vertical deformation and the shape of the contacted object. We will also mount the proposed sensor on the body of a humanoid robot for further testing.

Chapter 4

Tactile sensorization with an inductor

This chapter describes a flexible tactile sensor in which magnetorheological and non-magnetic elastomer sheets are simply laminated on an inductor. This sensor has potentially high durability against shocks since the sensing part has only flexible elastomer layers and a printed circuit. Because the magnetorheological elastomer (MRE) sheet contains iron particles, the distance between the MRE sheet and the inductor determines its inductance. Therefore, the sensor can detect surface deformation around the inductor by measuring the change in its inductance. The sensor response versus applied normal force curve and vertical deformation was obtained, and the signal-to-noise ratio (SNR) was found to be high (approximately 53 dB). We investigated the response properties with inductors having different sizes and confirmed that the SNRs were lower for the inductor with a smaller diameter. This result suggests a trade-off between the SNR and the density of the inductor layout. The results also indicate that the sensor has a point-symmetric bipolar spatial response with a large response region compared with the inductor diameter. We also investigated the changes in the inductance when metallic materials approach to the sensor surface because metallic materials can change the inductance without contact. The results demonstrate that (1) the inductance decreases when metal cubes approached to the inductor, and (2) the decrement of the inductance can be reduces by employing the MRE sheet with a large amount of iron particles. In addition, to measure contact force distributions with an array sensor using several inductors, interferences among inductors were investigated because our sensor works based on electromagnetic effect. We confirmed that the inductance increased when the neighbor inductor was activated, and that the amount of increase was reduced with a larger distance condition between the two inductors.

4.1 Background

Several types of flexible tactile sensors using elastic materials as covers have been developed; however, their properties such as the durability, maintainability, sensitivity, and mechanical complexity should be further improved. We previously developed a flexible sensor whose surface contains no transducers, wiring, and solids because these elements inside the flexible cover deteriorate the durability and maintainability, as shown in Chapter 3. The sensor surface consists of magnetorheological and nonmagnetic elastomer sheets while the sensor bottom has a magnet and magnetic transducer pair, which measures the magnetic flux that changes depending on the deformation of a magnetorheological elastomer (MRE) sheet containing iron particles.

In this study, we propose another type of flexible tactile sensor whose structure was simplified to improve the durability and reduce the mechanical complexity. We removed the magnet and magnetic transducer pair and installed a printed inductor instead. Since the MRE sheet contains iron particles, the distance between the MRE sheet and inductor determines its inductance. Hence, the sensor can detect surface deformation around the inductor by measuring the change in its inductance. It is predicted that an inductor with a large diameter could have a large response and large spatial response region. From the sensor structure, the sensor will have a point-symmetric spatial response at the center of the inductor, which will be also the most sensitive point, i.e., a peak position in the spatial response. However, the complex deformation of the dual-layer elastomer sheet makes it difficult to predict the sensor response.

In order to confirm these sensor characteristics, we investigated the response curve of the proposed sensor in terms of the applied normal force and signal-to-noise ratio (SNR) as fundamental properties of the sensor. As a preliminary experiment for implementing a large-area sensor, we also investigated the spatial responses with inductors having different sizes and examined the changes in the sensor response region and SNR depending on the inductor size. In addition, we investigated the sensor response caused by electromagnetic phenomenon, not by applied contact force, since the proposed sensor measures applied force as an inductance change, which could vary with external magnetic sources. First, we examined the sensor responses versus the approach of a metallic cube, which generate eddy currents with a magnetic field in the cube. The magnetic field would be generated in a direction to reduce the original magnetic field generated by the sensing inductor. Therefore, the inductance is expected to decrease in accordance with the approach of the metallic cube. Second, the magnetic interference between the inductors was investigated toward a large scale tactile sensing. To measure force distributions, the proposed sensor requires an inductor array; however, the magnetic fields generated by the inductors would interfere, and thus the inductances would also change by the interference.

4.2 Proposed sensor

This section provides an explanation of tactile sensorization method of a magnetorheological elastomer using an inductor.

4.2.1 Structure and Sensing Mechanism

Figure 4.1 shows the appearance of the proposed sensor and its cross-sectional schematic. An inductor is printed on a circuit board, which is covered by an MRE sheet and a nonmagnetic base elastomer (BE) sheet. The MRE sheet contains particles with a high magnetic permeability, e.g., iron particles.

In such a structure, the MRE sheet functions for an inductor as a magnetic core that increases the inductance while the inductor functions as a magnetic permeability transducer. The normal force applied to the sensor surface changes the distance between the inductor and the MRE sheet. This distance determines the inductance; thus, the sensor can measure the applied force as the inductance changes.

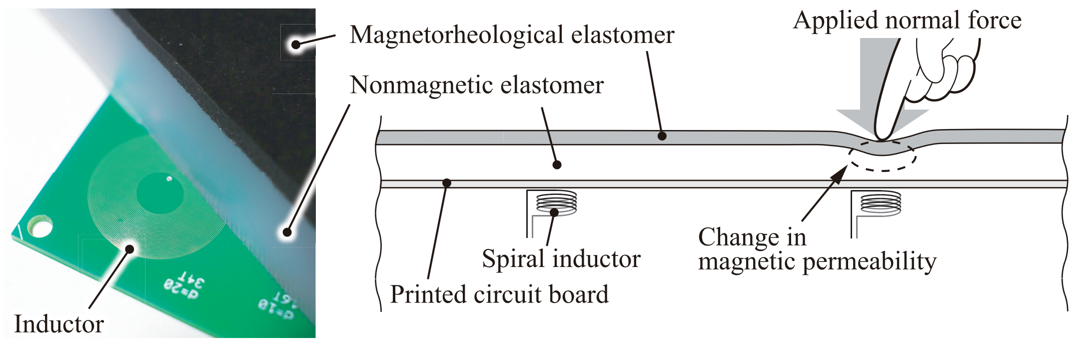

Figure 4.1: Appearance of the proposed sensor and its cross-sectional schematic. An spiral inductor is printed on a printed circuit board while magnetorheological and nonmagnetic base elastomer sheets cover the board.

Table 4.1: Characteristics of the prepared three spiral inductors

Type	Diameter (mm)	Number of turns	Initial inductance (µH)
A	20	32	51.3721
B	10	16	5.26445
C	8	14	2.73450

4.2.2 Fabricated Sensor

Figure 4.2 shows an appearance of the fabricated sensor. The size of the elastomer sheets was determined to be 150 mm on both sides. The thickness of the MRE and BE sheets were 10 mm and 2 mm, respectively. These layers were made of a platinum-cured silicone rubber (Smooth-On Inc., USA, Ecoflex 00-30). Iron particles with a diameter of 50 µm were mixed with the MRE at a volume ratio of 20 %.

Figure 4.3 illustrates the developed two-layered planar spiral inductor and the inductor parameters. The spiral inductor was printed on both surfaces of a rigid circuit board with a thickness of 1.6 mm. The trace width and the spacing between the traces were 0.1 mm. We prepared three inductors having different diameters, as listed in Table 4.2.2. The inductor diameters were set to the same diameter as the indenter (10 mm), a larger one (20 mm), and a smaller one (8 mm, the minimum diameter working in this setup).

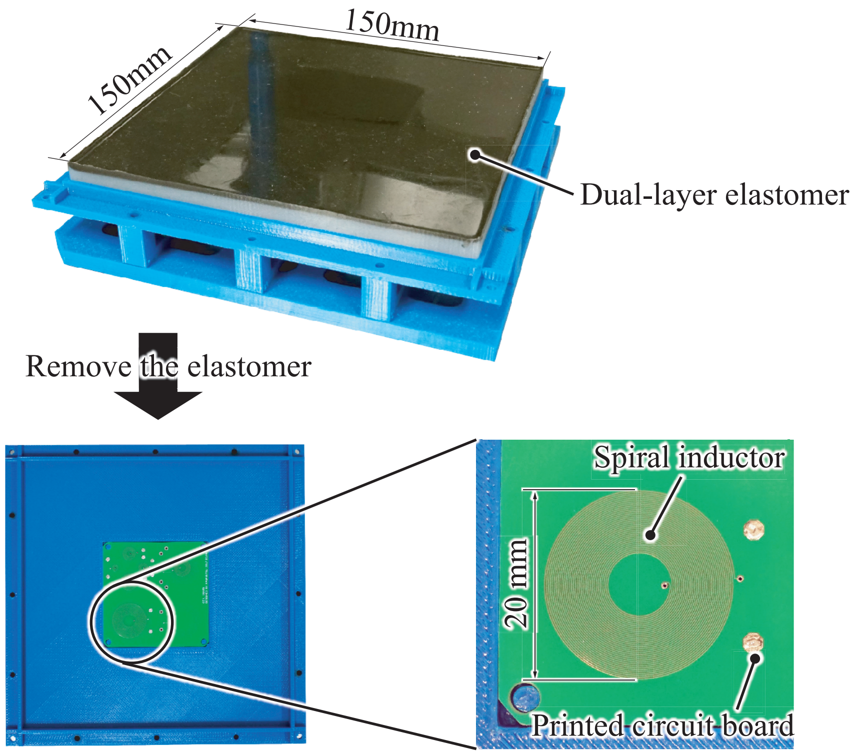

Figure 4.2: An appearance of the fabricated flexible tactile sensor. The sensor consists of a mangetorheological elastomer sheet, a non-magnetic elastomer sheet, and a printed circuit board holding a spiral inductor.

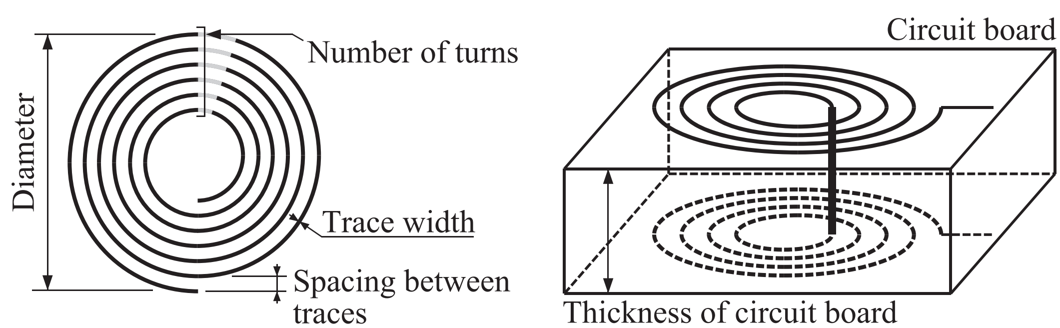

Figure 4.3: Inductor parameters of a two-layer planar spiral inductor printed on both surface of a rigid circuit board.

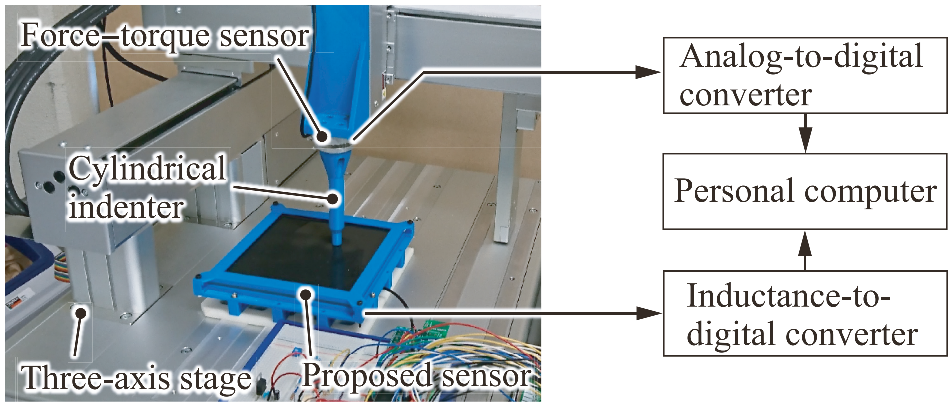

Figure 4.4: Experimental setup for measuring the sensor response curves. A normal force was applied to the sensor surface by a three-axis robot stage with a cylindrical indenter. A personal computer captured the inductance and the outputs of a force–torque sensor via an inductance-to-digital converter and analog-to-digital converter.

4.3 Experiments and results

Figure 4.4 shows the setup for investigating the sensor response. The proposed sensor was mounted to a three-axis robot stage (IAI Corp., Japan, TTA-C3-WA-30-25-10) with a force–torque sensor (F/T sensor; BL Autotech LTD., Japan, Mini 2/10-A) for measuring the applied force. The F/T sensor was equipped with a plastic cylindrical indenter with a diameter of 10 mm. A personal computer (PC) captured the output of the F/T sensor via a 16-bit analog-to-digital converter (CONTEC Corp., Japan, AI-1664LAX-USB). A 28-bit inductance-to-digital converter (Texas Instruments Corp., USA, LDC1614) measured the inductance values at 100 Hz and transmitted the values to the PC.

4.3.1 Sensor response curve

The sensor response curve with the type A inductor was measured in accordance with the following steps:

1. lower the indenter at a speed $V = 1$ mm/s until the surface of the sensor descends to depth of 6 mm, which corresponds to half of the thickness of the elastomer
2. wait for 10 s

3. raise the indenter to its initial position at a speed of V

4. wait for 10 s

5. repeat the above steps 10 times

Figure 4.5 shows the sensor response versus the applied normal force and vertical deformation. In both the plots, the insets show a magnification of the initial part of the curve. The solid line and dots are the average values of the measured inductance across 10 trials, and the shaded gray regions are twice the standard deviation (2σ) of the inductance. The arrows indicate the direction of the applied force. The measured inductance increased monotonically versus the applied normal force, although the curve exhibited hysteresis. In contrast, the inductance curve versus the applied vertical deformation has a small hysteresis compared to the one versus the applied normal force. To evaluate the measurement noise, we calculated the maximum variance, and this value was 7.609×10^{-7} µH^2. In addition, the SNR of 53.85 dB was obtained by the following equation: $20\log_{10}(A_S/A_N)$ where A_S is the maximum inductance change from the initial inductance and A_N is the maximum peak-to-peak inductance under no load. The small 2σ region compared with the sensor range also indicates the high repeatability of the inductance across 10 trials.

4.3.2 Spatial Response Properties

The spatial response should be investigated to determine a spatial layout of inductors for large-area implementation. An inductor with a small diameter allows a spatially massive implementation; however, miniaturization of the inductor could lower the sensitivity and SNR. To investigate the relationship between the sensor response and the diameter of the inductor, we used three inductors having different sizes, as listed in Table 4.2.2. The sensor responses were measured using the same equipment. Figure 4.6 illustrates the measurement region and positions of the spatial response. The black dots in the figure indicate the center positions where the load was applied, i.e., the center of the indenter. In accordance with the index numbers (1, 2, ..., 6561) of the dots, the indenter moved from $x = -40$ mm to $x = 40$ mm and from $y = -40$

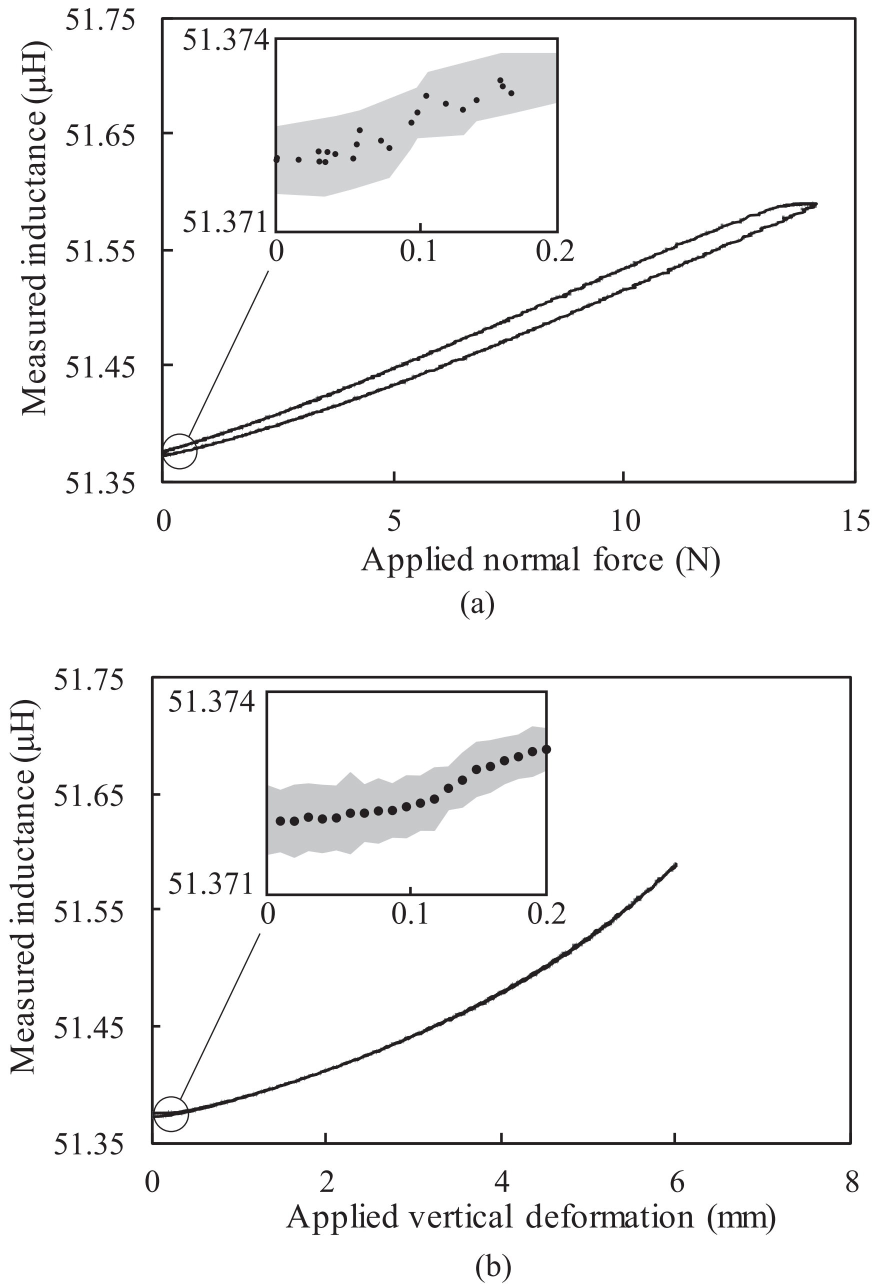

Figure 4.5: Measured sensor response curves versus (a) the applied normal force and (b) the applied vertical deformation across 10 trials. The inset shows a magnification of the initial part of the curve. The solid line and dots indicate the mean value of the inductance, and the arrows depict the direction of the applied normal force. The shaded region indicates twice the standard deviation (2σ) of the inductance.

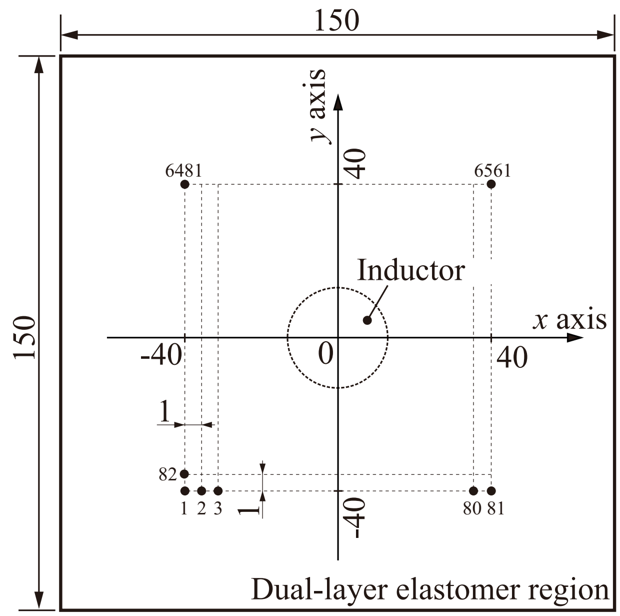

Figure 4.6: Measurement region and positions of the spatial response. The black dots indicate the center position of the applied load, i.e., the center of the indenter. The indenter was moved from $(x, y) = (-40, 40)$ to $(40, 40)$ in 1 mm steps based on the index numbers 1, 2, ..., 6,561 of the dots.

mm to $y = 40$ mm in 1-mm steps along each axis. The positions of the center of inductor corresponded to $(x,\, y) = (0,\, 0)$.

At each measurement position, the indenter was lowered from the sensor surface $Z_o = 0$ mm to 6 mm. By subtracting the initial inductance from the measure inductance, we measured the difference in the inductances at all measurement points.

Figure 4.7 shows the measured spatial response with the type A inductor, whose center was the coordinate origin. The colors indicate the different values of the inductance from its initial value. The response shape was bipolar whereas the one for conventional sensors is generally Gaussian-like. We describe such sensor response with three sensor parameters, i.e., the positive peak value and the average diameters of the positive and negative regions, because the measured bipolar response was almost point-symmetric. Table 4.3.2 summarizes these measured sensor parameters for three different inductors. The smaller inductors show a smaller variation in the inductance and SNRs; in contrast, the positive and negative response regions did not significantly change in accordance with the inductor diameter.

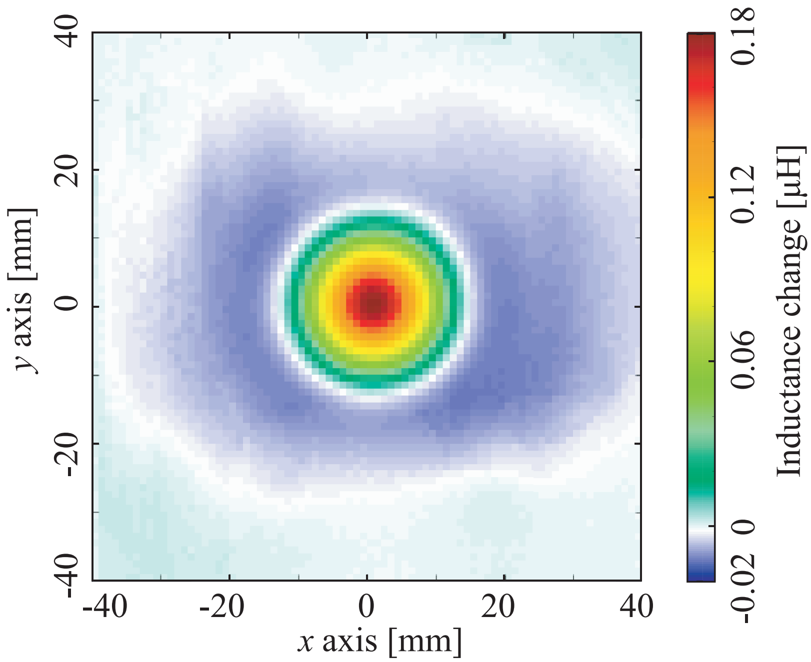

Figure 4.7: Spatial response of the sensor with a type A inductor. The color indicates that the inductance changed from its initial value.

Table 4.2: Summary of the measured responses.

Type	Positive peak (μH)	Diameter of positive response (mm)	Diameter of negative response (mm)	Signal-to-noise ratio (dB)
A	0.184721	25	68	53.85
B	0.010937	24	68	46.80
C	0.004181	22	68	41.80

4.3.3 Sensor response caused by approaching metallic materials

To investigate the sensor response caused by approaching metallic materials, a metallic cube was attached to the three-axis robot stage, instead of the plastic indenter. We here employed three kinds of metal, such as Aluminum (A5052), Steel (SS400), and Stainless steel (SUS304). The size of the metallic cube was 30 mm high, 30 mm wide, and 30 mm. The cube was approached to the sensor at the position where the

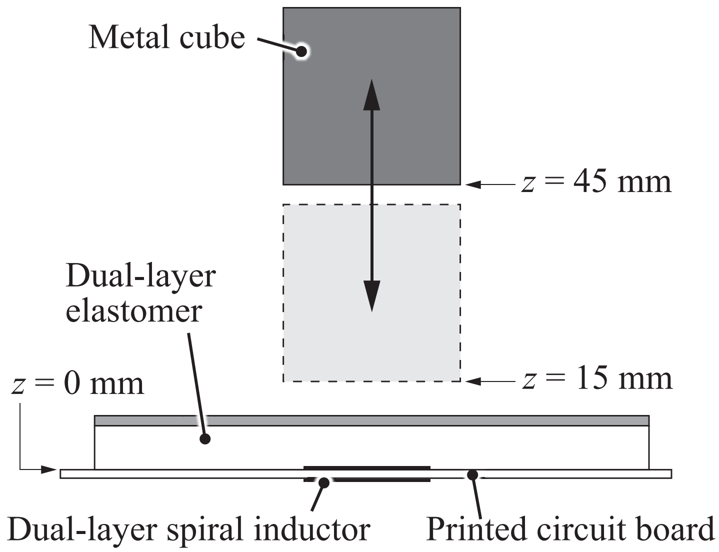

Figure 4.8: Experimental condition for investigating the sensor response versus approaching metal cube.

center of the cube and inductor matched as showed in Fig. 4.8. As the PCB surface was $z = 0$ mm, the bottom surface of the cube was moved $z = 15$ to $z = 45$ mm (here we define the PCB surface was $z = 0$ mm) totally 5 times.

Figure 4.9 indicates the inductance changes versus approaching three kinds of metallic cubes. The solid lines are average values across 5 trials. The results shows that the inductance monotonically decreased with approaching metallic cubes, and that the hysteresis in the response curves was small. The amounts of decrement were slightly different according to the employed metal.

The MRE sheet could function as a magnetic shield which can decrease the effect of approaching metallic material because the MRE sheet contains iron particles with a high magnetic permeability. Accordingly, the inductance changes versus approaching metallic material were investigated by using several MRE sheets with different thicknesses and volume ratio of contained iron particles. Table 4.3.3 summarizes the parameters of the employed nine different MRE sheets. The type A to type E MRE sheets have different thicknesses with an intervals of 1 mm and with the fixed volume ratio of iron particles of 20 %. In contrast, the type F to type I MRE sheets have different volume ratio of iron particles with an intervals of 10 % and with the fixed thickness of 2 mm. Here, the thickness of the BE sheet was fixed to 10 mm for all

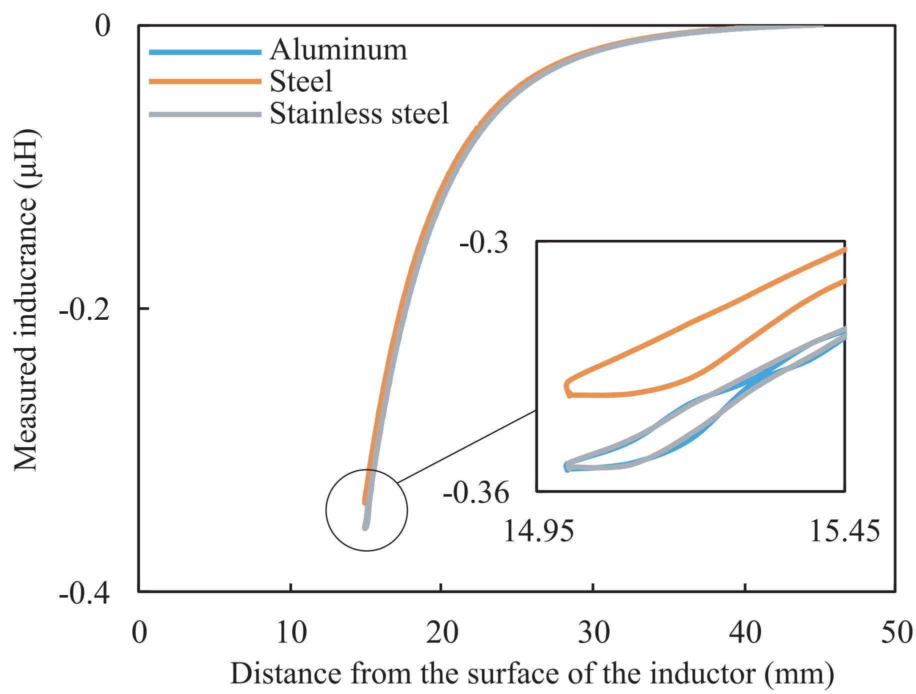

Figure 4.9: Measured inductance change versus the distance from the inductor. The solid line indicates the mean value of the inductance across 5 trials.

the MRE sheets.

With these nine different MRE sheets and three kinds of metal cubes, the inductance was measured with the same experimental procedure shown in Fig. 4.8. We here calculated the maximum decrement of each inductance change, and compared among nine MRE sheets. Figure 4.10 shows the maximum decrement of each inductance change with the Aluminum cube. Horizontal axis is the mass of iron particles in the MRE sheets. The maximum decrement of inductances were reduced in accordance with the thickness and volume ratio of iron particles of the MRE sheet. This tendency was also found in the condition using the other metal cubes and elastomers. The obtained results can be summarized as follows: (1) The maximum decrement of inductances were small when using thick MRE sheets. With the comparison between the MRE sheets with thickness of 1 mm and 5 mm, the maximum decrement of inductances were reduced 0.876, 0.882, and 0.854 times in Aluminum, Steel, Stainless steel conditions, respectively. (2) The maximum decrement of inductances were small

Table 4.3: Parameters of the MRE sheet.

Type	Thickness of the MRE sheet (mm)	Volume ratio of iron particles (%)	Mass of iron particles (g)
A	1	20	12.2
B	2	20	24.4
C	3	20	36.6
D	4	20	48.8
E	5	20	61.0
F	2	10	12.2
G	2	30	36.6
H	2	40	48.8
I	2	50	61.0

when using MRE sheets with larger volume ratio of iron particles. With the comparison between the MRE sheets with volume ratio of 10 % and 50 %, the maximum decrement of inductances were reduced 0.899, 0.919, and 0.918 times in Aluminum, Steel, Stainless steel conditions, respectively.

4.3.4 Interference between inductors

To investigate the interference between two inductors, we prepared another fabricated sensor and experimental setup. Figure 4.11 shows an appearance of another fabricated sensor. We employed inductors printed on a flexible printed circuit board (FPCB) while we employed the same elastomer used in the previous experiments. The spiral inductor with a diameter of 10 mm was printed on both surfaces of an FPCB with a thickness of 12.5 µm. The trace width and the spacing between the traces were 0.1 mm. In this experiment, we used two inductors mounted two different FPCB although each FPCB has four inductors. The inductor interval distance d between the two inductors can be adjusted by changing the mounting position of two FPCBs. We here define the two inductors as a target inductor, which is a measurement target, and a neighbor inductor.

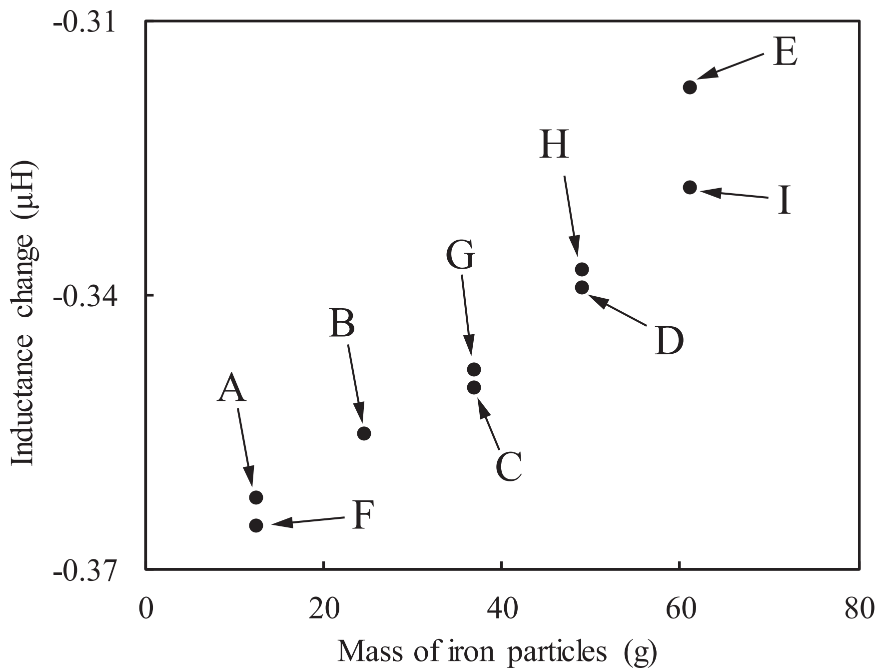

Figure 4.10: Maximum inductance change obtained with the nine different elastomers and the aluminum cube. The characters indicate the type of the elastomer.

This sensor was mounted on the tri-axis robot stage used in the previous experiments. Two inductance-to-digital converters were employed to measure and activate the target and neighbor inductor simultaneously.

First, we investigated the inductance change of the target inductor versus applied normal force when the neighbor inductor was deactivated. The experimental procedure was the same one used in Section 4.3.1. A 6-mm vertical deformation was applied to the surface of the elastomer totally 10 times.

Figure 4.12 shows the inductance change versus applied normal force. The solid line is the average values of the measured inductance across 10 trials, and the shaded gray regions are twice the standard deviation (2σ) of the inductance. The results demonstrates that the inductance monotonically increases with a high repeatability. The maximum change value of the inductance (i.e., the increment value from its initial inductance) was 0.0032 µH when a 6-mm vertical deformation was applied.

Next, we measured the inductance change of the target inductor without applying normal force when the neighbor inductor was activated. Figure 4.13 indicates

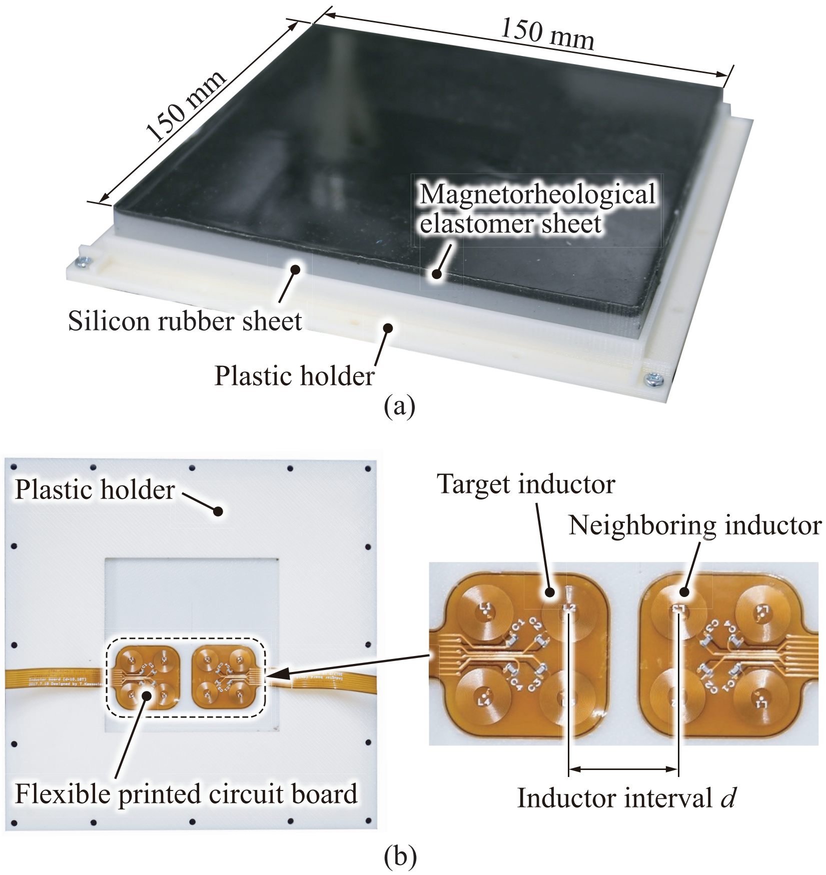

Figure 4.11: An appearance of the fabricated sensor for investigating the interference between two inductors: (a) appearance of the sensor; (b) bottom view of the sensor. The sensor consists of a mangetorheological elastomer sheet, a non-magnetic elastomer sheet, and flexible printed circuit boards holding spiral inductors.

the inductance change (i.e., the increment value from its initial inductance) versus the inductor interval distance d between the target and neighbor inductors. In this experiment, the distance d was changed from 10 mm to 30 mm with an interval of 5 mm; and the inductance was measured 10 times in each condition. The black dots are the average values of the measured inductance across 10 trials, and the error bars are twice the standard deviation (2σ) of the inductance. For reference, the dotted line is the inductance change when a 6-mm vertical deformation was applied, as measured the above experiment. The result shows that the inductance of the target inductor increased by activating the neighbor inductor even though no normal force was

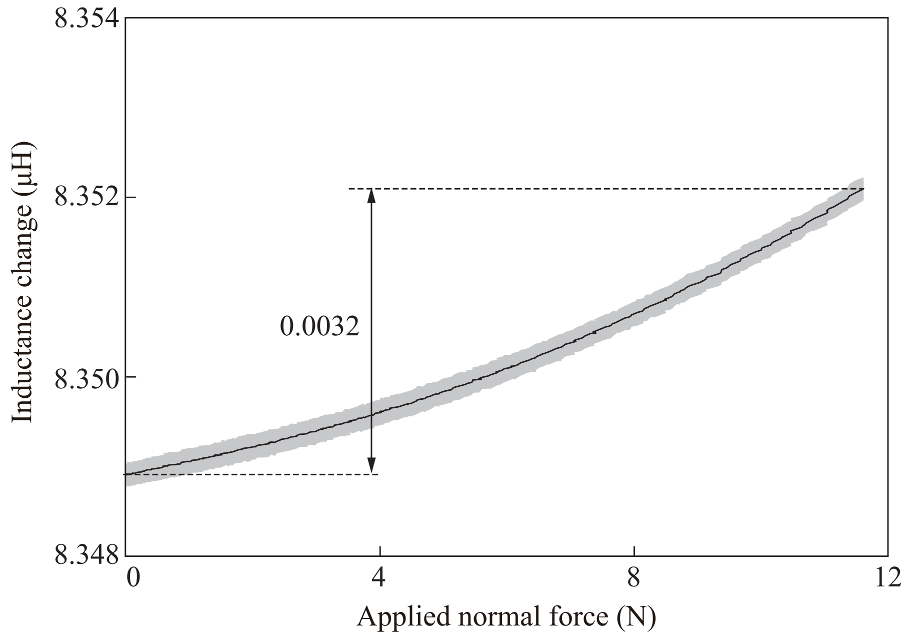

Figure 4.12: Inductance change versus the applied normal force across 10 trials. The solid line and shaded gray region indicate the mean value of the inductance and twice the standard deviation (2σ) of inductance, respectively. The inductance monotonically increases with the applied normal force.

applied. This amount of the inductance change was rapidly decayed in accordance with the inductor interval distance d. In addition, the error bar (i.e., 2σ value) was significantly small compared to the amount of the inductance change. Therefore, the activation of the neighbor inductor causes the increment of the inductance of the target inductor with a high repeatability.

We also investigated that whether the applied normal force affects the amount of the inductance change caused by activating the neighbor inductor. Figure 4.14 shows the comparison between the inductance changes versus the applied normal force when the neighbor inductor activated or not. This experiment also employed the same procedure described in Section 4.3.1; a vertical deformation of 6 mm was applied to the sensor surface. The inductor interval distance d was fixed to 20 mm which provides the small inductance change by activating the neighbor inductor compared to the one by applying normal force, as shown in Fig. 4.13. The black dotted line and gray solid line are the average values of the measured inductance when neighbor

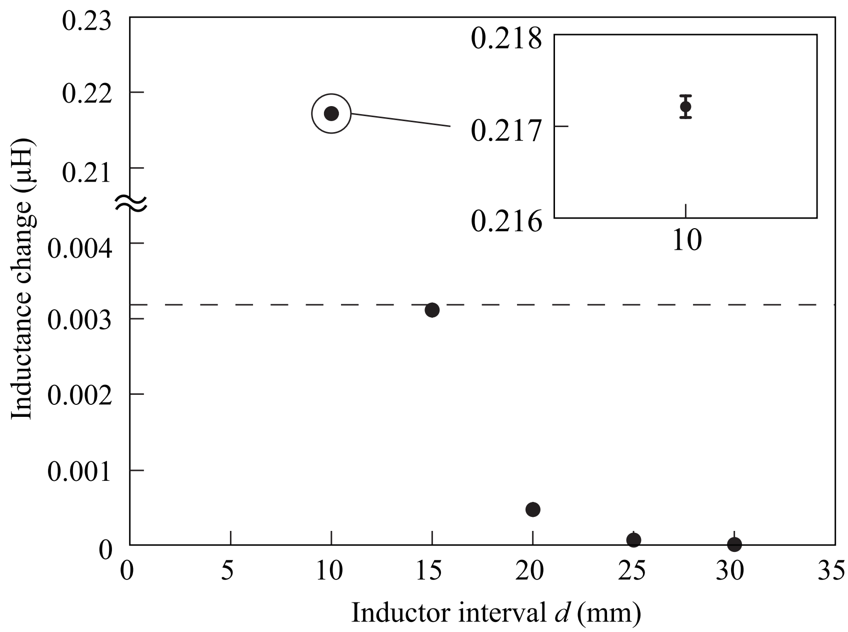

Figure 4.13: Inductor interval distance d versus inductance changed caused by the interference of two inductors. The dots and their error bars indicate the mean value and twice the standard division (2σ) of measure inductance change across 10 trials. For reference, the dotted line indicate the inductance change when a vertical deformation of 6 mm is applied.

inductor is deactivated or activated across 5 trials, respectively. Both the sensor response curve were well matched regardless of the amount of the applied vertical deformation. Therefore, interference between the two inductors can be suppressed by placing the two inductors with the inductor interval distance d which is enough to ignore the inductance change caused by activating the neighbor inductor.

4.4 Discussions

The monotonic response of the sensor indicates that the proposed sensor can measure the applied normal force by using only the inductor as a sensing transducer. Since the inductor can be easily implemented by the traces of a circuit board, the sensor can be fabricated at a lower cost compared with our previously proposed sensor using a magnetic sensor and magnet. The advantage is that a circuit board itself becomes the transducer without specific technologies.

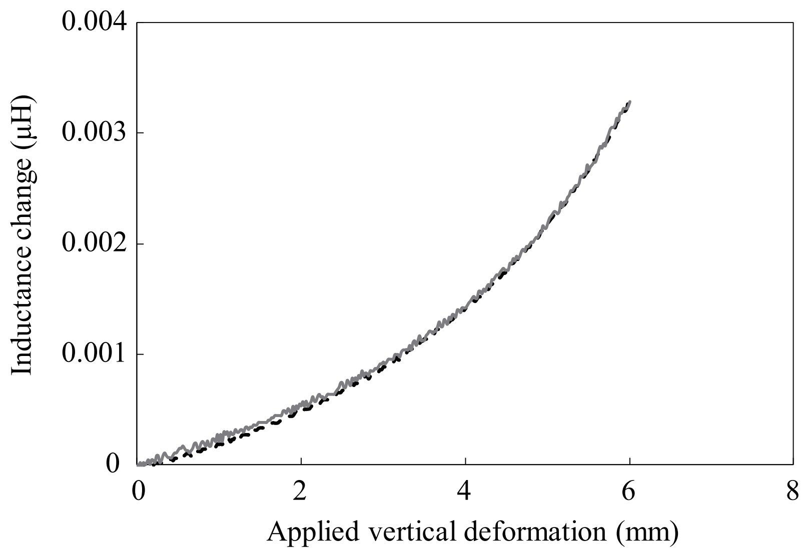

Figure 4.14: Inductance change versus applied vertical deformation. The solid and dotted lines indicate the mean value of measure inductance change when a neighbor inductor with an interval of 20 mm was driven or not driven across 5 trials, respectively.

The second experiments revealed that the spatial shape of the response was point-symmetric and bipolar. However, there was a slight distortion in the point-symmetric response for the negative response region. This distortion could be caused by the slightly nonuniform distribution of the iron particles in the handmade MRE layer due to the high sensitivity of the proposed sensor. The results also demonstrate that a negative response occurs when the sensor surface is pushed down at a certain distance from the inductor. This negative response can be explained by the following two mechanisms: 1) MRE stretching above the inductor decreases the permeability; thus, this lowers the inductance, which causes the negative response. Such MRE stretching can occur when the MRE is pushed down at some surface point because the MRE is stretched to the side and thinned; 2) BE bulging occurs around the inductor, in which the distance between the MRE and the inductor is extended by the BE, thereby causing the negative response. Such bulging can occur around the edge of the pushed region because the elastomer layers of the sensor are made of an incompressible material. Further analyses (e.g., observation of surface bulging) are required to conclude which mechanism causes the negative response. The bipolar response could be useful for detecting contact regions. In general, tactile sensor responses contain no information about the contact points, e.g., it is difficult to discriminate between a small force applied near the sensor and a large force applied far from the sensor. In contrast, the negative response of the proposed sensor indicates that the contact point is a certain distance from the inductor. Thus, the proposed sensor could express the information of a contact point, which could help to detect contact regions.

Table 2 indicates that small inductor has small inductance changes, and the SNR gradually decreased with the diameter. These results suggest a trade-off between the SNR and the density of the inductor layout. On the other hand, the diameters of the positive and negative response regions were larger than the inductor diameter. This is because the elastomer surface near the inductor smoothly deforms even though a contact force is applied to a region far from the inductor. Such a large response region can be utilized for a superresolution method [89] that can enhance the spatial resolution, even with a spatially sparse layout of the inductor. In future works, this method will be employed to balance the SNR and the spatial resolution.

4.4.1 Sensor response caused by approaching metallic materials

In the proposed sensor, the inductance decreased in accordance with approaching metallic cubes. This is because an eddy current is generated in the approaching metallic cubes [90]. The generated eddy current in the cubes occur in a direction to cancel the magnetic field originally generated by the inductor, resulting in a decrease in inductance. Since the amount of generated eddy current increases in accordance with the distance between the cubes and inductor, the decrement of the inductance also increases as the approach of the cubes. The decrement of the inductance differs depending on the type of metal because the amount of generated eddy current varies depending on the material properties of each metal.

The experiments using MRE sheets with different thickness and volume ratio of iron particles demonstrated that the decrement of the inductance cause by the approach of metal cubes decreased by using thick MRE sheet and/or with high volume ratio of iron particles. In contrast, Fig. 4.10 indicates that this decrement of the inductance is proportional to the mass of the iron particles contained in the MRE sheet. The decrements of the inductance were almost the same among the MRE sheets which contain the same mass of iron particles (as shown in Table 4.3.3, the type H and D MRE sheets have the same mass of the iron particles of 48.8 g although these MRE sheets have different thicknesses and volume ratios) That is, even if the thickness of the MRE sheet and the volume ratio of iron particles are different, if the mass of the contained iron powder is the same, almost the same reduction amount is shown These results suggests that it is important to employ a large amount of iron particles in the MRE sheet in order to reduce the decrement of the inductance caused by the approach of metallic materials.

4.4.2 Interference between two inductors

The experimental results demonstrates that the inductance of the target inductor increased when the neighbor inductor was activated. The inductance of the target inductor is determined by the amount of the magnetic flux penetrating the target inductor. When the neighbor inductor is activated, another magnetic flux generated by the neighbor inductor could enhance the magnetic flux generated by the target inductor. In addition, this strength of the enhancement could be large when both the inductor will placed close. This could be a feasible mechanism explaining that the inductance of the target inductor increases when the neighbor inductor is activated. Another feasible mechanism is that a mutual inductance between the two inductors could be added both the inductors. One of the future work is to discuss the electromagnetic phenomena occurred by approaching two activated inductors.

The increment of the inductance (here we define ΔN) caused by the activation of the neighbor inductor has a high repeatability across 10 trials. Therefore, given both the inductor interval d and the activation status of the neighbor inductor, this increment ΔN could be compensated. However, it is difficult to know when and which inductor is activated in a large amount implementation of the inductor for a large scale tactile sensation. This is because that the synchronization of large amount of inductance-to-digital converter makes a measurement system complicated.

A feasible approach to avoid the interference is to place two inductors with an enough distance d in which the increment of the inductance by activating the neighbor inductor ΔN is sufficiently small compared to the increment of the inductance by applying contact force (we define here ΔS). As shown in Fig. 4.12, the maximum ΔS was 0.0032 µH when a vertical deformation of 6 mm was applied. In comparison with these ΔS and ΔN, ΔN was larger than ΔS with the inductor interval d of less than 15 mm. Therefore, when two inductors are placed with the d of less than 15 mm, it is difficult to discriminate the inductance change caused by the applying contact force or activation of the neighbor inductor. In contrast, ΔN was enough smaller than ΔS with the inductor interval d of over 20 mm. In addition, Fig. 4.14 demonstrates that this relationship did not change when contact force was applied. Consequently, in this setting, two inductors should be placed with d of over 20 mm to avoid the interference.

As we discussed above, the interference can be avoided by placing inductors with an inductor interval of over 20 mm when employed an inductor with a diameter of 10 mm. In contrast, the spatial density of inductors determines spatial resolution of measurable contact force distribution. Therefore, a certain application may require more high density spatial implementation of inductors. Here, important characteristics are spatial response region of each inductor and the degree of overlapping their spatial response regions. The experiments investigated the spatial response region of an inductor with a diameter of 10 mm, and found that the response region was circular with a radius of 12 mm from the center of the inductor. This suggests that there are overlapping portions in some response regions even if the inductors are placed with an interval of 20 mm. Lepora et al. [89] demonstrated that the spatial response between the two sensors can be interpolated using a tactile superresolution technology by providing overlap in the response regions of the two tactile sensors, and therefore the spatial resolution can be high compared to the spatial density of the sensors. Even in our proposed sensor, there is a possibility that the degradation of the spatial resolution, which occurs when the distance between the inductors is increased in order to avoid interference, could be interpolated using such a tactile superresolution technique. This is also a future work for achieving a high spatial resolution without an interference.

4.5 Summary

This chapter proposed a tactile sensorization method of a magnetorheological elastomer based on an inductance measurement. We investigated the sensor responses with the real experiments using the fabricated sensors. The obtained results can be summarized as follows:

1. the sensor can measure the applied normal force with low noise (an SNR of 53 dB), even though the sensor structure is very simple and easy to fabricate.
2. the sensor has a point-symmetric bipolar spatial response whose center corresponds the center of the inductor.
3. the sensor has a trade-off between the diameter of the response region and its SNR.
4. the inductance decreases in accordance with the approach of metallic materials because of a generated eddy current in the metallic material.
5. a magnetic interference between inductors increases inductance, and the amount of increase is large with the short distance between the inductor.

We will try to mount such inductors onto a flexible printed circuit board for implementing the sensor onto a complex surface such as robot skin. In other future work, the three-axis forces will be obtained by improving the sensor structure.

Chapter 5

Tri-axis tactile sensorization with four inductors

This chapter describes a tri-axis tactile sensorization method, and a flexible and soft tactile sensor that measures the tri-axis force based on inductance measurement. The proposed sensor has four spiral inductors printed on a flexible circuit board and a mounted cylindrical elastomer (silicon rubber). A disk-shaped magnetorheological elastomer (ferromagnetic marker) is embedded in the cylindrical elastomer and its three-dimensional displacement is estimated by monitoring the inductance changes of the four inductors. In this study, we investigated the relationship between the applied tri-axis force and inductance changes. Our results can be summarized as follows: (1) the inductance changes of the four inductors were monotonic and linear against the applied normal and shear force; (2) the applied tri-axis force could be estimated well with linear functions of the sum and difference of the measured inductances; (3) the estimation error of the tri-axis force increased when a larger force was applied and/or faster contact speeds were used.

5.1 Background

Flexible and soft tactile sensors play important roles in robotic systems interacting with unknown objects. A number of studies have proposed various types of tactile sensors (see reviews [17,18,91]) using elastic materials as their surface coverings. This is because flexible and soft sensor surfaces can fit the complex surfaces of objects safely both for the objects and the robot itself. In contrast, sensors containing soft materials suffer from several technical issues related to deteriorations in the fundamental properties of tactile sensors such as durability, sensitivity, and mechanical simplicity.

As one solution for these issues, we previously proposed and developed a flexible tactile sensor in which a sheet-shaped magnetorheological elastomer (MRE), which is a ferromagnetic silicon rubber, is laminated on a sheet-shaped silicon rubber covering a flexible circuit board with a spiral inductor, as described in Chapter 4. Because the MRE contains iron particles with a high magnetic permeability, the distance between the MRE and inductor determines its inductance. Thus, the inductance increases/decreases in accordance with the descent/ascent of the MRE around the inductor, respectively. In the previous study, we demonstrated that the sensor could measure applied normal forces by monitoring the inductance of the inductor. The advantages of this sensor can be summarized as follows: 1) high durability–it has a durable structure against shocks and heavy loads because the flexible and soft surface where the contact force is applied contains no fragile electric transducers or wiring; 2) high sensitivity–it is sensitive to small forces because it directly captures surface deformations of the outermost soft MRE layer; 3) simple structure–its structure is simple and damaged surfaces are therefore easy to replace because the surface elastomer sheets are placed on the circuit board without any wire connections.

One of the biggest remaining issues is that the sensor cannot measure the tri-axis force, because of its structure. In this study, we improve the tactile sensor so that it can measure the tri-axis force without deteriorating the above advantages of the sensor. As shown in Fig. 5.1, the proposed tri-axis tactile sensor consists of four inductors, a disk-shaped MRE (hereafter called ferromagnetic marker or marker), and a cylindrical elastomer made of a silicon rubber. In this structure, applied normal and shear forces cause a vertical and horizontal displacement of the ferromagnetic marker, respectively. As a result, the inductances of the four inductors indicate the three-dimensional (3D) position of the ferromagnetic marker. It is expected that: 1) the summation value of all inductances indicates the magnitude of an applied normal force because the vertical distances between the marker and every inductor decrease simultaneously; 2) the difference of the four inductance values indicates the direction

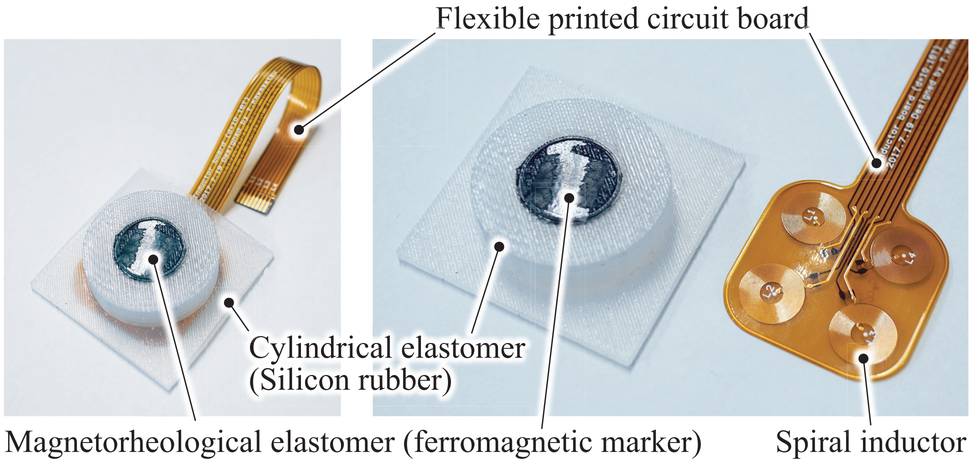

Figure 5.1: Appearance of the proposed tri-axis tactile sensor. The sensor consists of four spiral inductors printed on a flexible printed circuit board (FPCB) and a disk-shaped magnetorheological elastomer (MRE; ferromagnetic marker) embedded in a cylindrical elastomer made of a silicon rubber. The inductances of the inductors are determined by the positional relationship between the ferromagnetic marker and each inductor because the marker contains iron particles with a high magnetic permeability. Therefore, the sensor can estimate applied tri-axis forces by monitoring the inductance changes caused by three-dimensional (3D) displacements of the marker.

and magnitude of an applied shear force because the horizontal distances between the marker and every inductor decreases or increases depending on the positions of the inductors. In contrast, the ferromagnetic marker itself is deformed by the contact force because the marker is made with a highly flexible and soft silicon rubber. Such deformation of the ferromagnetic marker might affect the expected inductance changes mentioned above. In addition, the non-linear rubber elasticity might cause a nonlinear change in inductance. Therefore, the relationship between the applied tri-axis force and inductance should be investigated to enable the measurement of the tri-axis force.

In order to investigate this relationship, we measured the sensor responses by using the developed sensor. The results can be summarized as follows: 1) the inductance changes of the four inductors were monotonic and linear against an applied normal and shear force; 2) the applied tri-axis force could be estimated well with linear functions of the sum and difference of the measured inductances; 3) the estimation error of the tri-axis force increased against a larger force or faster contact speeds.

5.2 Proposed Tri-axis Tactile Sensor

This section provides details of the developed sensor and its sensing mechanism.

5.2.1 Developed sensor

We developed a four-inductor array to measure displacements of the ferromagnetic marker. As shown in Fig. 5.2(a), each inductor is printed on a flexible printed circuit board (FPCB) as a thin two-layer spiral inductor. In this study, we employed an FPCB manufacturing service (P-ban.com Corp., Japan). The FPCB is 30-mm wide, 30-mm long (except for the connecter part), and 12.5-µm thick. Each inductor has a diameter of 10 mm, and the number of turns is set to 16 in each layer. The trace width and spacing between the traces are both 100 µm. The thickness of the trace is set to 35 µm. In this study, we employed an inductance-to-digital converter that measures the inductances by detecting the resonant frequency on an LC parallel resonance circuit. Hence, a ceramic capacitor with a capacitance of 330 pF was connected in parallel with each inductor.

The design parameters of an inductor, such as the width and thickness of a trace, and the spacing between the traces, were determined to achieve a high Q factor in the LC parallel resonance circuit (please refer to [90] for more information). The trace width and spacing between traces should be narrow because the number of turns can be increased to achieve a high sensitivity. Therefore, we determined the width and spacing as 100 µm, which is the minimum value acceptable for the manufacturing service. In contrast, the thickness of the traces should be thick as much as possible because the parasitic resistance of the inductor should be reduced to achieve a higher Q factor. Therefore, we determined the thickness as 35 µm, which is the maximum value acceptable for the manufacturing service. As a reference, the Q factor in this study was 28.3 at a resonance frequency of 3.22 MHz, which was calculated by an inductor design tool [90].

Four inductors are arranged at equal intervals of 15 mm in the x- and y-directions, as illustrated in Fig. 4.1(b). Figure 4.1(c) shows an illustration of the sensor configuration for the experiments in this study. A plastic holder supports both the cylindrical elastomer containing the ferromagnetic marker and the FPCB containing the inductors. The bottom surface of the marker is raised by 8 mm from the FPCB top surface. The diameter and thickness of the ferromagnetic marker are set to 15 and 3 mm, respectively, while the diameter and thickness of the cylindrical elastomer are 30 and 10 mm, respectively. The ferromagnetic marker and cylindrical elastomer are composed of a platinum-cured silicone rubber (Ecoflex 00-30, Smooth-On, Inc., USA). To construct the ferromagnetic marker, iron particles with a diameter of 50 µm were mixed with the platinum-cured silicon rubber at a volume ratio of 40% before curing, and was poured into a disk-shaped female mold until cured (Fig. 5.3 (a)). Subsequently, the ferromagnetic marker was placed at the bottom of another female mold, and the platinum-cured silicon rubber was poured into the mold until cured (Fig. 5.3 (b)).

5.2.2 Sensing mechanism

The aggregation of iron particles are supported elastically on the inductors in the proposed sensor. Because the ferromagnetic marker containing iron particles function as a magnetic core for the inductors, the positional relationship between the marker and inductor determines its inductance (see also [92]). As shown in Figs. 5.1 and 5.2, the ferromagnetic marker is placed in the center of the four-inductor array where the marker is slightly raised from the array surface. Because the tri-axis force applied to the sensor surface causes a 3D displacement of the marker above the inductors, their inductances change in accordance with the distance between the marker and each inductor. In this structure, vertical displacements of the marker along the z-axis induced by the normal force F_z will increase the inductances of all the inductors. In contrast, horizontal displacements of the marker along the x- or y-axes induced by shear forces F_x or F_y will increase/decrease the inductances of the inductors where the marker approaches/departs.

We assume that the applied force can be approximated by calculating the summation and difference of the four inductances as follows:

$$\begin{aligned} L_x &= (L_1 + L_4) - (L_2 + L_3) \\ L_y &= (L_1 + L_2) - (L_3 + L_4) \\ L_z &= L_1 + L_2 + L_3 + L_4 \end{aligned} \tag{5.1}$$

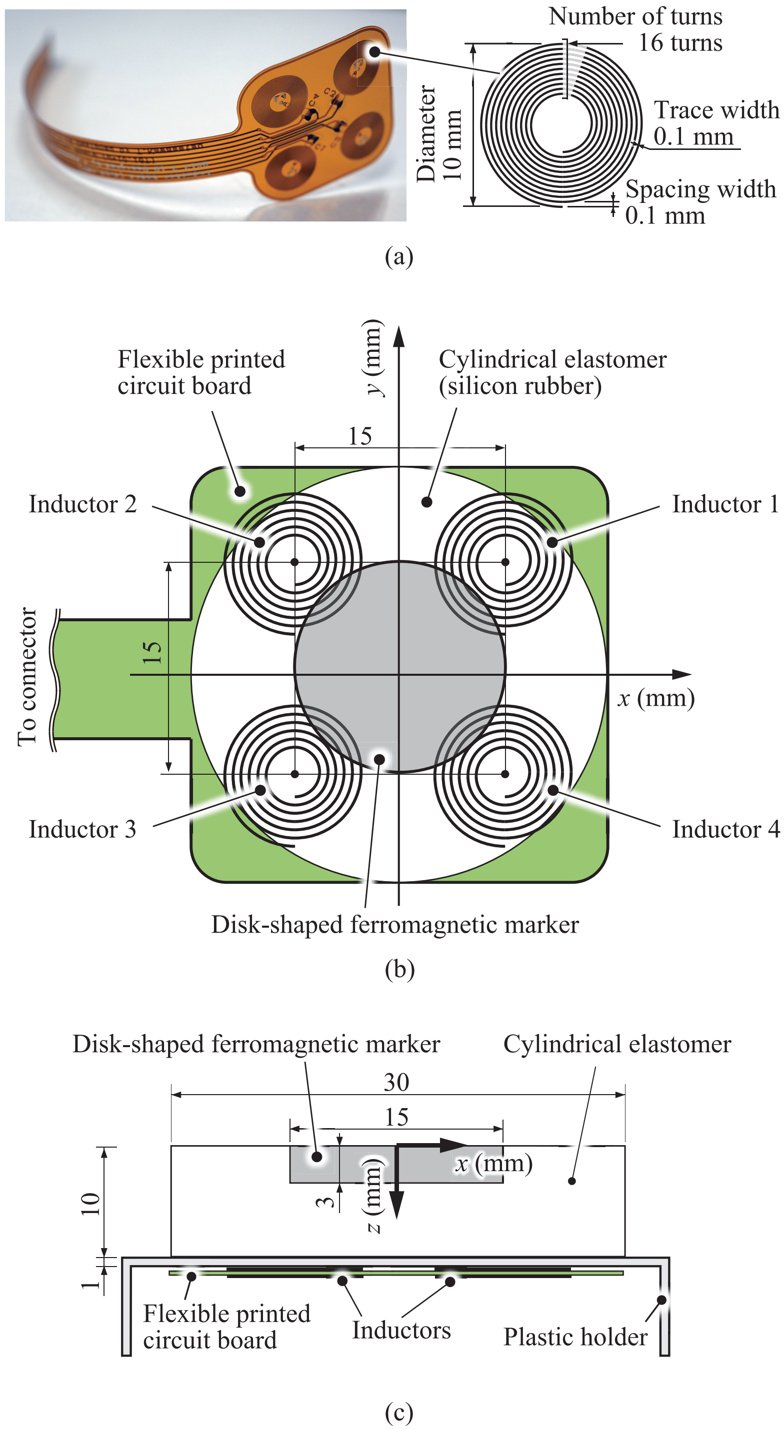

Figure 5.2: Schematic and design parameters of the developed tri-axis tactile sensor: (a) Design parameters for an inductor printed on the FPCB; (b) arrangement of inductors and ferromagnetic marker in x-y plane; (c) arrangement of inductors and ferromagnetic marker in x-z plane.

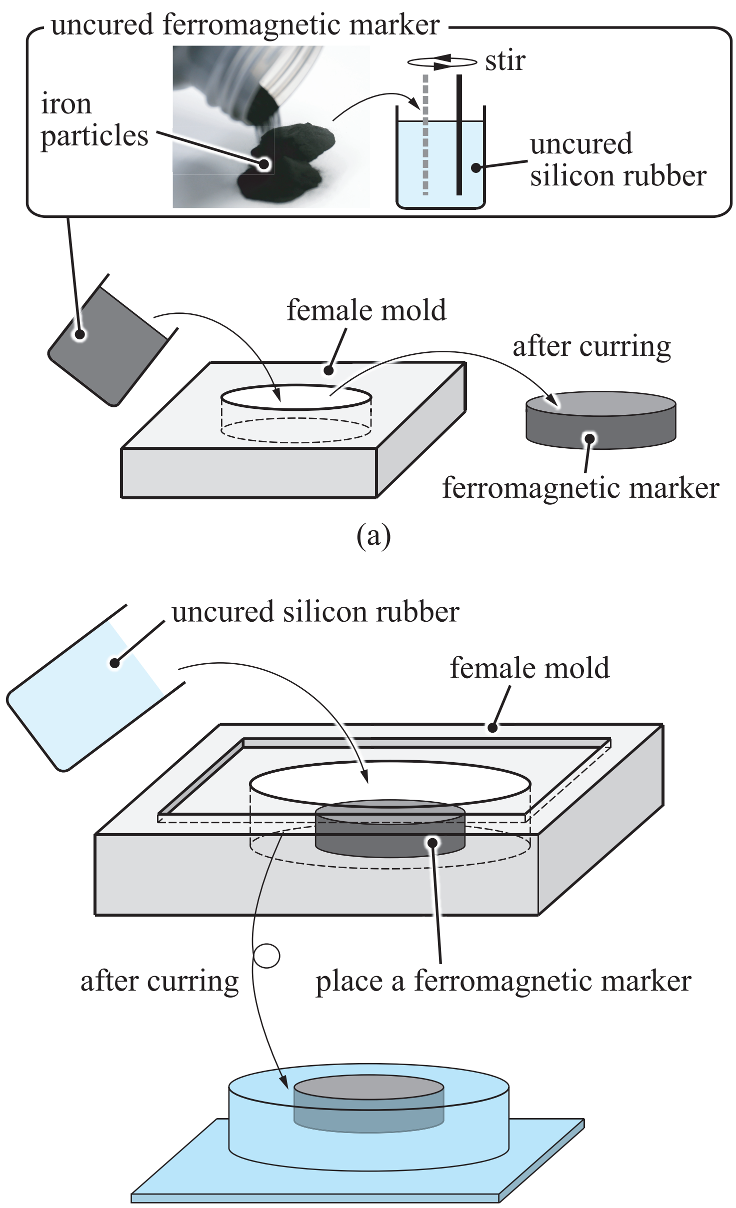

(b)

Figure 5.3: Fabrication processes: (a) a ferromagnetic marker; (b) a cylindrical elastomer containing the ferromagnetic marker.

where L_i is the measured inductance of the i-th inductor. L_x and L_y are the differences in inductances along the x- or y-axes, while L_z is the summation of all inductances. The tri-axis forces F_x, F_y, and F_z are considered to be estimated from these converted inductances L_x, L_y, and L_z, respectively, by determining the relationship between these values.

5.3 Experiments

The sensor response versus applied tri-axis force was measured with the experimental setup illustrated in Fig. 5.4. The developed sensor is attached to a tri-axis robot stage (TTA-C3-WA-30-25-10, IAI Corp., Japan) holding a force–torque sensor (F/T sensor; Mini 2/10-A, BL Autotech Ltd., Japan). As a contact target, a flat surface plastic indenter is attached to the tip of the F/T sensor. A personal computer (PC) captures the outputs of the F/T sensor via a 16-bit analog-to-digital converter (AI-1664LAX-USB, CONTEC Corp., Japan). A 28-bit inductance-to-digital converter (LDC1614EVM [90], Texas Instruments Corp., USA) captures the inductances of the sensor and sends their values to the PC via an Arduino board (Arduino Uno, Italy). In this experiment, the inductances of four inductors were measured one-by-one by switching the inductor activated with 200 µA. The sampling period of both outputs of the F/T sensor and converted inductances was set to 20 ms.

Before the experiments, we measured the initial inductances of the four inductors, i.e., inductances under no load; the inductances were as follows: $L_1 = 8.2053$, $L_2 = 8.2588$, $L_3 = 8.1966$, and $L_4 = 8.2516$ µH.

5.3.1 Sensor calibrations

We investigated the sensor responses versus the applied tri-axis force to determine the relationships between the tri-axis force and the converted inductances calculated using Eq. 1. First, the normal force F_z was applied to the sensor by lowering the indenter at a speed of 0.1 mm/s until the surface of the sensor descended to a depth of 2.5 mm. Figure 5.5 shows the changes in the converted inductance L_z versus the applied normal force F_z. The measured shear forces F_x and F_y and converted

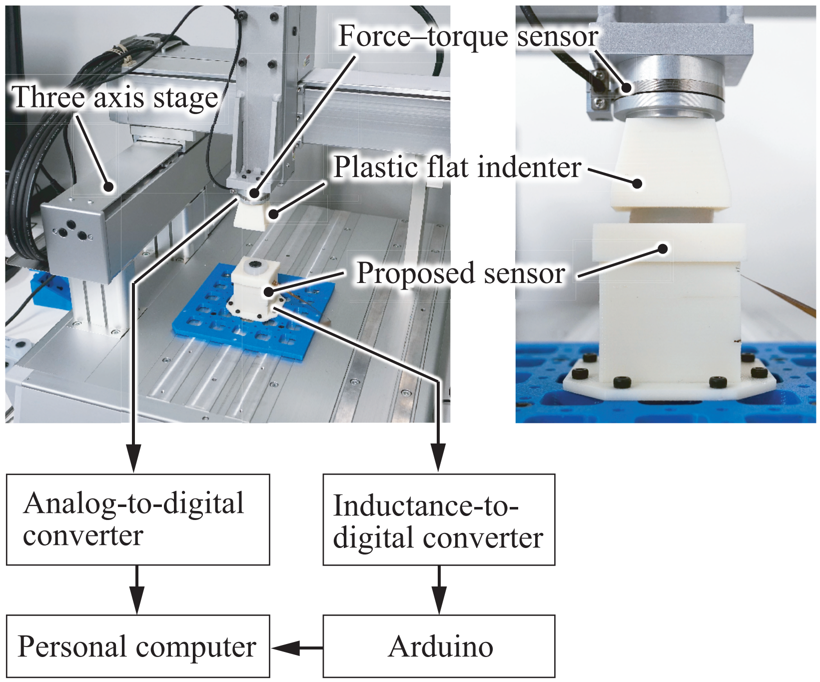

Figure 5.4: Experimental setup for investigating the sensor responses. The proposed sensor is mounted on a three-axis robot stage holding a force–torque sensor (F/T sensor). Contact force is applied to the sensor using a plastic flat object attached to the tip of the F/T sensor. An inductance-to-digital converter measures the inductances and sends them to a personal computer (PC), while an analog-to-digital converter captures the output of the F/T sensor and sends it to the PC.

inductances L_x and L_y are also depicted for reference because F_x and F_y were lightly applied to the sensor surface even when the application of F_z was intended. The solid line and shaded gray regions indicate the mean value and twice the standard deviation (2σ) of each inductance value across 10 trials, respectively. The dotted line indicates the mean value of the measured shear forces F_x and F_y across 10 trials. The result demonstrates that the value of L_z monotonically and linearly increases with the applied normal force F_z, while the values of L_x and L_y do not significantly increase with F_z. Therefore, the applied normal force F_z can be estimated by employing a linear function of L_z, i.e., the summation of the four inductances.

Next, the shear forces F_x and F_y were applied to the sensor with the following procedure: (1) apply a vertical deformation of 1 mm before applying a shear force; (2) horizontally move indenter ± 6 mm from the origin along x- or y-axes. Figure

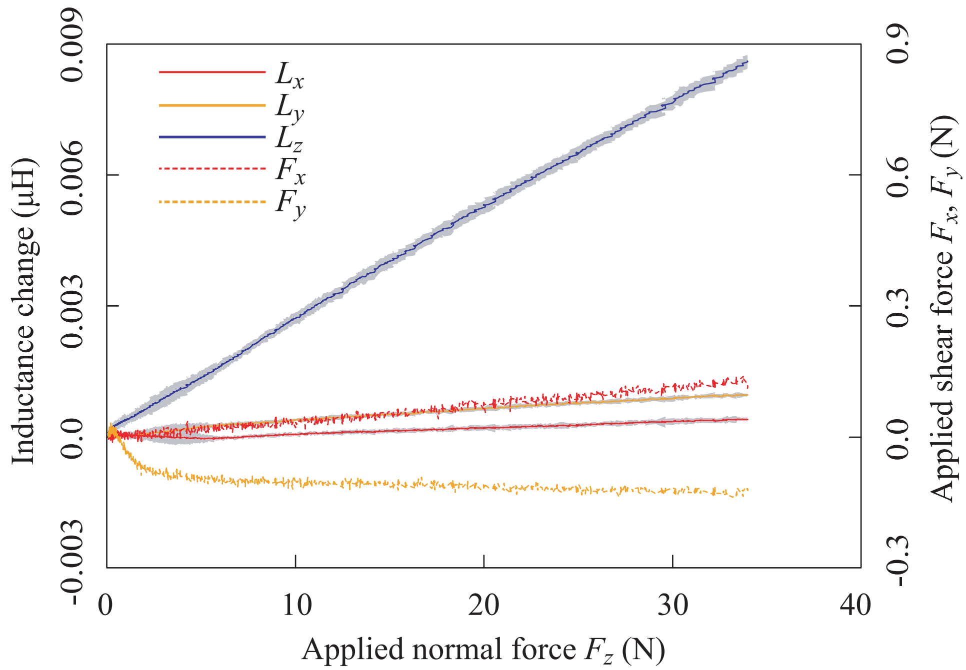

Figure 5.5: Converted inductances L_x, L_y, and L_z versus the applied normal force F_z across 10 trials. The solid and dotted lines indicate the mean value of the converted inductance and applied shear force, respectively. The shaded region indicates twice the standard deviation (2σ) of each inductance. The inductance value L_z increases with the applied normal force, while L_x and L_y do not significantly increase.

5.6 shows the converted inductance L_x versus the applied shear force F_x, while Fig. 5.7 shows the converted inductance L_y versus the applied shear force F_y. In these plots, the other measured axis force and converted inductances are also depicted for reference. The solid line and shaded regions indicate the mean value and twice the standard deviation (2σ) of each inductance across 10 trials, respectively. The dotted line indicates the mean value of the other measured axis force across 10 trials. These results indicate that the values of L_x and L_y also monotonically and linearly increase with the applied shear force F_x and F_y. Therefore, the applied shear forces F_x and F_y can also be estimated by employing a linear function of L_x and L_y, i.e., the difference of the four inductances (Eq. 1).

From these results, the tri-axis force applied to the proposed sensor can be estimated based on the three converted inductance values of L_x, L_y, and L_z because these values monotonically, linearly, and almost independently increase in accordance

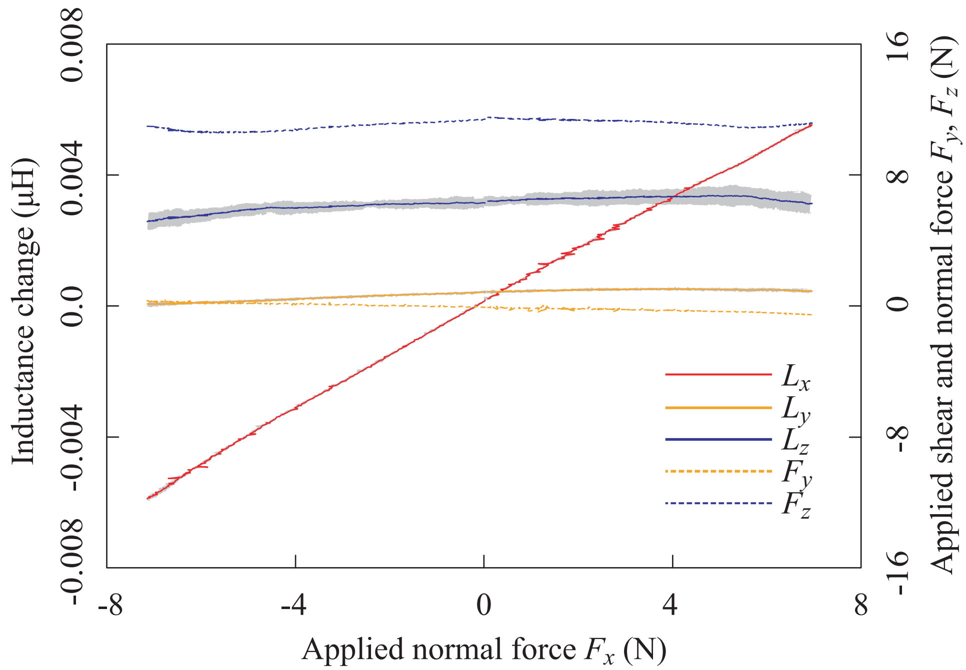

Figure 5.6: Converted inductances versus the applied shear force F_x across 10 trials. The solid and dotted lines indicate the mean values of the converted inductance and applied shear and normal force, respectively. The shaded region indicates twice the standard deviation (2σ) of the inductance. The result demonstrates that the converted inductance value L_x increase in accordance with the applied shear force F_x, while L_z does not significantly increase.

with the applied shear forces F_x and F_y, and normal force F_z, respectively. Thus, the tri-axis force can be simply estimated from these inductance values as follows:

$$\begin{aligned} F_x &= a_x L_x + b_x \\ F_y &= a_y L_y + b_y \\ F_z &= a_z L_z + b_z \end{aligned} \tag{5.2}$$

where a_i and b_i are constant values. A least-squares method was applied to obtain these constant values; these values were estimated as follows by using the results presented in Figs. 5.5, 5.6, and 5.7: $a_x = 1.239 \times 10^3$, $b_x = -0.05104$, $a_y = 1.192 \times 10^3$, $b_y = -0.4377$, $a_z = 3.889 \times 10^3$, and $b_z = -0.4855$. In addition, the fitting errors R were $R_x = 0.9961$, $R_y = 0.9900$, $R_z = 0.9989$.

To evaluate the measurement noise, we calculated the maximum variance of L_x,

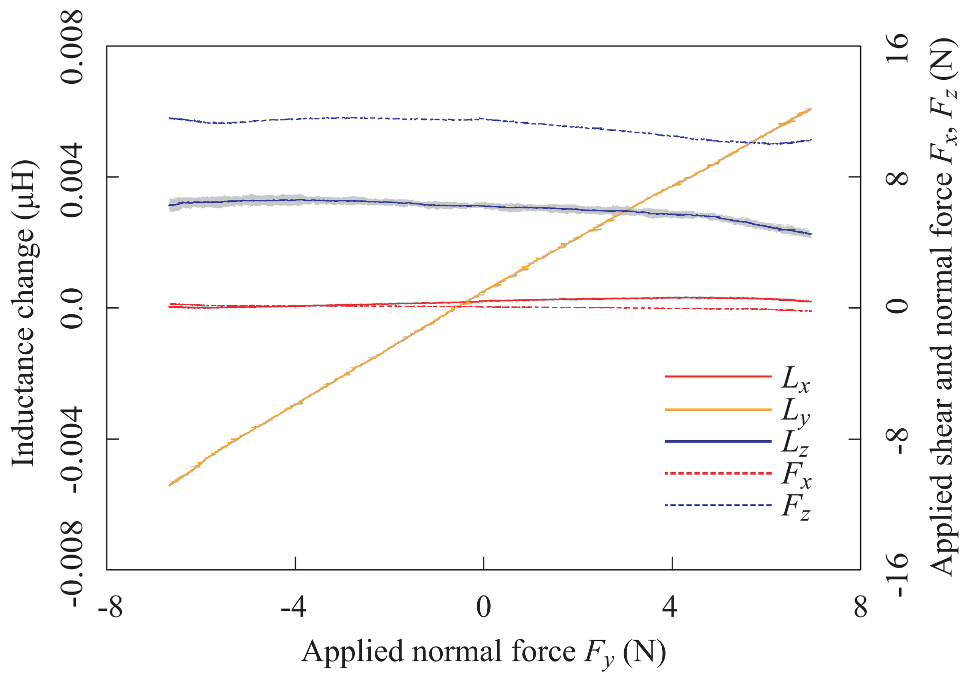

Figure 5.7: Converted inductances versus the applied shear force F_y across 10 trials. The solid and dotted lines indicate the mean values of the converted inductance and applied shear and normal force, respectively. The shaded region indicates twice the standard deviation (2σ) of the inductance. The result demonstrates that the converted inductance value L_y increase in accordance with the applied shear force F_y, while L_z does not significantly increase.

L_y, and L_z when applying F_x, F_y, and F_z, respectively; these values were 3.445×10^{-9}, 1.237×10^{-8}, and 1.427×10^{-8} μH^2 for L_x, L_y, and L_z, respectively. From Figs. 5.6 and 5.7, the small 2σ regions of L_x and L_y compared to their range of inductance change demonstrate a high repeatability of those inductances across 10 trials. In contrast, the 2σ region of L_z shown in Fig. 5.5 is larger compared with that of L_x and L_y. In addition, the signal-to-noise ratio (SNR) was evaluated using the following equation: $20\log10(A_S/A_N)$ where A_S is the maximum peak-to-peak inductance change from the initial inductance and A_N is the maximum peak-to-peak inductance change under no load. The SNRs of L_x, L_y, and L_z were 40.77, 42.53, and 34.19 dB, respectively. To evaluate the sensitivity of the sensor, we calculated the minimum detectable force S for three orthogonal directions; these values can be calculated using the results in Figs. 5.5, 5.6, and 5.7, as well as the obtained noise levels: $S_x = 94.4$ mN, $S_y = 173$

mN, and $S_z = 444$ mN.

5.3.2 Tri-axis force sensing

We next evaluated the estimated tri-axis force based on the obtained relationship between the applied force and inductance change, as described in Section IV-A. The tri-axis forces were simultaneously applied to the sensor with the following procedure:

1. apply a vertical deformation of 0.5 mm with a contact speed of 20 mm/s.

2. horizontally move indenter to the position $(x, y) = (3, -3)$ with a contact speed of 1 mm/s.

3. move indenter to the position $(x, y) = (-3, 3)$ with a contact speed of 20 mm/s

4. apply additional 0.5-mm vertical deformation with a contact speed of 20 mm/s.

5. repeat 2) to 4) until the applied vertical deformation reaches 2 mm.

Figure 5.8 represents the relationship between the estimated force and applied tri-axis force versus time. The solid gray line indicates the applied tri-axis force F measured with the F/T sensor, while the solid black line indicates the estimated tri-axis force F_{est} based on the measured inductances. In addition, the dotted red line represents the estimation error, i.e., $F - F_{est}$, for reference. The result demonstrates a good agreement between the estimated tri-axis force and the applied tri-axis force. However, the estimation error increases under a large applied normal force. In addition, the estimation error is large during the fast contact condition, i.e., during the procedure of (3) described above. To evaluate the estimation error, we calculated the root mean squared errors (RMSE) between the estimated and measured tri-axis forces. We measured the tri-axis force 10 times with the same procedure described above, and obtained the average and variance of the RMSEs, as summarized in table 5.1.

Table 5.1: Root mean squared errors between the estimated and measured tri-axis force across 10 trials

	F_x	F_y	F_z
average (N)	0.455	0.704	1.21
variance (N^2)	0.761×10^2	0.435×10^2	9.49×10^2

5.4 Discussions

This section first summarizes the sensor response curves describing the relationship between the inductance changes and the applied tri-axis force. Then, we discuss the estimation results of the applied tri-axis force based on the assumed linear function. Finally, we summarize the advantages of the proposed sensor.

5.4.1 Sensor calibration and tri-axis force sensing

The experimental results indicate that the proposed tri-axis tactile sensor can measure the three-axis force by monitoring the changes in the inductances from the four inductors. In this study, we define three converted inductance values L_x, L_y, and L_z as the simple summation or difference of the four inductances (Eq. 1), and we found that the relationship between these values and the applied tri-axis force can be given with a simple linear function (Eq. 2), although the sensor consists of a highly soft rubber.

The result in Section IV-B demonstrates that the sensor can estimate the tri-axis force based on the inductance values by using the obtained linear functions described in Eq. 2. We found that the estimation errors increased with the applied normal force. One potential reason for this estimation error could be the deformation of the ferromagnetic marker itself. The marker could deform when a large contact force was applied because the marker itself is composed of a highly soft and flexible silicon rubber. This deformation of the marker will become large under a large applied contact force and cause the estimation error. Therefore, the proposed sensor works well under a contact force that causes little to no deformations of the marker. In this study, the ferromagnetic marker deformed because we employed the same soft silicon rubber with the cylindrical elastomer to construct the ferromagnetic marker. Employing a ferromagnetic marker composed of a hard-type rubber could reduce the deformation of the marker; however, employing such a hard-type rubber deteriorates the softness of the surface rubber. Therefore, one of the issues is that the deformation of the ferromagnetic marker should be reduced without employing the hard-type rubber.

The result also indicates that the estimation error was large during the fast contact condition, e.g., the force curves at about 5, 15, and 25 s in Fig. 5.8. We also found that the estimated force had a time-delay compared to the measured force during the fast contact condition. This time-delay appears to be caused by the viscosity of the employed rubbers because the deformation of the rubbers requires a few transient times because of its viscosity. Therefore, the output of the proposed sensor has a short time delay to the actual applied force. One of the solutions to this issue is the use of another low-viscosity elastic material instead of the silicon rubber holding the ferromagnetic marker (e.g., a soft sponge) as we employed in our previous study [93].

5.4.2 Advantages of the proposed sensor

The structure of the proposed sensor is quite simple: an elastic material holding a rubber with iron particles is simply placed on four spiral inductors. In the proposed sensing mechanism, a trace on an FPCB itself (i.e., an inductor) becomes a tactile transducer. The proposed sensor can be mounted on a complex surface because the sensor only consists of a soft and stretchable surface rubber and a bendable FPCB. In this study, we employed a printed circular spiral inductor as the sensing inductor for the following reasons: first, printed circular spiral inductors enable us to fabricate thin FPCB easier compared to other inductors, e.g. rectangular, triangular spiral coils or wound up coils; second, the spatial response properties of printed circular spiral inductors have been investigated in our previous study [92]. Although the sensing mechanism allows us to employ other inductor shapes, the sensitivity and accuracy of tri-axis force measurements would depend on the inductors type. One of the future issues is to investigate how inductor shape affects its sensor response.

The greatest advantage of the sensor is that the sensor surface is composed of only a soft and stretchable rubber, and this surface rubber can be placed to the outside of the frame containing its measurement circuit inside (as we placed the rubber on the plastic holder holding the FPCB). This separation between the rubber and the FPCB with the corresponding measurement circuits leads to a number of advantages: 1) the fragile elements such as the printed circuits and ceramic capacitors are protected from the contact force to reach. Thus, the proposed sensor has high durability against large contact forces; 2) it is easy to replace its surface when the surface is damaged; 3) the sensor can be used in water, which has an equivalent magnetic permeability as air, because the sensor structure can be waterproof by placing the sensing elements inside a waterproof holder. We are certain these advantages will facilitate a number of applications of the proposed sensor.

5.5 Summary

This chapter introduced a flexible tri-axis tactile sensor using four spiral inductors and a ferromagnetic marker embedded in a cylindrical elastomer made of a silicon rubber. In this study, we measured the sensor responses using the developed sensor in order to investigate the relationship between the applied tri-axis force and inductance changes. The experiments demonstrated that the proposed sensor can simply estimate the applied tri-axis force based on simple linear functions of three converted inductance values, i.e., the summation and difference of four inductances. In contrast, we also found that a large applied force can cause a large estimation error because the soft ferromagnetic marker itself can be deformed with respect to the applied force.

In this study, we mounted an FPCB and rubbers on a flat plastic holder. As one of future works, the proposed sensor could be mounted to an arbitrary surface shape on a complex-shaped surface (e.g., a curved surface) and the effect to its response property upon deformation of the FPCB and rubbers could be investigated. An additional step is to mount the proposed sensor on the tip of a robot hand or body of a robot for further testing. We are certain that the simple-structured proposed sensor of high durability will accelerate the utilization of tactile sensors in robots. One of the issues for future discussions is the extent to which external magnetic sources such as electric motors and movable metallic parts of the robot itself can deteriorate the sensor performance.

The advantage of our sensor for miniaturization is that only the printed inductor circuits and ferromagnetic particles are required in the sensing areas. This simple structure potentially enables us to fabricate a sensor with a smaller taxel size and thinner thickness than the ones fabricated in this study. This miniaturization is one of our future issues.

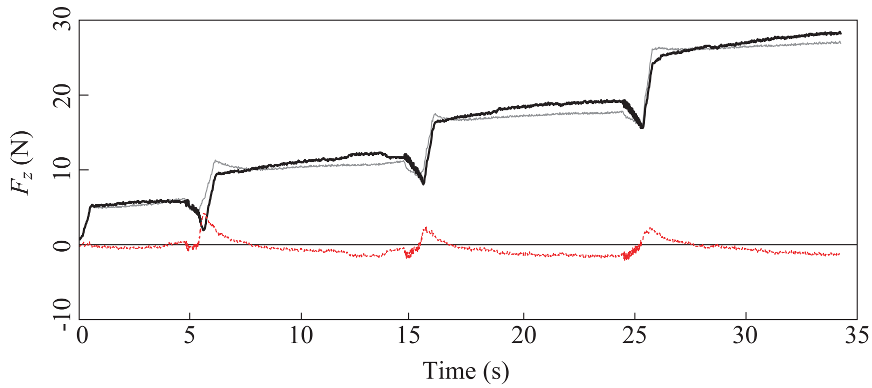

(a)

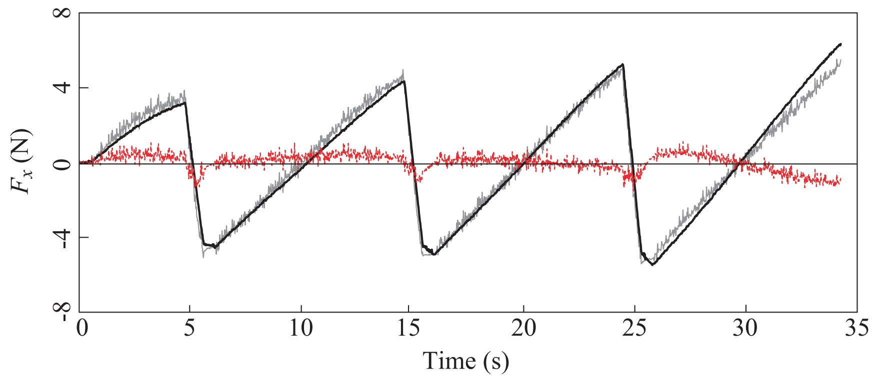

(b)

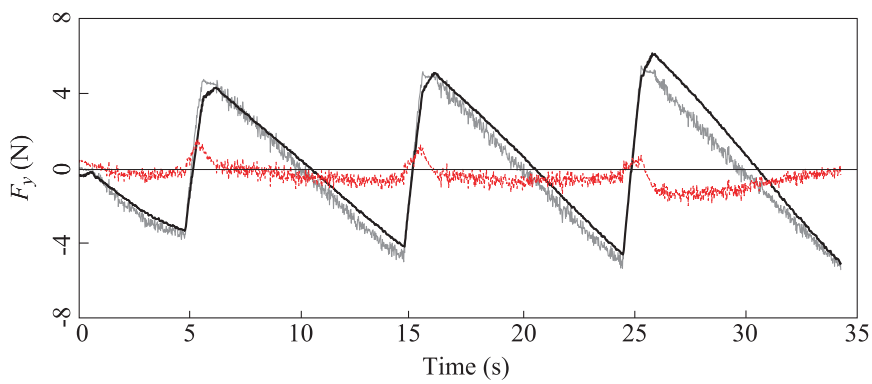

(c)

Figure 5.8: Comparison between measured and estimated tri-axis force applied to the proposed sensor: (a) applied normal force F_z versus time; (b), (c) applied shear force F_x and F_y versus time, respectively. The solid gray line indicates the measured tri-axis force with the F/T sensor (i.e., reference force), while the solid black line indicates the estimated tri-axis force based on the measured inductance values. The dotted red line indicates the estimation error (i.e., difference of the measured and estimated force) for reference.

Chapter 6

Discussion

This chapter first discusses the differences between the two proposed approaches. Next, the proposed sensing mechanisms offer several advantages in practical applications. The advantages, sensor performance and limitations, and directions for future development are provided.

6.1 Difference between the proposed approaches

This dissertation proposed two approaches for tactile sensorization of an MRE by employing different transducers and sensing mechanisms. The two approaches can be considered the same since the both measure the applied contact force as a displacement of the MRE caused by the applied force. In this sense, there is no differences between the two approaches in terms of the information obtained. However, the structure of the first approach can provide the capability to obtain rich information that cannot be obtained with the second approach.

In the first approach, a magnetic source and its transducer, i.e., a permanent magnet and magnetic transducer, were separated. The second approach employed an inductor that functioned as both a magnetic source and magnetic permeability transducer. This separated structure can adjust sensor performance. A feasible approach is to employ an electromagnet as a magnetic source instead of the permanent magnet used in this dissertation. In Chapter 3, we employed a permanent magnet as a magnetic source; thus, the magnetic field generated by the magnet was temporally static.

However, by employing an electromagnet, we can 1) adjust the magnitude of the magnetic field; and 2) generate a magnetic field with temporal variation. Therefore, the sensor performance, e.g., sensitivity and spatial response region, can be dynamically tuned by adjusting the magnitude of the magnetic field. Furthermore, we employed a magnetic transducer by measuring the magnitude of the magnetic field penetrating the body along a one-dimensional axis. It is expected that richer information about distribution changes in the magnetic field can be obtained when a magnetic transducer measuring 3D changes in the magnetic field is employed. Consequently, these ideas for the first sensorization approach will yield rich tactile information that cannot be obtained with the second approach. To obtain rich tactile information, these ideas should be addressed in future works.

In contrast, the large magnitude of the magnetic field generated by a permanent magnet or an electromagnet has several disadvantages. First, a soft MRE sheet could be slightly deformed by the magnetic force generated by the magnet as well as the applied contact force because the magnetic force attracts the iron particles in the soft MRE sheet. This attraction may cause a large amount of hysteresis in the sensor response curves. Second, magnetic field interference between the magnets could occur when some magnet and magnetic transducer pairs are installed in large area for tactile sensing. This interference makes it difficult to predict the sensor response.

In summary, although the two proposed approaches are similar; the separated structure of the magnetic source and its transducer in the first approach has the potential to measure rich tactile information. In contrast, the second approach has several advantages with respect to its simple structure, as discussed in Chapters 4 and 5. Therefore, we have to choose which tactile sensor is suitable for certain applications. Further investigation and discussions are required to determine whether the first approach can obtain richer tactile information that the second approach.

6.2 Advantages of the proposed approaches

This dissertation considered the development of three kind of tactile sensors based on the two proposed tactile sensorization approaches. We hope that these sensors will facilitate the employment and utilization of tactile sensations in various fields as well as the field of robotics. This section summarizes the advantages of the proposed sensors.

6.2.1 Advantages in practical applications

The biggest advantage of the proposed sensors is the achievement of high durability against severe applied contact force. The sensor surface consists of only elastic silicon rubber and an MRE made of silicon rubber without transducers or electrical wiring. Both sensing mechanisms enable us to insert a frame between the sensor surface and transducers when the frame material has sufficiently low magnetic permeability compared to that of MREs. This means that the sensor surface where the contact force is applied can be completely separated from the transducer and related elements, such as electrical wiring and measurement circuit. Hence, the applied contact force does not reach the fragile and delicate transducers and related elements. In addition, this separation structure enables the fabrication of a flexible tactile sensor that is waterproof because the inserted frame prevents liquid from entering the sensor. This waterproof performance will be important in practical and specific applications.

High durability of the sensor can be achieved by employing a thicker sensor surface. The sensor surface made of elastic material functions as a shock absorber to protect the inside of the sensor from a large applied force. The shock absorption performance can be enhanced by employing thicker elastic material. However, a thick sensor surface will diminish sensor performance such as sensitivity and spatial resolution. Shimojo pointed out that an elastic material placed on a tactile transducer functions as a low-pass filter. In contrast, the proposed approaches can avoid the effect of this low-pass filtering by the elastic material because the transducers can measure the displacement of the outermost surface, i.e., the MRE. Therefore, the proposed sensors can avoid the deteriorations of sensitivity and spatial resolution.

Another advantage is high maintainability. As described above, the sensor has a high durability against large contact force. However, attrition and deterioration of the dual-layer elastomer are unavoidable under physical contact. Subsequently, the dual-layer elastomer, where contact force is applied, must be replaced in practical applications. In the proposed sensors, the dual-layer elastomer is simply placed on the PCB because the elastomer does not contain any transducer and electrical wiring. Therefore, we can easily replace the elastomer when damaged.

The simple structure of both proposed sensors is another important advantage. In both sensors, the dual-layer elastomer, in which the MRE is laminated onto or embedded into a nonmagnetic elastomer, is placed on a PCB holding the transducer. This simple structure enables us to fabricate the sensor easily. Owing to this simple structure, the sensors described in Chapters 4 and 5 can be fabricated at a low-cost because the sensor employs only the dual-layer elastomer and a PCB with traces. In other words, the sensor does not require any additional transducers because an inductor printed on a PCB with traces functions as a magnetic permeability transducer without special technology.

As described in Chapter 5, the inductor can be fabricated on a bendable flexible PCB which can be installed on a complex surface, e.g., a curved surface. The bendability of the sensor is important for several applications, including the implementation of tactile sensors to a complex surface.

6.2.2 Adjustability of sensor performances

Another advantage of the proposed sensors is that sensor performance can be easily adjusted by modifying the sensor structure parameters. The proposed approaches measure the displacement of the outermost MRE surface of the dual-layer elastomer as a distribution change in magnetic permeability around the MRE using a magnet and magnetic transducer, or using an inductor. Therefore, the material characteristics of the dual-layer elastomer and MRE as well as their structural parameters determine the relationship between the displacement and applied contact force.

Sensitivity

Sensitivity against applied contact force can be increased with several approaches. One approach is increasing the amount of magnetic particles in the MRE because a large amount of magnetic particles will increase the magnetic permeability of the MRE. From the sensing mechanisms, a large change in magnetic permeability leads a large sensor response, i.e., large changes in magnetic field or inductance in both approaches. The drawback of increasing magnetic particles is that the softness of the elastic material containing the particles diminishes. Hence, the amount of magnetic particles should be determined to meet the sensitivity and softness requirements of individual applications. A similar approach is employing a thick MRE to increase the sensitivity because a large MRE volume can hold a large amount of magnetic particles.

Another approach is the employment of a dual-layer elastomer with a thin and soft non-magnetic elastomer. Shorter distance between the transducers and MRE will generate a larger change in magnetic permeability. In addition, a softer non-magnetic elastomer will be well deformed against even a small contact force; hence, the displacement of magnetic particles will increase. However, a thinner and softer surface will decrease the measurement range of the contact force because the surface will reach its bottom surface with few applied forces.

The parameters of transducers and other related elements can adjust the sensitivity while the above approaches are related to the sensor surface structure. In the sensor described in Chapter 3, the employment of a strong magnet is a feasible approach to enhance sensitivity. This is because the large magnitude of the magnetic field generated by the magnet causes a large change in magnetic field when contact force is applied. We can apply the same idea to the sensor employing an inductor as a magnetic permeability transducer. An inductor with a large diameter has a large inductance change, i.e., high sensitivity to the applied contact force as shown in Chapter 4. The magnitude of change in inductance will increase in accordance with the original inductance value since an inductor with a large inductance generates a large magnitude of magnetic field. Increasing the number of turns of the inductor is another approach to increase the original inductance. However, in both sensors, the large magnitude of the generated magnetic field could reduce the spatial resolution. Hence, this is an another trade-off between sensitivity and spatial resolution.

Measurement range

The measurement range against applied contact force can be adjusted by modifying the softness and thickness of the dual-layer elastomer. Since the proposed sensing mechanisms measure the applied contact force as displacement of the MRE, the amount of displacement determines the measurement range of the contact force. Therefore, employing harder and thicker non-magnetic elastomer will increase the measurement range because a large contact force can be applied before the MRE approaches to its bottom surface.

Spatial resolution

In the sensor employing an inductor, the spatial resolution, i.e., diameter of spatial response, can be changed by modifying the diameter of the inductor, as shown in Chapter 4. This is because the region of the generated magnetic field can expand in accordance with the diameter of the inductor. Therefore, high spatial resolution can be achieved by employing an inductor with a small diameter. On the other hand, we found that the diameter of the spatial response is not directly proportional to the diameter of the inductor, and that the diameter of the spatial response is larger than that of the inductor. This can be attributed to the spatial low-pass filtering effect of the elastic surface of the sensor [13]. In addition, an inductor with a small diameter will reduce its sensitivity and signal-to-noise (S/N) ratio. Hence, the diameter of an inductor should be determined to balance parameters such as spatial resolution, sensitivity, and S/N ratio in accordance with its applications.

6.3 Issues of the proposed approach

The proposed tactile sensors could be solutions for open issues in conventional tactile sensors by providing the number of advantages discussed above. However, the sensors also have several issues that needed to be addressed for practical applications.

The proposed sensors employ electromagnetic phenomenon to measure the applied contact force. In applications requiring the measurement of force distributions, the number of proposed sensors should be installed like an array. However, electromagnetic interference can occur when the sensors are installed close each other.

The tactile sensor described in Chapter 3 employs a magnet and magnetic transducer pair. To fabricate this sensor array, we have to install several pairs; therefore, the sensor surface will have numerous magnets. The magnetic field generated by these magnets will interfere each other, and this interference will cause difficulty in predicting how the magnetic field changes in accordance with applied contact force. Similarly, the sensor described in Chapters 4 and 5 employs an inductor as a magnetic permeability transducer. To fabricate the sensor array, we have to mount several inductors. These inductors also generate magnetic field when measuring inductance; thus, there will be interference between each inductors.

Consequently, we cannot avoid the electromagnetic interference in both proposed approaches. One of our future works will be to investigate how sensor response is changed by interference. In addition, the issue of compensations for interference must be addressed in the near future. Another interesting approach is to utilize this interference to obtain rich tactile information. The interference between magnets or inductors generates a complex magnetic field which makes it difficult to predict the sensor response. However, such a complex change in magnetic field against applied contact force might yield additional information that cannot be obtained without interference. Investigation of this interference is included in future work for enriching tactile information.

6.4 An insight for a tactile hardware filter

An interesting finding in this dissertation is that the proposed sensors have a bipolar spatial response that can be fitted with a difference-of-Gaussian function. From the experimental results and discussions in Chapter 3, we conclude that the negative response in the bipolar spatial response can be derived from the incompressibility of the employed nonmagnetic elastomer in the dual-layer elastomer. Generally, a tactile sensor covered with an elastic material has a Gaussian-like spatial response as its center position corresponds to the most sensitive point of the employed tactile transducers. This is because that the elastic surface for a tactile transducer functions as a spatial low-pass filter according to Shimojo [13]. Therefore, this bipolar spatial response in the proposed sensing mechanism is also a different point from the conventional tactile sensors.

The question is whether this bipolar response is useful in tactile sensation. The answer is yes in certain applications because the proposed tactile sensor has the potential to function as tactile hardware filter. A difference-of-Gaussian function, which is employed as a fitting function for the observed spatial response, is known as an edge-enhancement filter in the visual processing field. This suggests that the proposed sensor has the potential to extract tactile edge-enhancement information at the hardware level when using an array of tactile sensors.

Edge-enhancement in tactile information processing will be important for detecting the edges of the contact region. Physiology studies have shown that tactile receptors in humans respond to the edge of the contact target. These studies suggest that edge information can help measure and extract rich and essential tactile information in humans. Thus, the proposed sensor with edge-enhancement hardware filtering will play important role in tactile information processing.

Hardware spatial filtering will help in effective tactile information processing, especially in the case of applications using a large number of tactile sensors, e.g., whole body tactile sensation of a humanoid robot. This is because spatial filtering generally has high computational costs.

This dissertation investigated the spatial response using only one cylindrical indenter with a flat contact surface. However, the shape of the spatial response will depend on the shape of indenter because the sensor response is determined by the deformation shape of the MRE sheet. Although we assumed that the contact point, i.e., the number of indenters, was single in the experiments described Chapters 3 and 4, the spatial response will also depend on the number of contact points. Therefore, we have to investigate how the spatial response of the proposed sensor changes under various contact conditions. This investigation is one of the future issue to be addressed to utilize the hardware filter-like spatial response in tactile information processing.

Chapter 7

Conclusion

This dissertation dealt with the tactile sensorization of highly-deformable material for enriching physical interaction. For this purpose, two approaches were proposed. This chapter summarizes the proposed approaches for tactile sensorization of an MRE using electromagnetic phenomena, and describes the results obtained in the experiments. Furthermore, several research issues to be resolved in future works are presented and discussed.

7.1 Summary of the proposed approaches

This dissertation proposed two tactile sensorization methods by employing an MRE as a key component. Chapter 3 addressed the approach for tactile sensorization of the MRE by employing a magnet and magnetic transducer pair. Chapter 4 introduced the approach for tactile sensorization of the MRE by employing an inductor as a magnetic permeability transducer. Chapter 5 expanded the approach described in Chapter 4 to measure tri-axis force with the proposed tactile sensor. The following sections provide the details of the proposed sensorization approaches and summarize the experimental results and findings obtained.

7.1.1 Tactile sensorization of a magnetorheological elastomer based on a magnetic field measurement

Chapter 3 presented the approach for actile sensorization of the MRE based on magnetic field measurements using a magnet and magnetic transducer pair. We evaluated the sensor response versus applied normal force by conducting the following experiments: simulations by a finite element method with a simple model of the proposed sensor, evaluation of sensor response curves with several fabricated sensors under different contact speeds, and investigation of the spatial response of the sensor.

The simulation and experimental results suggest that 1) the proposed sensor can estimate the applied normal force by measuring the change in the magnetic field; and 2) the sensor performance, such as sensitivity and measurement range against contact force, can be tuned by adjusting the thickness of each elastomer in the dual-layer elastomer. In addition, the viscosity of the dual-layer elastomer caused a time-delay in the sensor response under fast contact condition. Another findings is that the spatial response of the sensor is a bipolar response, which has both positive and negative response areas versus the applied normal force. We conclude that this bipolar response can be derived from the incompressibility of the non-magnetic elastomer in the dual-layer elastomer by conducting an investigation of the spatial response with a compressive sponge sheet instead of an incompressive nonmagnetic elastomer.

7.1.2 Tactile sensorization of a magnetorheological elastomer based on an inductance measurement

Chapter 4 introduced the approach for tactile sensorization of the MRE based on inductance measurement using only an inductor instead of a magnet and magnetic transducer pair used in Chapter 3. We evaluated the sensor response versus applied normal force by conducting several experiments on sensor response curves and spatial responses with several fabricated sensors.

The results indicates that 1) the proposed sensor can estimate the applied normal force by measuring the change in the inductance; and 2) an inductor with a large diameter has a large inductance change, i.e., a large sensor response and large S/N ratio. The spatial response of the sensor is a bipolar response because of the incompressibility of the nonmagnetic elastomer in the dual-layer elastomer. We found that an inductor with a large diameter has a large diameter of spatial response. Subsequently, we conclude that there is a trade-off between the sensitivity and spatial resolution of the sensor.

An expanded study of this approach was covered in Chapter 5. Chapter 5 provided the approach for tri-axis tactile sensorization of the MRE based on the inductance measurement using four inductors. This approach employed a disk-shaped MRE and four inductors, whereas the previous approach employed a sheet shaped MRE and one inductor. The proposed sensor can estimate the applied tri-axis force by monitoring the 3D displacement of the disk-shaped MRE from the sum or difference of four inductances, while the tactile sensors described in Chapters 3 and 4 can only measure applied normal force. We also investigated the sensor response versus applied tri-axis force by conducting several experiments.

The results can be summarized as follows: 1) the applied tri-axis force can be estimated with the three converted inductance values, which are sum and difference of the four inductances; and 2) the converted inductances changed monotonically and linearly against the applied normal and shear force. We also found that the estimation error of the tri-axis force increased when a larger force was applied and/or faster contact speeds were used. This estimation error occurred under the large contact force condition because the disk-shaped MRE, which functions as a displacement marker, can be deformed owing to its extreme softness. In addition, the viscosity of the employed elastic materials can cause estimation errors under fast contact condition.

7.2 Future works

This dissertation proposed two methods for the tactile sensorization of an MRE, and investigated fundamental sensor responses with a single sensor under certain experimental conditions. As we discussed in Chapter 6, a number of future works must be conducted in order to investigate sensor responses precisely for real robot applications. One of these is to extend the proposed sensor to large-area tactile sensing, i.e., development of a tactile sensor array. Tactile sensing is generally employed to obtain the distribution of contact force as well as force sensing at a certain contact point. A tactile sensor array using the proposed sensorization approaches can be obtained by implementing an array of a magnet and magnetic transducer pairs, or an inductor. However, these will cause electromagnetic interference between each the element in the array, as discussed in Chapter 6. We will continue to investigate and discuss sensor responses by magnetic field simulation or real experiments with a fabricated tactile sensor array.

The proposed tactile sensorization approaches provide three kinds of flexible and soft tactile sensors that can overcome the issues with conventional tactile sensors. Therefore, the proposed sensors are applicable to any field requiring tactile sensing as well as the field of robotics. Another future works include discussing and developing flexible tactile sensors for various applications not limited to robotics.

Bibliography

[1] Hanna Yousef, Mehdi Boukallel, and Kaspar Althoefer. Tactile sensing for dexterous in-hand manipulation in robotics—a review. Sensors and Actuators A: physical, Vol. 167, No. 2, pp. 171–187, 2011.

[2] Chiara Lucarotti, Calogero Maria Oddo, Nicola Vitiello, and Maria Chiara Carrozza. Synthetic and bio-artificial tactile sensing: A review. Sensors, Vol. 13, No. 2, pp. 1435–1466, 2013.

[3] David Silvera-Tawil, David Rye, and Mari Velonaki. Artificial skin and tactile sensing for socially interactive robots: A review. Robotics and Autonomous Systems, Vol. 63, pp. 230–243, 2015.

[4] 篠田裕之. 皮膚の力学的構造に隠れている知能 (「人間における知能の力学的理解特集号」). システム/制御/情報, Vol. 46, No. 1, pp. 28–34, 2002.

[5] 篠田裕之. 器用な手の皮膚と触覚. 日本ロボット学会誌, Vol. 18, No. 6, pp. 767–771, 2000.

[6] Shan Luo, Joao Bimbo, Ravinder Dahiya, and Hongbin Liu. Robotic tactile perception of object properties: A review. Mechatronics, Vol. 48, pp. 54–67, 2017.

[7] Saleem Khan, Leandro Lorenzelli, and Ravinder S Dahiya. Technologies for printing sensors and electronics over large flexible substrates: a review. IEEE Sensors Journal, Vol. 15, No. 6, pp. 3164–3185, 2015.

[8] Chiara Bartolozzi, Lorenzo Natale, Francesco Nori, and Giorgio Metta. Robots with a sense of touch. Nature materials, Vol. 15, No. 9, p. 921, 2016.

[9] Ryosuke Tajima, Satoshi Kagami, Masayuki Inaba, and Hirochika Inoue. Development of soft and distributed tactile sensors and the application to a humanoid robot. Advanced Robotics, Vol. 16, No. 4, pp. 381–397, 2002.

[10] Marika Hayashi, Takashi Sagisaka, Yui Ishizaka, Tomoaki Yoshikai, and Masayuki Inaba. Development of functional whole-body flesh with distributed three-axis force sensors to enable close interaction by humanoids. In Intelligent Robots and Systems, 2007. IROS 2007. IEEE/RSJ International Conference on, pp. 3610–3615. IEEE, 2007.

[11] Tomoyuki Noda, Takahiro Miyashita, Hiroshi Ishiguro, and Norihiro Hagita. Super-flexible skin sensors embedded on the whole body self-organizing based on haptic interactions. Human-Robot Interaction in Social Robotics, p. 183, 2012.

[12] Philipp Mittendorfer, Eiichi Yoshida, and Gordon Cheng. Realizing whole-body tactile interactions with a self-organizing, multi-modal artificial skin on a humanoid robot. Advanced Robotics, Vol. 29, No. 1, pp. 51–67, 2015.

[13] Makoto Shimojo. Spatial filtering characteristic of elastic cover for tactile sensor. In Robotics and Automation, 1994. Proceedings., 1994 IEEE International Conference on, pp. 287–292. IEEE, 1994.

[14] Perla Maiolino, Marco Maggiali, Giorgio Cannata, Giorgio Metta, and Lorenzo Natale. A flexible and robust large scale capacitive tactile system for robots. IEEE Sensors Journal, Vol. 13, No. 10, pp. 3910–3917, 2013.

[15] Masanori Goka, Hiroyuki Nakamoto, and Satoru Takenawa. A magnetic type tactile sensor by gmr elements and inductors. In Intelligent Robots and Systems (IROS), 2010 IEEE/RSJ International Conference on, pp. 885–890. IEEE, 2010.

[16] Akihiko Yamaguchi and Christopher G Atkeson. Combining finger vision and optical tactile sensing: Reducing and handling errors while cutting vegetables. In Humanoid Robots (Humanoids), 2016 IEEE-RAS 16th International Conference on, pp. 1045–1051. IEEE, 2016.

[17] Ravinder S Dahiya, Giorgio Metta, Maurizio Valle, and Giulio Sandini. Tactile sensing–from humans to humanoids. IEEE transactions on robotics, Vol. 26, No. 1, pp. 1–20, 2010.

[18] Brenna D Argall and Aude G Billard. A survey of tactile human–robot interactions. Robotics and autonomous systems, Vol. 58, No. 10, pp. 1159–1176, 2010.

[19] Ravinder S Dahiya, Philipp Mittendorfer, Maurizio Valle, Gordon Cheng, and Vladimir J Lumelsky. Directions toward effective utilization of tactile skin: A review. IEEE Sensors Journal, Vol. 13, No. 11, pp. 4121–4138, 2013.

[20] 多田泰徳, 細田耕, 浅田稔. 内部に触覚受容器を持つ人間型柔軟指. 日本ロボット学会誌, Vol. 23, No. 4, pp. 482–487, 2005.

[21] Koh Hosoda, Yasunori Tada, and Minoru Asada. Anthropomorphic robotic soft fingertip with randomly distributed receptors. Robotics and Autonomous Systems, Vol. 54, No. 2, pp. 104–109, 2006.

[22] Nobuyuki Futai, Kiyoshi Matsumoto, and Isao Shimoyama. A flexible micromachined planar spiral inductor for use as an artificial tactile mechanoreceptor. Sensors and Actuators A: Physical, Vol. 111, No. 2-3, pp. 293–303, 2004.

[23] Lucie Viry, Alessandro Levi, Massimo Totaro, Alessio Mondini, Virgilio Mattoli, Barbara Mazzolai, and Lucia Beccai. Flexible three-axial force sensor for soft and highly sensitive artificial touch. Advanced Materials, Vol. 26, No. 17, pp. 2659–2664, 2014.

[24] Yu-Ming Huang, Nan-Chyuan Tsai, and Jing-Yao Lai. Development of tactile sensors for simultaneous, detection of normal and shear stresses. Sensors and Actuators A: Physical, Vol. 159, No. 2, pp. 189–195, 2010.

[25] Hidetoshi Takahashi, Akihito Nakai, Nguyen Thanh-Vinh, Kiyoshi Matsumoto, and Isao Shimoyama. A triaxial tactile sensor without crosstalk using pairs of piezoresistive beams with sidewall doping. Sensors and Actuators A: Physical, Vol. 199, pp. 43–48, 2013.

[26] Lucia Beccai, Stefano Roccella, Luca Ascari, Pietro Valdastri, Arne Sieber, M Chiara Carrozza, and Paolo Dario. Development and experimental analysis of a soft compliant tactile microsensor for anthropomorphic artificial hand. IEEE/Asme Transactions on Mechatronics, Vol. 13, No. 2, pp. 158–168, 2008.

[27] Kenichiro Kanao, Shingo Harada, Yuki Yamamoto, Wataru Honda, Takayuki Arie, Seiji Akita, and Kuniharu Takei. Highly selective flexible tactile strain and temperature sensors against substrate bending for an artificial skin. RSC Advances, Vol. 5, No. 38, pp. 30170–30174, 2015.

[28] Daiki Hirashima, Tatsuya Uematsu, Masayuki Sohgawa, Wataru Mito, Takeshi Kanashima, Masanori Okuyama, and Haruo Noma. Fabrication of a flexible array for tactile sensors with microcantilevers and the measurement of the distribution of normal and shear forces. Japanese Journal of Applied Physics, Vol. 50, No. 6S, p. 06GM02, 2011.

[29] Nawid Jamali and Claude Sammut. Majority voting: Material classification by tactile sensing using surface texture. IEEE Transactions on Robotics, Vol. 27, No. 3, pp. 508–521, 2011.

[30] Murat Gel and Isao Shimoyama. Force sensing submicrometer thick cantilevers with ultra-thin piezoresistors by rapid thermal diffusion. Journal of micromechanics and microengineering, Vol. 14, No. 3, p. 423, 2003.

[31] Hyung-Kew Lee, Jaehoon Chung, Sun-Il Chang, and Euisik Yoon. Normal and shear force measurement using a flexible polymer tactile sensor with embedded multiple capacitors. Journal of Microelectromechanical Systems, Vol. 17, No. 4, pp. 934–942, 2008.

[32] A Fassler and C Majidi. Soft-matter capacitors and inductors for hyperelastic strain sensing and stretchable electronics. Smart Materials and Structures, Vol. 22, No. 5, p. 055023, 2013.

[33] S Wattanasarn, K Noda, K Matsumoto, and I Shimoyama. 3d flexible tactile sensor using electromagnetic induction coils. In Micro Electro Mechanical Systems (MEMS), 2012 IEEE 25th International Conference on, pp. 488–491. IEEE, 2012.

[34] Mitsuhiro Hakozaki, Atsushi Hatori, and Hiroyuki Shinoda. A sensitive skin using wireless tactile sensing elements. In TECHNICAL DIGEST OF THE SENSOR SYMPOSIUM, Vol. 18, pp. 147–150. Citeseer, 2001.

[35] Jaemin Kim, Mincheol Lee, Hyung Joon Shim, Roozbeh Ghaffari, Hye Rim Cho, Donghee Son, Yei Hwan Jung, Min Soh, Changsoon Choi, Sungmook Jung, et al. Stretchable silicon nanoribbon electronics for skin prosthesis. Nature communications, Vol. 5, p. 5747, 2014.

[36] Sungwon Lee, Amir Reuveny, Jonathan Reeder, Sunghoon Lee, Hanbit Jin, Qihan Liu, Tomoyuki Yokota, Tsuyoshi Sekitani, Takashi Isoyama, Yusuke Abe, et al. A transparent bending-insensitive pressure sensor. Nature nanotechnology, Vol. 11, No. 5, p. 472, 2016.

[37] Xiandi Wang, Lin Dong, Hanlu Zhang, Ruomeng Yu, Caofeng Pan, and Zhong Lin Wang. Recent progress in electronic skin. Advanced Science, Vol. 2, No. 10, 2015.

[38] Michael Leineweber, Georg Pelz, Michael Schmidt, Holger Kappert, and Günter Zimmer. New tactile sensor chip with silicone rubber cover. Sensors and Actuators A: Physical, Vol. 84, No. 3, pp. 236–245, 2000.

[39] Alexander Schmitz, Perla Maiolino, Marco Maggiali, Lorenzo Natale, Giorgio Cannata, and Giorgio Metta. Methods and technologies for the implementation of large-scale robot tactile sensors. IEEE Transactions on Robotics, Vol. 27, No. 3, pp. 389–400, 2011.

[40] Alexander Schmitz, Marco Maggiali, Marco Randazzo, Lorenzo Natale, and Giorgio Metta. A prototype fingertip with high spatial resolution pressure sensing for the robot icub. In Humanoid Robots, 2008. Humanoids 2008. 8th IEEE-RAS International Conference on, pp. 423–428. IEEE, 2008.

[41] Hyung-Kew Lee, Jaehoon Chung, Sun-Il Chang, and Euisik Yoon. Real-time measurement of the three-axis contact force distribution using a flexible capacitive polymer tactile sensor. Journal of Micromechanics and Microengineering, Vol. 21, No. 3, p. 035010, 2011.

[42] Z Chu, PM Sarro, and S Middelhoek. Silicon three-axial tactile sensor. Sensors and Actuators A: Physical, Vol. 54, No. 1-3, pp. 505–510, 1996.

[43] F Zhu and JW Spronck. A capacitive tactile sensor for shear and normal force measurements. Sensors and Actuators A: Physical, Vol. 31, No. 1-3, pp. 115–120, 1992.

[44] Jose Gerardo Vieira da Rocha, Pedro Filipe Antunes da Rocha, and Senentxu Lanceros-Mendez. Capacitive sensor for three-axis force measurements and its readout electronics. IEEE transactions on instrumentation and measurement, Vol. 58, No. 8, pp. 2830–2836, 2009.

[45] Axaykumar Rana, Jean-Philippe Roberge, and Vincent Duchaine. An improved soft dielectric for a highly sensitive capacitive tactile sensor. IEEE Sensors Journal, Vol. 16, No. 22, pp. 7853–7863, 2016.

[46] Ting Zhang, Hong Liu, Li Jiang, Shaowei Fan, and Jing Yang. Development of a flexible 3-d tactile sensor system for anthropomorphic artificial hand. IEEE sensors Journal, Vol. 13, No. 2, pp. 510–518, 2013.

[47] Alin Drimus, Gert Kootstra, Arne Bilberg, and Danica Kragic. Design of a flexible tactile sensor for classification of rigid and deformable objects. Robotics and Autonomous Systems, Vol. 62, No. 1, pp. 3–15, 2014.

[48] Gereon H Büscher, Risto Kõiva, Carsten Schürmann, Robert Haschke, and Helge J Ritter. Flexible and stretchable fabric-based tactile sensor. Robotics and Autonomous Systems, Vol. 63, pp. 244–252, 2015.

[49] Haopeng Wang, Debao Zhou, and Jianguo Cao. Development of a skin-like tactile sensor array for curved surface. IEEE Sensors Journal, Vol. 14, No. 1, pp. 55–61, 2014.

[50] Makoto Shimojo, Akio Namiki, Masatoshi Ishikawa, Ryota Makino, and Kunihiko Mabuchi. A tactile sensor sheet using pressure conductive rubber with electrical-wires stitched method. IEEE Sensors journal, Vol. 4, No. 5, pp. 589–596, 2004.

[51] Yasunori Tada, Masahiro Inoue, Toshimi Kawasaki, Yasushi Kawahito, Hiroshi Ishiguro, and Katsuaki Suganuma. A principle and characteristics of a flexible and stretchable tactile sensor based on static electricity phenomenon. Journal of the Robotics Society of Japan, Vol. 26, No. 2, pp. 210–216, 2008.

[52] 稲葉雅幸, 星野由紀子, 井上博允. 導電性ファブリックを用いた全身被覆型触覚センサスーツ. 日本ロボット学会誌, Vol. 16, No. 1, pp. 80–86, 1998.

[53] Oliver Kerpa, Karsten Weiss, and Heinz Worn. Development of a flexible tactile sensor system for a humanoid robot. In Intelligent Robots and Systems, 2003.(IROS 2003). Proceedings. 2003 IEEE/RSJ International Conference on, Vol. 1, pp. 1–6. IEEE, 2003.

[54] Takashi Minato, Yuichiro Yoshikawa, Tomoyuki Noda, Shuhei Ikemoto, Hiroshi Ishiguro, and Minoru Asada. Cb2: A child robot with biomimetic body for cognitive developmental robotics. In Humanoid Robots, 2007 7th IEEE-RAS International Conference on, pp. 557–562. IEEE, 2007.

[55] Makoto Shimojo, Takuma Araki, Seiichi Teshigawara, Aigou Ming, and Masatoshi Ishikawa. A net-structure tactile sensor covering free-form surface and ensuring high-speed response. In Intelligent Robots and Systems, 2007. IROS 2007. IEEE/RSJ International Conference on, pp. 670–675. IEEE, 2007.

[56] Toshiharu Mukai, Masaki Onishi, Tadashi Odashima, Shinya Hirano, and Zhiwei Luo. Development of the tactile sensor system of a human–interactive robot ”ri–man”. IEEE Transactions on Robotics, Vol. 24, No. 2, pp. 505–512, 2008.

[57] Yoshiyuki Ohmura, Yasuo Kuniyoshi, and Akihiko Nagakubo. Conformable and scalable tactile sensor skin for curved surfaces. In Robotics and Automation, 2006. ICRA 2006. Proceedings 2006 IEEE International Conference on, pp. 1348–1353. IEEE, 2006.

[58] Philipp Mittendorfer and Gordon Cheng. Humanoid multimodal tactile-sensing modules. IEEE Transactions on robotics, Vol. 27, No. 3, pp. 401–410, 2011.

[59] 保坂紗智子. 全身触覚をもつ赤ちゃんロボットの開発. 第 24 回日本ロボット学会学術講演会予稿集, 2006, 2006.

[60] 伍賀正典, 中本裕之, 武縄悟, 貴田恭旭. 磁気式触覚センサの小型化と性能評価 (機械力学, 計測, 自動制御). 日本機械学会論文集 C 編, Vol. 76, No. 772, pp. 3640–3647, 2010.

[61] Lorenzo Jamone, Lorenzo Natale, Giorgio Metta, and Giulio Sandini. Highly sensitive soft tactile sensors for an anthropomorphic robotic hand. IEEE sensors Journal, Vol. 15, No. 8, pp. 4226–4233, 2015.

[62] Sina Youssefian, Nima Rahbar, and Eduardo Torres-Jara. Contact behavior of soft spherical tactile sensors. IEEE sensors Journal, Vol. 14, No. 5, pp. 1435–1442, 2014.

[63] Yanjie Liu, Haijun Han, Tao Liu, Jingang Yi, Qingguo Li, and Yoshio Inoue. A novel tactile sensor with electromagnetic induction and its application on stick-slip interaction detection. Sensors, Vol. 16, No. 4, p. 430, 2016.

[64] Tito Pradhono Tomo, Sophon Somlor, Alexander Schmitz, Lorenzo Jamone, Weijie Huang, Harris Kristanto, and Shigeki Sugano. Design and characterization of a three-axis hall effect-based soft skin sensor. Sensors, Vol. 16, No. 4, p. 491, 2016.

[65] Hongbo Wang, Greg de Boer, Junwai Kow, Ali Alazmani, Mazdak Ghajari, Robert Hewson, and Peter Culmer. Design methodology for magnetic field-based soft tri-axis tactile sensors. Sensors, Vol. 16, No. 9, p. 1356, 2016.

[66] Eduardo Torres-Jara, Iuliu Vasilescu, and Raul Coral. A soft touch: Compliant tactile sensors for sensitive manipulation, 2006.

[67] James J Clark. A magnetic field based compliance matching sensor for high resolution, high compliance tactile sensing. In Robotics and Automation, 1988. Proceedings., 1988 IEEE International Conference on, pp. 772–777. IEEE, 1988.

[68] Damith Suresh Chathuranga, Zhongkui Wang, Yohan Noh, Thrishantha Nanayakkara, and Shinichi Hirai. Magnetic and mechanical modeling of a soft

three-axis force sensor. IEEE Sensors Journal, Vol. 16, No. 13, pp. 5298–5307, 2016.

[69] Satoru Takenawa. A magnetic type tactile sensor using a two-dimensional array of inductors. In Robotics and Automation, 2009. ICRA'09. IEEE International Conference on, pp. 3295–3300. IEEE, 2009.

[70] Hiroyuki Nakamoto, Masanori Goka, Satoru Takenawa, and Yasuaki Kida. A magnetic type tactile sensor using gmr elements and inductors. Transactions of the Japan Society of Mechanical Engineers, Part C, Vol. 76, No. 766, pp. 1476–1482, 2010.

[71] 堀井隆斗, 長井志江, 浅田稔. 磁性エラストマーを利用した磁気式触覚センサ. ロボティクス・メカトロニクス講演会 2014 講演論文集, 2014.

[72] Tito Pradhono Tomo, Alexander Schmitz, Wai Keat Wong, Harris Kristanto, Sophon Somlor, Jinsun Hwang, Lorenzo Jamone, and Shigeki Sugano. Covering a robot fingertip with uskin: A soft electronic skin with distributed 3-axis force sensitive elements for robot hands. IEEE Robotics and Automation Letters, Vol. 3, No. 1, pp. 124–131, 2018.

[73] Kazuto Kamiyama, Kevin Vlack, Terukazu Mizota, Hiroyuki Kajimoto, K Kawakami, and Susumu Tachi. Vision-based sensor for real-time measuring of surface traction fields. IEEE Computer Graphics and Applications, Vol. 25, No. 1, pp. 68–75, 2005.

[74] A Takagi, Y Yamamoto, M Ohka, H Yussof, and SC Abdullah. Sensitivity-enhancing all-in-type optical three-axis tactile sensor mounted on articulated robotic fingers. Procedia Computer Science, Vol. 76, pp. 95–100, 2015.

[75] A Takagi, Y Yamamoto, M Ohka, H Yussof, and SC Abdullah. Sensitivity-enhancing all-in-type optical three-axis tactile sensor mounted on articulated robotic fingers. Procedia Computer Science, Vol. 76, pp. 95–100, 2015.

[76] Kazuto Kamiyama, Hiroyuki Kajimoto, Naoki Kawakami, and Susumu Tachi. Evaluation of a vision-based tactile sensor. In Robotics and Automation, 2004.

Proceedings. ICRA'04. 2004 IEEE International Conference on, Vol. 2, pp. 1542–1547. IEEE, 2004.

[77] Yuji Ito, Youngwoo Kim, and Goro Obinata. Robust slippage degree estimation based on reference update of vision-based tactile sensor. IEEE Sensors Journal, Vol. 11, No. 9, pp. 2037–2047, 2011.

[78] Rui Li, Robert Platt, Wenzhen Yuan, Andreas ten Pas, Nathan Roscup, Mandayam A Srinivasan, and Edward Adelson. Localization and manipulation of small parts using gelsight tactile sensing. In Intelligent Robots and Systems (IROS 2014), 2014 IEEE/RSJ International Conference on, pp. 3988–3993. IEEE, 2014.

[79] Luke Cramphorn, Benjamin Ward-Cherrier, and Nathan F Lepora. Tactile manipulation with biomimetic active touch. In Robotics and Automation (ICRA), 2016 IEEE International Conference on, pp. 123–129. IEEE, 2016.

[80] Akihiko Yamaguchi and Christopher G Atkeson. Combining finger vision and optical tactile sensing: Reducing and handling errors while cutting vegetables. In Humanoid Robots (Humanoids), 2016 IEEE-RAS 16th International Conference on, pp. 1045–1051. IEEE, 2016.

[81] Kazuto Kamiyama, Hiroyuki Kajimoto, Masahiko Inami, Naoki Kawakami, and Susumu Tachi. A vision-based tactile sensor. In International Conference on Artificial Reality and Telexistence, pp. 127–134, 2001.

[82] Kazuhiro Shimonomura, Hiroto Nakashima, and Kentaro Nozu. Robotic grasp control with high-resolution combined tactile and proximity sensing. In Robotics and Automation (ICRA), 2016 IEEE International Conference on, pp. 138–143. IEEE, 2016.

[83] 熊谷建汰, 下ノ村和弘. イベントベースカメラを用いた高時間・空間分解能触覚センサ. 計測自動制御学会第 18 回 SI 部門講演会 (SI2017), 2017.

[84] 熊谷建汰, 下ノ村和弘. イベントベースカメラを用いた分布型触覚センサのロボットハンドへの適用. 日本機械学会ロボティクス・メカトロニクス講演会 2018, 2018.

[85] Hongbo Wang, Junwai Kow, Gd Boer, Dominic Jones, Ali Alazmani, and Peter Culmer. A low-cost, high-performance, soft tri-axis tactile sensor based on eddy-current effect. In IEEE Sensors, 2017.

[86] 加嶋俊大. 磁性流体および磁性エラストマーを用いたソフトアクチュエータの研究, 2013.

[87] J Andrew Pruszynski and Roland S Johansson. Edge-orientation processing in first-order tactile neurons. Nature neuroscience, Vol. 17, No. 10, p. 1404, 2014.

[88] Shan Luo, Wenxuan Mou, Kaspar Althoefer, and Hongbin Liu. Novel tactile-sift descriptor for object shape recognition. IEEE Sensors Journal, Vol. 15, No. 9, pp. 5001–5009, 2015.

[89] Nathan F Lepora, Uriel Martinez-Hernandez, Mathew Evans, Lorenzo Natale, Giorgio Metta, and Tony J Prescott. Tactile superresolution and biomimetic hyperacuity. IEEE Transactions on Robotics, Vol. 31, No. 3, pp. 605–618, 2015.

[90] Texas Instruments. Inductance-to-digital converter chip ldc1614. `http://www.ti.com/product/LDC1614/`.

[91] Hanna Yousef, Mehdi Boukallel, and Kaspar Althoefer. Tactile sensing for dexterous in-hand manipulation in robotics–a review. Sensors and Actuators A: physical, Vol. 167, No. 2, pp. 171–187, 2011.

[92] Takumi Kawasetsu, Takato Horii, Hisashi Ishihara, and Minoru Asada. Size dependency in sensor response of a flexible tactile sensor based on inductance measurement. In SENSORS, 2017 IEEE, pp. 1–3. IEEE, 2017.

[93] Takumi Kawasetsu, Takato Horii, Hisashi Ishihara, and Minoru Asada. Mexican-hat-like response in a flexible tactile sensor using a magnetorheological elastomer. Sensors, Vol. 18, No. 2, p. 587, 2018.

Published Papers by the Author

Articles in Journal

1. Takumi Kawasetsu, Takato Horii, Hisashi Ishihara, and Minoru Asada, “ Flexible Tri-axis Tactile Sensor Using Spiral Inductor and Magnetorheological Elastomer ”. *IEEE Sensors Journal*, vol.18, no.14, pp.5834–5841, 2018.

2. Takumi Kawasetsu, Takato Horii, Hisashi Ishihara, and Minoru Asada, “Mexican-Hat-Like Response in a Flexible Tactile Sensor Using a Magnetorheological Elastomer ”. *Sensors*, vol.18, no.2, pp.587, 2018.2.

3. 川節拓実, 堀井隆斗, 石原尚, 浅田稔. “ 磁性・非磁性エラストマを積層した磁気式触覚センサの基礎特性解析 ”. 日本 *AEM* 学会誌, Vol.24, No.3, pp.204-209, 2016.12.

Papers in Proceedings of International Conferences

1. Takumi Kawasetsu, Takato Horii, Hisashi Ishiara, and Minoru Asada. ”Size dependency in spatial response property of elastomeric tactile sensor laminated on inductor coil”. In *Proceedings of the IEEE Sensors Conference*, 2017.

2. Takumi Kawasetsu, Takato Horii, Hisashi Ishiara, and Minoru Asada. “ Towards rich representation learning in a tactile domain: a flexible tactile sensor providing a vision-like feature based on the dual inductor ”. In *Proceedings of the 5th International Conference on Human-Agent Interaction workshop on Representation learning for human and robot cognition*, 2017.

3. Takumi Kawasetsu, Takato Horii, Hisashi Ishiara, and Minoru Asada. “ Magnetorheological elastomer-gel tactile sensor with an electromagnet ”. In *Proceedings of the ICRA 2017 Workshop on The Robotic Sense of Touch*, 2017.

4. Takumi Kawasetsu, Takato Horii, Hisashi Ishiara, and Minoru Asada. “ Difference of Gaussian like feature enhances object classification accuracy in magnetorheological elastomer-gel tactile sensor ”. In *Proceedings of the Humanoids 2016 Workshop on Tactile sensing for manipulation: new progress and challenges*, 2016.

5. Takumi Kawasetsu, Takato Horii, Hisashi Ishiara, and Minoru Asada. “Towards rich physical human-robot interaction: A novel magnetic-type flexible tactile sensor that detects its surface deformation ”. In *Proceedings of the ICRA 2016 Workshop on human-robot interfaces for enhanced physical interactions*, 2016.

6. Takumi Kawasetsu, Takato Horii, Hisashi, Ishiara and Minoru Asada. “ A magnetic type tactile sensor that detects deformation of its surface made of dual layer elastomer ”. In *Proceedings of the Workshop “ From Robotics to Cognitive Interaction and Beyond ”*, 2016.

7. Takumi Kawasetsu, Takato Horii, Hisahi Ishihara, and Minoru Asada. “Toward humanlike tactile sensation: magnetic type tactile sensor with dual-layer elastomer ”. The 2nd International Workshop on Cognitive Neuroscience Robotics, 2016.

8. Takumi Kawasetsu, Takato Horii, Hisashi Ishihara, and Minoru Asada. “ Deformation response of a flexible tactile sensor made of magnetorheological and nonmagnetic elastomers ”. Workshop on Cognitive Development for Friendly Robots and Rehabilitation, 2015.

Papers in Proceedings of Japanese Conferences

1. 川節拓実, 堀井隆斗, 石原尚, 浅田稔. “ 磁性エラストマとスパイラルコイルを用いた柔軟触覚センサのアレイ化 ”. ロボティクス・メカトロニクス講演会 2018, 福岡, 2018.

2. 福田康平, 川節拓実, 石原尚, 堀井隆斗, 中村亮一, 川平洋, 浅田稔. “腹腔鏡手術手技評価のための縫合結紮トレーニングパッドの三軸力覚センサ化”. ロボティクス・メカトロニクス講演会 2018, 福岡, 2018.

3. 川節拓実, 堀井隆斗, 石原尚, 浅田稔. “磁性エラストマと平面コイルを用いたインダクタンス測定に基づく柔軟触覚センサの開発”. 第 26 回 MAGDA コンファレンス, 金沢, 2017.

4. 川節拓実, 堀井隆斗, 石原尚, 浅田稔. “磁性エラストマを用いた柔軟な 3 軸力覚センサ”. 第 35 回日本ロボット学会学術講演会, 埼玉, 2017.

5. 川節拓実, 堀井隆斗, 石原尚, 浅田稔. “Difference of Gaussian 様空間応答を示す磁気式柔軟触覚センサ”. 第 34 回日本ロボット学会学術講演会, 山形, 2016.

6. 川節拓実, 堀井隆斗, 石原尚, 浅田稔. “磁性・非磁性エラストマを用いた磁気式触覚センサの磁場解析”. ロボティクス・メカトロニクス講演会 2016, 横浜, 2016.

7. 川節拓実, 堀井隆斗, 石原尚, 浅田稔. “磁性エラストマを用いた磁気式触覚センサの特性評価”. 第 16 回計測自動制御学会システムインテグレーション部門講演会予稿集, 愛知, 2015.

8. 川節拓実, 堀井隆斗, 石原尚, 浅田稔. “磁性・非磁性エラストマを積層した磁気式触覚センサの基礎特性解析”. 第 24 回 MAGDA コンファレンス, 宮城, 2015.

Patent

1. 特許出願 2017-170627. 川節拓実, 堀井隆斗, 石原尚. 触覚センサ, 大阪大学, 出願日 2017 年 9 月 5 日.

2. 特許出願 2016-146070. 川節拓実, 堀井隆斗, 石原尚, 仲田好宏, 浅田稔, 細田耕, 宮下敬宏. 変形測定装置, 株式会社国際電気通信基礎技術研究所, 出願日 2016 年 7 月 26 日.

Award

1. 日本ロボット学会研究奨励賞, 2018.
2. ロボカップジャパンオープン 2018 日本ロボット学会賞, 2018.
3. 第 24 回 MAGDA コンファレンス 優秀ポスター講演論文賞, 2015.